LIGHT ODD-ODD NUCLEI

THERMAL NEUTRON CAPTURE STUDIES OF SOME LIGHT ODD-ODD NUCLEI

by

ABUL FAIZ MOHAMMED ISHAQ,

B.Sc. (Hons.), M.Sc.

A Thesis

Submitted to the Faculty of Graduate Studies

in Partial Fulfilment of the Requirements

for the Degree

Doctor of Philosophy

McMaster University

September, 1972

DOCTOR OF PHILOSOPHY (1972)

McMASTER UNIVERSITY
Hamilton, Ontario

TITLE: Thermal Neutron Capture Studies of Some Light Odd-Odd Nuclei.

AUTHOR: Abul Faiz Mohammed Ishaq,

B.Sc. (Hons.), M.Sc. (Karachi University)

SUPERVISOR: Dr. T. J. Kennett

NUMBER OF PAGES: vii, 165

SCOPE AND CONTENTS:

Thermal neutron capture studies have been made of the odd-odd nuclei, ^{20}F, ^{24}Na, ^{28}Al, ^{32}P, ^{36}Cl and ^{40}K. The gamma ray spectra have been studied using a Ge(Li) pair spectrometer and revised decay schemes are presented for these nuclei. The Q-values and gamma ray multiplicities have been obtained for the reactions studied. The average partial widths for primary M1 and E1 transitions have been calculated for the six nuclei and compared with the theoretical estimates. The features of the capture gamma ray spectra are discussed and it is observed that for the six nuclei studied, the total intensity in the spectrum above the energy of 0.3 times the Q-value is nearly the same (~1.4 photons/capture).

ACKNOWLEDGEMENTS

I wish to thank the members of my supervisory committee, Dr. T. J. Kennett, Dr. W. V. Prestwich and Dr. K. Fritze for their advice and interest during the course of this work. I owe my sincerest gratitude to my Research Director, Dr. T. J. Kennett, for his ready and capable assistance and encouragement. I am also indebted to Dr. W. V. Prestwich for many enlightening discussions.

This work could not have been completed without the assistance of my research associates. I am particularly thankful to Tony Colenbrander for his participation in the work on ^{28}Al and for the use of several of his computer programs, and to Andy Robertson and Armando Lopez for their help with the electronics.

Thanks are also due to the Reactor and Health Physics staff for their cooperation and assistance.

I am very grateful to Mrs. W. Prestwich for the fast and accurate typing of this manuscript.

Finally, I would like to thank the Government and the people of Canada for the award of a Commonwealth Scholarship. This work has been supported financially by the National Research Council of Canada and the Government of Ontario.

TABLE OF CONTENTS

	Page
CHAPTER I - Introduction	1
1.1 The (n,γ) Reaction	1
1.2 Radiation Widths	5
1.3 Porter-Thomas Distribution	12
1.4 Nuclear Level Densities	14
1.5 Spectral Features	15
1.6 Absolute Intensities	17
CHAPTER II - Experimental Details	19
2.1 The Tangential Irradiation Facility	19
2.2 The Ge(Li) Pair Spectrometer	21
2.3 The Data Acquisition System	23
2.4 Energy Measurements	24
2.5 Relative Intensity Measurements	29
CHAPTER III - Thermal Neutron Capture Studies	31
3.1 The $^{27}Al(n,\gamma)^{28}Al$ Reaction	31
3.2 The $^{35}Cl(n,\gamma)^{36}Cl$ Reaction	51
3.3 The $^{31}P(n,\gamma)^{32}P$ Reaction	71
3.4 The $^{19}F(n,\gamma)^{20}F$ Reaction	79
3.5 The $^{23}Na(n,\gamma)^{24}Na$ Reaction	92
3.6 The $^{39}K(n,\gamma)^{40}K$ Reaction	104
CHAPTER IV - Transition Strengths	117
4.1 Composite Capture State	117
4.2 Transition Strengths	121
4.3 Discussion and Conclusions	141
CHAPTER V - Spectral Features	149
5.1 Q-values and Multiplicities	149
5.2 Spectral Features	149
5.3 Detailed Analysis of ^{36}Cl Spectrum	157
REFERENCES	159

LIST OF TABLES

NUMBER	TITLE	PAGE
2-1	The Energies of Calibration Standards	26
3-1	The Observed Transitions in ^{28}Al	33
3-2	The Q-Value for the $^{27}Al(n,\gamma)^{28}Al$ Reaction	42
3-3	The Decay Modes of ^{28}Al Levels	46
3-4	The Transitions in ^{38}Cl	54
3-5	The Observed Transitions in ^{36}Cl	55
3-6	The Q-value for the $^{35}Cl(n,\gamma)^{36}Cl$ Reaction	64
3-7	The Decay Modes of ^{36}Cl Levels	65
3-8	The Intensities of Strong Low Energy Transitions in ^{36}Cl	69
3-9	The Observed Transitions in ^{32}P	73
3-10	The Q-value for the $^{31}P(n,\gamma)^{32}P$ Reaction	77
3-11	The Decay Modes of ^{32}P Levels	79
3-12	The Observed Transitions in ^{20}F	84
3-13	The Decay Modes of ^{20}F Levels	90
3-14	The Observed Transitions in ^{24}Na	94
3-15	The Q-value for the $^{23}Na(n,\gamma)^{24}Na$ Reaction	100
3-16	The Decay Modes of ^{24}Na Levels	102
3-17	The Transitions Attributed to ^{42}K	106
3-18	The Observed Transitions in ^{40}K	107
3-19	The Q-value for the $^{39}K(n,\gamma)^{40}K$ Reaction	115
4-1	The Primary M1 Transitions in ^{20}F	124
4-2	The Primary M1 Transitions in ^{24}Na	126
4-3	The Primary E1 Transitions in ^{24}Na	127
4-4	The Primary M1 Transitions in ^{28}Al	129
4-4	The Primary E1 Transitions in ^{28}Al	130
4-6	The Primary M1 Transitions in ^{32}P	132
4-7	The Primary E1 Transitions in ^{32}P	133
4-8	The Primary M1 Transitions in ^{36}Cl	135
4-9	The Primary E1 Transitions in ^{36}Cl	136
4-10	The Primary M1 Transitions in ^{40}K	139

LIST OF TABLES

NUMBER	TITLE	PAGE
4-11	The Primary E1 Transitions in ^{40}K	140
4-12	A Summary of Transition Strengths	142
4-13	The Other Primary Transitions in ^{28}Al	144
4-14	The Estimates of Degrees of Freedom	148
5-1	A Summary of Q-value Measurements	150
5-2	The Gamma Ray Multiplicities	151
5-3	The Average Energies of Primary Transitions	154
5-4	The Variation of I_x with E_x	156

LIST OF FIGURES

NUMBER	CAPTION	FOLLOWING PAGE NO.
2-1	The Tangential Irradiation Facility	19
2-2	The Sample Holder/Carrier	20
2-3	The Capture Gamma Ray Spectrum of Melamine	23
2-4	A Block Diagram of the Data Acquisition System	23
2-5	The Relative Efficiency of the Ge(Li) Pair Spectrometer	30
3-1	The Capture Gamma Ray Spectrum of Aluminum	32
3-2	The Decay Scheme of ^{28}Al	45
3-3	The Capture Gamma Ray Spectrum of Chlorine	52
3-4	The Decay Scheme of ^{36}Cl	63
3-5	The Capture Gamma Ray Spectrum of Phosphorus	72
3-6	The Decay Scheme of ^{32}P	77
3-7	The Capture Gamma Ray Spectrum of Fluorine	83
3-8	The Capture Gamma Ray Spectrum of Sodium	93
3-9	The Capture Gamma Ray Spectrum of Potassium	105
4-1	The Reduced Intensities of Primary E1 Transitions in ^{36}Cl	145
4-2	The Reduced Intensities of Primary E1 Transitions in ^{40}K	145
4-3	The Reduced Intensities of Primary M1 Transitions in ^{28}Al	146
		146
5-1	The Total and Primary Spectra of ^{20}F	153
5-2	The Total and Primary Spectra of ^{24}Na	153
5-3	The Total and Primary Spectra of ^{28}Al	153
5-4	The Total and Primary Spectra of ^{32}P	153
5-5	The Total and Primary Spectra of ^{36}Cl	153
5-6	The Total and Primary Spectra of ^{40}K	153
5-7	The Cumulative Spectra of Members of Two Step Cascades in ^{36}Cl	158
5-8	The Cumulative Spectra of Members of Three Step Cascades in ^{36}Cl	158

CHAPTER I

INTRODUCTION

A study of the gamma ray spectrum emitted after neutron capture in nuclei provides information about nuclear binding energies, gamma ray transition probabilities and the level structure of nuclei.

Several review articles concerning the (n,γ) work have been written[Ba 60, Ba 61, Mo 65, Mo 70]. In this chapter a brief description of the (n,γ) reaction and the related topics is presented.

1.1 THE (n,γ) REACTION

When neutrons are incident on a nucleus of mass A, they may undergo potential scattering or form a compound nucleus with mass number A + 1. The energy balance for compound nucleus formation may be written as:

$$M(Z,A) + M_n + E_n = M(Z,A+1) + B_n + E_n \qquad (1.1)$$

where E_n = energy of incident neutron in the center of mass system,

$M(Z,A)$ = mass of the target nucleus,

M_n = mass of neutron,

$M(Z,A+1)$ = mass of the product nucleus in its ground state, and

B_n = binding energy of the last neutron in the product nucleus.

The total excitation energy of the compound nucleus is then the sum of B_n and E_n. For low energy incident neutrons and for nonfissionable nuclei, the highly excited compound nucleus may usually de-excite by emitting a neutron, which leaves the target nucleus in its ground state, or by emitting a photon and leaving the product nucleus in one of its bound states.

The total cross-section for slow neutron interactions in nonfissionable nuclei, for an isolated resonance, is given by,

$$\sigma_T = 4\pi R^2 + \frac{\sigma_o}{1+x^2}\left[\frac{\Gamma_n}{\Gamma} + \frac{2R}{\lambda_0}\,x\right] + \frac{\sigma_o}{1+x^2}\,\frac{\Gamma_\gamma}{\Gamma}\,\sqrt{\frac{E_o}{E_n}} \qquad (1.2)$$

where $\sigma_o = 4\pi\,\lambda_o^2\,g\,\Gamma_n/\Gamma$,

$x = 2(E_n - E_o)/\Gamma$,

Γ = total width of the resonance,

Γ_γ = radiation width,

Γ_n = neutron width,

R = effective radius of the target nuclei for neutrons,

E_o = neutron energy at resonance,

λ_o = wavelength of neutron at resonance,

$g = (2J+1)/2(2I+1)$

J = spin of the resoance, and

I = spin of the target nucleus.

In equation (1.2) the first term gives the cross-section for potential scattering. The second term is the resonance scattering cross-section and includes the part arising from coherent interference between potential and resonance scattering. The third term gives the resonance capture cross-section.

In equation (1.2) it has been assumed that only s-wave neutrons may interact with an appreciable cross-section. This is a safe assumption in the case of thermal neutrons. Assuming that the s-wave and p-wave scattering strength functions are equal, the ratio of the average p-wave total cross-section to the average s-wave total cross-section for slow neutrons is given by:

$$\frac{\sigma_T(l=1)}{\sigma_T(l=0)} = 3(kR)^2$$

where k is the wave vector of the incident neutron. For thermal neutrons and R = 5 fermis, this ratio is found to be $\sim 10^{-8}$ and p-wave capture may be neglected.

When the compound nucleus de-excites by emitting one or more gamma quanta to reach the ground state of the product nucleus, all the excitation energy is radiated except for a small nuclear recoil component. An estimate of the reaction energy is then the sum of the gamma ray transition energies for a set of m transitions forming a cascade from the capture state to the ground state of the product nucleus.

Therefore one may write

$$Q = \sum_m \left[E_{\gamma_m} + \frac{E_{\gamma_m}^2}{2M(Z,A+1)c^2} \right] \qquad (1.3)$$

where E_{γ_m} is the observed energy of the mth member of the cascade and the second term on the right hand side is the correction for nuclear recoil. In the case of thermal neutron capture, the reaction energy, Q, is equal to the binding energy of the last neutron, because E_n is very small compared to Q, and may be neglected.

After s-wave neutron capture, the compound nucleus may be formed with spin I-1/2 or I + 1/2, where I is the spin of the target nucleus. If the thermal neutron capture cross-section is dominated by a resonance then the spin of the compound nucleus would correspond to that of the resonance. If this is not the case, then the compound nucleus may be formed with either spin value with relative probabilities determined by the shape and proximity of resonances with the two possible spins.

Under certain conditions the (n,γ) reaction may proceed without the formation of a compound nucleus. In the process, usually termed direct capture, the nucleus undergoes a radiative transition before the captured neutron has shared its energy with the target nucleons. The conditions under which direct capture can be generally comparable on importance to compound nucleus formation are:

a. that capture takes place in regions for from resonances in nuclei where levels are widely spaced, and

b. that gamma ray transitions are allowed to relatively pure single particle states in the product nucleus.

Usually a correlation between the intensities of neutron capture gamma rays and proton groups from the (d,p) reaction for the same final states is considered to be an indication of the direct capture process since the (d,p) reaction is believed to be a mainly direct process (Bo 59).

1.2 Radiation Widths

The measurements of the total radiation widths, Γ_γ have indicated that these do not vary too much from nucleus to nucleus or from resonance to resonance. This is understandable because the capture state possesses a large number of possible decay channels so that the total radiation width represents a kind of average over individual lifetimes.

The total radiation width is the sum of partial radiation widths for all available bound states in the product nucleus.

$$\Gamma_\gamma = \sum_i \Gamma_{\gamma_i} = \sum_i f_i \Gamma_\gamma \qquad (1.4)$$

where f_i is the fractional intensity of the transition from the capture state to the ith bound state expressed as the number of photons per capture. Since the transition intensities are

usually expressed as number of photons per hundred captures, one may rewrite the above expression as

$$\Gamma_\gamma = \sum_i I_i \quad \Gamma_\gamma \times 10^{-2}, \text{ and} \tag{1.5}$$

$$\Gamma_{\gamma_i} = I_i \, \Gamma_\gamma \times 10^{-2}. \tag{1.6}$$

where I_i is the percent intensity.

The use of first-order time-dependent perturbation theory gives the partial width, $\Gamma_\gamma(i,f)$, for a gamma transition from state i to state f as

$$\Gamma_\gamma(i,f) = \frac{2\pi}{\hbar} | \langle f|0|i\rangle |^2 \rho_f \tag{1.7}$$

where ρ_f is the density of final states associated with the emitted photon and $\langle f|0|i\rangle$ is the matrix element of the interaction Hamiltonian 0. Unfortunately, the nuclear wave functions are not known exactly, and one has to assume a model set of wave functions to evaluate the form of the matrix element.

The change in parity and angular momentum caused by a radiative transition are characterized by the nature and the multipole order of the transition. If L is the angular momentum removed by the radiation, then conservation of angular momentum gives:

$$|J_i - J_f| < L < (J_i + J_f) \tag{1.8}$$

where J_i and J_f are the spins of the initial and the final states. The parity change, $\Delta\pi$, is given by,

$$\Delta\pi = (-)^{L} \text{ for electric, and}$$

$$\Delta\pi = (-)^{L+1} \text{ for magnetic transitions.}$$

The estimates of transition probabilities for electric and magnetic transitions have been obtained by Weisskopf (We 51) using the extreme one particle model. These are given by:

$$\tau_\gamma^{-1}\,(E1) = \frac{4.4(L+1)}{L\left|(2L+1)!!\right|^2}\left(\frac{3}{L+3}\right)^2\left(\frac{E_\gamma}{197}\right)^{2L+1} R^{2L} \times 10^{21}\ \text{sec}^{-1}$$

and

$$\tau_\gamma^{-1}\,(M1) = \frac{1.9(L+1)}{L\left|(2L+1)!!\right|^2}\left(\frac{3}{L+3}\right)^2\left(\frac{\gamma}{197}\right)^{2L+1} R^{2L-2} \times 10^{21}\ \text{sec}^{-1}$$

where τ_γ is the mean lifetime, related to Γ_γ by $\tau_\gamma\Gamma_\gamma = \bar{h}$. In the above expressions E and M stand for electric and magnetic radiation, L is the multipalarity E_γ the energy of the transition expressed in MeV, and R the nuclear radius expressed in fermis. A reasonable approximation for the nuclear radius is

$$R = r_o\, A^{1/3}$$

where r_o is a constant and A the mass number of the nucleus.

Since the transition probability decreases rapidly with increasing multipolarity, it can usually be safely assumed that all primary transitions observed in the (n,γ) reaction are dipole in character because there are a large number of bound states available for the transitions to proceed from the capture state.

An evaluation of the Weisskopf expressions for dipole transition probabilities, using a value of 1.2 fermis for r_o, gives the results (Sk 66).

$$\Gamma_W(E1) = 6.75 \times 10^{-2} A^{2/3} E_\gamma^3 \text{ eV} \qquad (1.9)$$

and

$$\Gamma_W(M1) = 2.07 \times 10^{-2} E_\gamma^3 \text{ eV} \qquad (1.10)$$

where E_γ is expressed in MeV.

The Weisskopf estimates for magnetic multipole transitions are obtained by assuming that the square of the matrix element for magnetic transitions is $10(\hbar/McR)^2$ times the square of the matrix element for the electric transition, where c is the velocity of light. This is a rather crude approximation and in particular one would expect this factor to depend upon L. Moszkowski (Mo 55) has replaced the factor 10 by

$$\frac{L+3}{L+2} \left(\mu_p L - \frac{L}{L+1}\right)^2$$

where μ_p is the intrinsic magnetic moment of proton expressed in nuclear magnetons. While for higher magnetic multipole transitions this modification increases the speed considerably, it is found that for M1 radiation

$$\Gamma_M(M1) = 0.93\ \Gamma_W(M1).$$

Thus, this refinement does not produce any appreciable change in the radiation width for magnetic dipole transitions.

A modification proposed by Wilkinson[Wi 60] for the Weisskopf estimates for electric multipole transitions is the inclusion of the so-called "effective charge factor". This arises due to the finite mass and charge of the nucleus. If the nucleus has mass A and charge Z and a proton is radiating, then the other Z-1 protons radiate in opposition to the radiating proton and their accleration is A-1 times smaller. Then for E1 transitions, the total radiation is, roughly,

$$(1-Z/A)^2 \Gamma_W \approx 1/4\Gamma_W$$

Similarly, for transitions involving neutrons, the radiation is due to the charges on the rest of the nucleus which is of the order $(Z/A)^2\Gamma_W \approx 1/4\Gamma_W$.

For highly excited states in nuclei the level spacings are much smaller and we should expect configuration mixing to take place and transitions to be correspondingly discouraged. Thus, for transitions from highly excited states, one would expect radiation widths to be smaller by a factor D/D_o[Bl 52] where D is the average spacing between levels with the same spin and parity as the radiating state near the excitation energy and D_o is some characteristic single particle level spacing. Wilkinson[Wi 60], while examining then current (n,γ) data recommended 3 MeV and 10 MeV values to be used for D_o when treating E1 and M1 radiation respectively. The expected partial radiation widths may then be obtained in terms of

Weisskopf estimates as:

$$\Gamma_{\gamma\rho}(\mathrm{E1}) = \frac{1}{4}\,\Gamma_W(\mathrm{E1})\,\frac{D}{D_o} \qquad \text{eV} \qquad (1.11)$$

and

$$\Gamma_{\gamma\rho}(\mathrm{M1}) = \Gamma_W(\mathrm{M1})\,\frac{D}{D_o} \qquad \text{eV} \qquad (1.12)$$

where D and D_o are in same units.

The observed partial radiation widths are widely distributed quantities (Po 56) and to compare these with the predicted values one must average over a large sample. In practice it is difficult to get a large enough sample and the uncertainties in the values of average partial radiation widths are high. Before taking the average the energy dependence must be removed. We may define a quantity, the transition strength, as the ratio of the observed to the expected partial radiation width. Then, we can write for the average transition strengths.for E1 and M1 radiation,

$$T(\mathrm{E1}) = \frac{\langle\Gamma_{\gamma i}\rangle_{\mathrm{E1}}}{\Gamma_{\gamma\rho}(\mathrm{E1})}$$

$$T(\mathrm{M1}) = \frac{\langle\Gamma_{\gamma i}\rangle_{\mathrm{M1}}}{\Gamma_{\gamma\rho}(\mathrm{M1})}$$

where the pointed brackets indicate that an average has been taken. Substituting for $\Gamma_{\gamma i}$ and $\Gamma_{\gamma\rho}$, we obtain

$$T(\mathrm{E1}) = 0.59\langle I/E^3\rangle_{\mathrm{E1}}\,\frac{\Gamma_\gamma\, D_o}{A^{2/3} D} \qquad (1.13)$$

$$T(\mathrm{M1}) = 0.48\,\langle I/E^3\rangle_{\mathrm{M1}}\,\frac{\Gamma_\gamma\, D_o}{D} \qquad (1.14)$$

where the quantity $\langle I/E^3 \rangle$ is in %/MeV^3, Γ_γ is in eV and D and D_o are expressed in the same units.

Another approach to the problem of electric dipole transitions is to make use of the giant dipole resonance observed in photonuclear reaction. This possibility has been investigated by Axel (Ax 62) who used the Lorentz line shape and the relation between the photonuclear absorption cross-section and the average width for the ground state transition, $\langle \Gamma_{\gamma o} \rangle$, to obtain the approximate relationships,

$$\langle \Gamma_{\gamma o} \rangle / D = K_1 \, E^5 \, A^{8/3} \qquad \text{for } E \approx 7 \text{ MeV}, \qquad (1.15)$$

$$\langle \Gamma_{\gamma o} \rangle / D = K_2 \, E^4 \, A^{7/3} \qquad \text{for } E \leq 3 \text{ MeV} \qquad (1.16)$$

where K_1 and K_2 are constants which may be evaluated by using the parameters of the giant dipole resonance. In deriving the above relationships an $A^{-1/3}$ dependence has been used for the energy of the dipole giant resonance.

The energy dependence obtained in the above relationships refers to ground state transitions from different initial states, whereas the (n,γ) data yield information about transitions from a fixed initial state to different final states. However, it has been argued by Bollinger and Thomas (Bo 67) that if it is assumed that the excited states in nuclei have their own giant resonances (similar to the ground state giant resonance but shifted towards higher energy by an amount equal to the energy of the excited state) then the energy dependence of radiation widths will depend only upon the gamma ray

energy, regardless of whether it is the initial or the final state that is varying in energy. The evidence for the existence of a giant resonance for the first excited state in ^{12}C has been obtained by Allas et al (Al 64) from their study of the radiative capture of protons in ^{11}B. If one assumes this to be true for all excited states of all nuclei, then equations (1.11) and (1.12) yield the average radiation widths for their respective energy ranges, independent of the position of initial and final states.

1.3 Porter-Thomas Distribution

It has been shown by Porter and Thomas (Po 56) that the correct probability density function for nuclear reaction widths is one of the family of chi-squared distributions. These functions can be represented by the relationship,

$$P_\nu(x) = \frac{(\nu/2)}{\Gamma(\nu/2)} \left(\frac{\nu x}{2\bar{x}}\right)^{\frac{\nu}{2}-1} \exp\left(-\frac{\nu x}{2\bar{x}}\right) \qquad (1.17)$$

where ν is a parameter referred to as the number of degrees of freedom, x is the reduced width and $\bar{x}$ the mean reduced width. They have also shown that in the case of a single-channel process in a compound nuclear reaction, the distribution is expected to be characterized by one degree of freedom.

A simple argument given by Carpenter (Ca 62) showing that the partial radiation widths are expected to follow a chi-squared distribution is presented here. Since the compound nucleus is a highly excited system, it is expected that the

wave function describing the state would be extremely complicated. To get the matrix element $\langle f|0|i\rangle$, one has to integrate over the configuration space. Let us assumes that the configuration space can be broken into small cells which are small enough that there are a large number of such cells in the configuration space but large enough that the integrand changes its sign several times within each cell. In this case it is possible for each cell to make a positive or a negative contribution to the matrix element, independant of other cells. The use of the "central limit" theorem then assures that the sums of these contributions (matrix elements for different final states) will follow a normal distribution with zero mean. The squares of matrix elements will then be distributed as a chi-squared with one degree of freedom.

In the absence of a dominating resonance, the thermal neutron capture reaction is no longer a single channel process and one cannot always expect a $\nu = 1$ distribution for partial radiation widths. It has recently been shown by Bollinger (Bo 71a) that $\nu = 1$ is still the expected result, irrespective of the number of resonances that are contributing, as long as only one spin state is involved. This is based upon the assumption that $D^2/\Gamma_r^2 >> 1$ (where D is the average level spacing and Γ_r the total width of rth resonance) which is true for most nuclei. Thus, for nuclei with target spin zero the partial radiation widths are expected to have a distribution characterized by one degree of freedom. However, if both spin states

contribute to the thermal capture cross -section, then the distribution would be a chi-squared with a value of ν lying between 1 and 2 depending upon the relative magnitude of the two components.

1.4 NUCLEAR LEVEL DENSITIES

The statistical theory of nuclear level densities has received considerable attention in the past. The treatment of the nucleus as a gas of two types of fermions by Bethe[Be 36,Be37] yields the relationship:

$$\rho(E) \sim \exp \sqrt{aE} \qquad (1.18)$$

where $\rho(E)$ is the level density at excitation energy E and a is a constant. This relationship agrees with experimental findings at high excitation energies but is not applicable at low energies.

It was observed by Ericson[Er 59] that a plot of log N vs. E, where N is the cummulated number of levels up to energy E, could be fitted by a straight line over a few MeV. This gives the relation

$$N = \exp (E-E_o)/T \qquad (1.19)$$

where E_o and T are parameters chosen to fit the data. The parameter T is usually called the nuclear temperature. The level densities show a deviation from this form at high energies where T can no longer be assumed constant.

Gilbert et al[Gi 65, Gi65a] have treated the subject in detail including a discussion of the energy at which the transition from one behaviour to the other occurs.

The spin distribution has been reviewed by Ericson[Er 60] who derived the relationship.

$$\rho(E,J) = \frac{2J+1}{2\sigma_m^2} \exp\left[-(J+1/2)^2/2\sigma_m^2\right] \rho(E) \qquad (1.20)$$

with $$\rho(E) = \sum_J \rho(E,J)$$

In this equation, σ_m is a spin dependence parameter and J is the angular momentum. This relationship is based on the random coupling of the angular momenta and is essentially model-independent.

1.5 Spectral Features

The complexity of the gamma ray spectra after thermal neutron capture increases with the mass number since the number of available energy levels below the nuetron separation energy becomes larger. Also, the spectra of odd-odd nuclei are more complicated then those of neighboring even-even or even-odd nuclei. This is, again, due to the higher level density in odd-odd nuclei.

If the level density is high enough, then one can calculate the gross shape of the expected gamma ray spectrum after thermal neutron capture from statistical considerations. To calculate the primary gamma ray spectrum, one needs to know the energy dependence of the transition probability and the

level density. To a first approximation one may treat the E1 and M1 radiation as a single class of transitions, since the two have the same energy dependence and the amplitudes are highly distributed anyway. Then, using the appropriate form of the level density, one can write,

$$S(E)dE = CE^3 \rho(Q-E)\ dE \qquad (1.21)$$

for the primary spectrum in the energy interval dE. Here C is a constant which may be evaluated by integrating the above expression from 0 to Q and normalizing to 100%. A comparison of the calculated spectrum with the experimentally observed primary spectrum, will then allow one to test the energy dependence of the transition probability and the level density formulation. The prime requirement for any meaningful inference to be obtained is that the primary transition density is high enough that the uncertainties introduced by the wide distribution of individual radiation widths are low. Unfortunately, this condition is not usually met in light nuclei and for heavier nuclei where the level densities are high enough, one is usually unable to make a significant analysis of the observed spectrum.

A quantity which has received some attention in the past is the multiplicity, or the average number of gamma rays emitted per neutron capture, defined by

$$M = \frac{\Sigma I_i}{100} \qquad (1.22)$$

where the intensities are in percent and the summation extends over all transitions. Once the absolute intensities are calculated, the multiplicity may be easily obtained and a knowledge of the decay scheme is not required.

The multiplicity is actually a weighted sum of the intensities associated with the different cascade orders in the decay of the compound nucleus. The latter quantities could prove more useful in formulating a cascade model for the decay of the compound nucleus but are more difficult to obtain because they require a knowledge of the decay scheme.

This subject will be treated in more detail in Chapter V.

1.6 Absolute Intensities

It is difficult to directly measure the absolute intensities of gamma rays because the finite sizes of targets introduce effects such as self-shielding, self absorption and complicated solid angles. However, relative intensities may be obtained readily once the relative efficiency of the spectrometer system has been determined.

The relative intensities of the observed gamma rays may be put on an absolute scale by requiring that the sum of the intensities of all primary transitions equal 100 per cent.

$$\sum_i I_{pi} = 100\% \qquad (1.23)$$

This process of normalization, however, requires a knowledge of the decay scheme.

Since the reaction energy, Q, is released once per neutron capture, it follows that,

$$\frac{\sum_i E_i I_i}{Q} = 100\% \qquad (1.24)$$

where the summation extends over all transitions. This provides an alternate procedure for the normalization of intensities with the condition that all the components in the gamma ray spectrum have been identified but not accounted for in the decay scheme.

In some cases, the product nuclei are themselves unstable and beta-decay with subsequent gamma ray emission. A measurement of the intensity of such a transition in the daughter nucleus may provide yet another method of normalization of intensities. This process is sufficiently accurate only when:

a. the half-life of the product nucleus is not too long,

b. the energy of the transition in the daughter nucleus lies in the region where the relative efficiency calibration of the spectrometer system is reliable, and

c. in the case of branching, the percent yield of of the transition is accurately known.

CHAPTER II

EXPERIMENTAL DETAILS

A brief description of the experimental facility is presented in this chapter along with a summary of the procedure used for the extraction of energies and intensities of gamma rays from the observed spectra.

2.1 THE TANGENTIAL IRRADIATION FACILITY

The experiments were performed at the McMaster Nuclear Reactor using the Tangential Irradiation Facility which has been described by Nichol et al (Ni 70). It has since been modified to allow sample changing during reactor operation. A brief account of this will be given.

The layout of the facility is shown in Fig. 2-1. It consists of an evacuated aluminum target chamber, an in-pool collimator and an external collimator. The target chamber consists of an aluminum tube approximately 2 m long and having an out diameter of 7.6 cm. The tube can be placed in the pool on "V" shaped supports and secured in position by lead weights attached to both ends. Initially, the tube was lowered in the pool with the help of stranded stainless steel aircraft cables attached to each end and was evacuated by a 1/4" diameter aluminum tube, attached to the flange at the rear end, extending to the surface of the pool. In this setup, the reactor had to be shutdown and the core moved to allow the target chamber

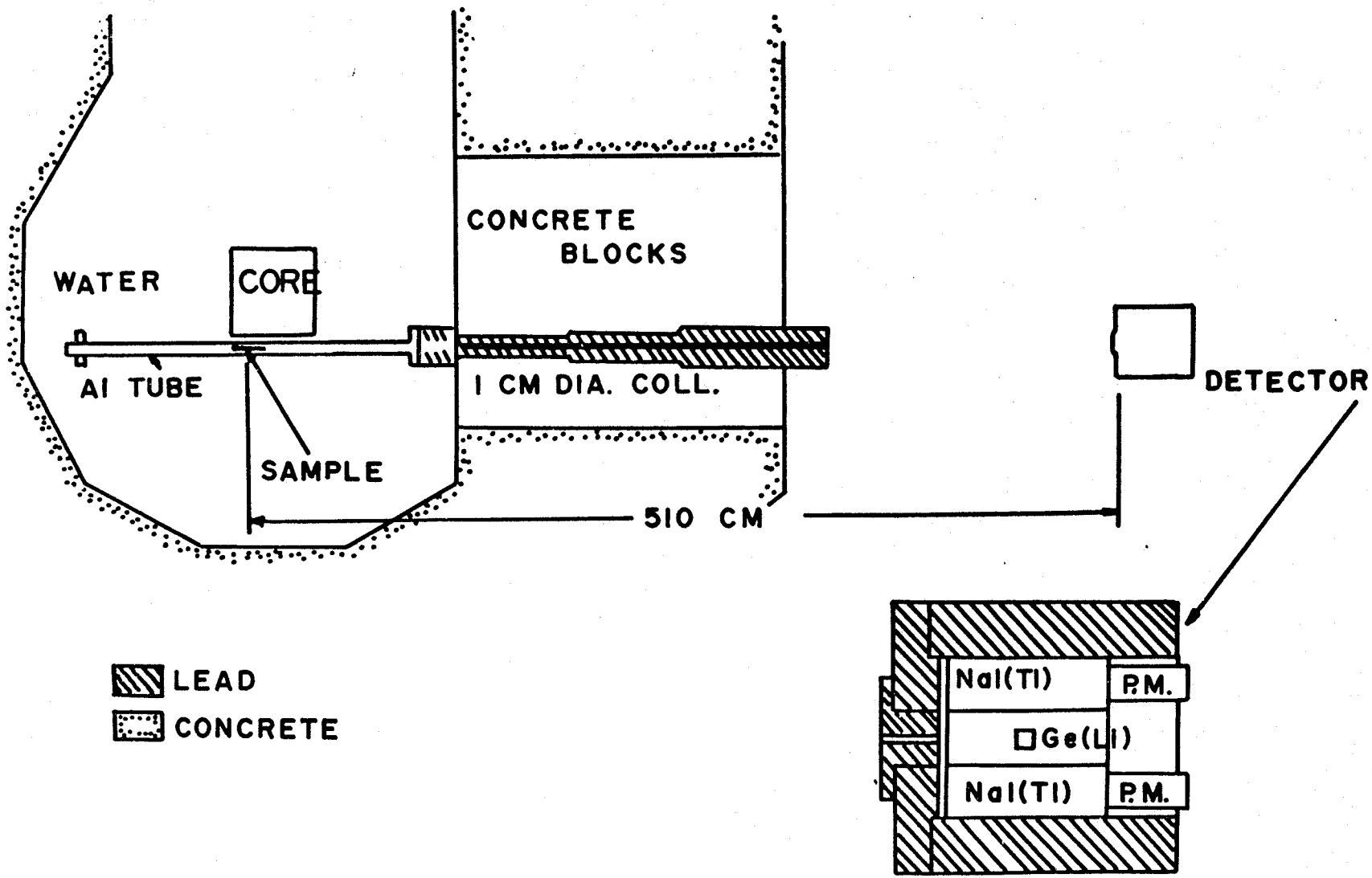

Fig. 2-1 The layout of the tangential irradiation facility.

tube to be removed which made target changing a rather tedious operation. To allow target changing during reactor operation a "T" shaped extension was made to the target chamber at the target position which connected to a chamber at the surface of the pool via PVC tubing. This allows one to lower a sample through the PVC tubing into the target chamber. A target seat in the target chamber allows accurate positioning of the sample usually dispatched in a properly shaped graphite container (see Fig. 2-2). The chamber at the surface of the pool has an auxiliary extension tube (extending four feet under water) for the storage of hot samples pulled out from irradiation position. The whole system can be sealed and either evacuated during normal counting or pressurized with nitrogen for mixed source calibration.

The internal collimator consists of a 15 cm diameter, 23 cm long lead annulus with an aperture of 3 cm. To remove thermal neutrons from the beam, discs of ^{6}LiF packed in aluminum containers are situated at each end of the collimator.

The external collimator is located in the thermal column vault which is isolated from the pool by a 25 cm thick aluminum plate. A small region of this plate was thinned down to 0.6 cm to allow the gamma ray beam to pass without much loss. The external collimator is 190 cm long having an aperture of 1 cm. The stepped square shaped aluminum collimator is filled with a mixture of lead and polyethylene shot.

The thermal neutron flux at target position is of the order of 10^{13} neutrons/cm^2/sec.

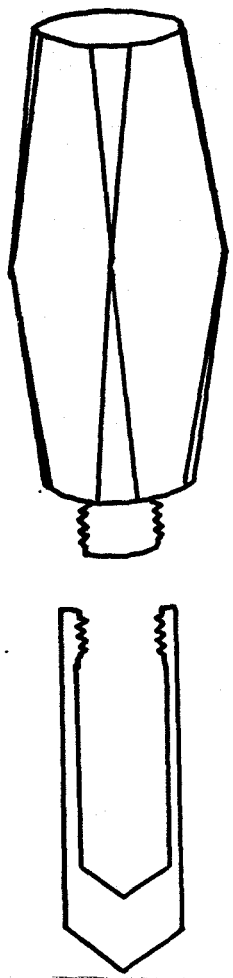

Fig. 2-2 The thru tube sample holder/carrier.

2.2 THE Ge(Li) PAIR SPECTROMETER

While Ge(Li) detectors have very good energy resolution they still suffer from the disadvantage of a complicated response function. The incident gamma ray photon may interact within the detector by one or more of the following processes:

a. Photoelectric effect

b. Compton scattering

c. Pair production.

The pair production event is possible only if the photon energy is higher than 1022 keV. In this case the photon produces a positron-electron pair with the rest of the photon energy transferred as the kinetic energy of the pair. When the positron comes to rest after losing its energy through collisions, it annihilates with another electron. This process usually releases two annihilation photons (511 keV) at 180^{o} to each other. If one of the annihalation photons escapes the detector without interacting then the energy absorbed by the detector is $E\gamma-M_{o}c^{2}$, where $E\gamma$ is the incident gamma ray energy and M_{o} is the rest mass of an electron. If both annihilation quanta escape undetected then the energy recorded is $E\gamma-2M_{o}c^{2}$, and the events may be called double escape events. This gives rise to single and double escape peaks. The total response then consists of photo, single escape and double escape peaks over a Compton background. This response is not only complicated

and redundant, but the single and double escape peaks interfere with other photopeaks.

The response of the Ge(Li) detector can be very much simplified by using it in a pair spectrometer mode, i.e. only looking at the double escape events. This can be achieved by surrounding the detector with a NaI annulus and identifying double escape events by the detection of two annihilation photons. The strong directional correlation of annihilation quanta makes this process highly efficient.

The Ge(Li) detectors used were 15-20 cc active volume devices fabricated here using the techniques reported by Fiedler et al[Fi66]. A NaI annulus 23 cm in diameter and 15 cm long, which is optically divided into quadrants, surrounded the Ge(Li) detector. The double escape events were identified by the detection of 511 keV annihilation photons in the diametrically opposite quadrants of the NaI annulus.

Ideally, the response of the pair spectrometer to monochromatic gamma radiation of energy E_γ would be a peak (a delta function folded in with the detector resolution) at energy $E_\gamma - 2M_oc^2$. Actually, however, the response consists of the peak at $E_\gamma - 2M_oc^2$, a continuous distribution below this energy and a tail on the high energy side. The continuous distribution is mainly due to energy loss caused by escaping bremmstrahlung radiation emitted by the electrons slowing down in the detector and by electrons leaving the

active volume of the detector. It could also be caused by the radiation reaching the detector after (single or multiple) scattering in the collimator. The high energy tail is produced by the deposition of small amount of energy by escaping annihilation quanta. Because of the poor resolution of NaI detector, the window setting for the identification of annihilation quanta has to be made wide enough and a small loss in energy cannot be easily sensed. The process of random adding could also contribute to the tail on the high energy side of the peak.

The observed spectrum after thermal neutron capture in melamine is shown in Fig. 2-3. The main background contributions, in this and other spectra, are the 4440 keV peak from ^{12}C, 3684 and 4946 keV from ^{13}C, 2223 keV from ^{2}H and 7724 keV line from ^{28}Al.

2.3 THE DATA ACQUISITION SYSTEM

The block diagram of the data acquisition system is shown in Fig. 2-4. A Nuclear Data (ND 3300) pulse height analyzer equipped with a 12 bit, 30 MHz analog-to-digital converter (ADC) is used to accumulate the spectra.

The signals from the Ge(Li) detector, mixed with the output of a dual reference precision pulser are amplified using a Tennelac (TC 135) preamplifier and a Tennelac (TC 200) amplifier and fed in the analyzer ADC through an adjustable delay circuit.

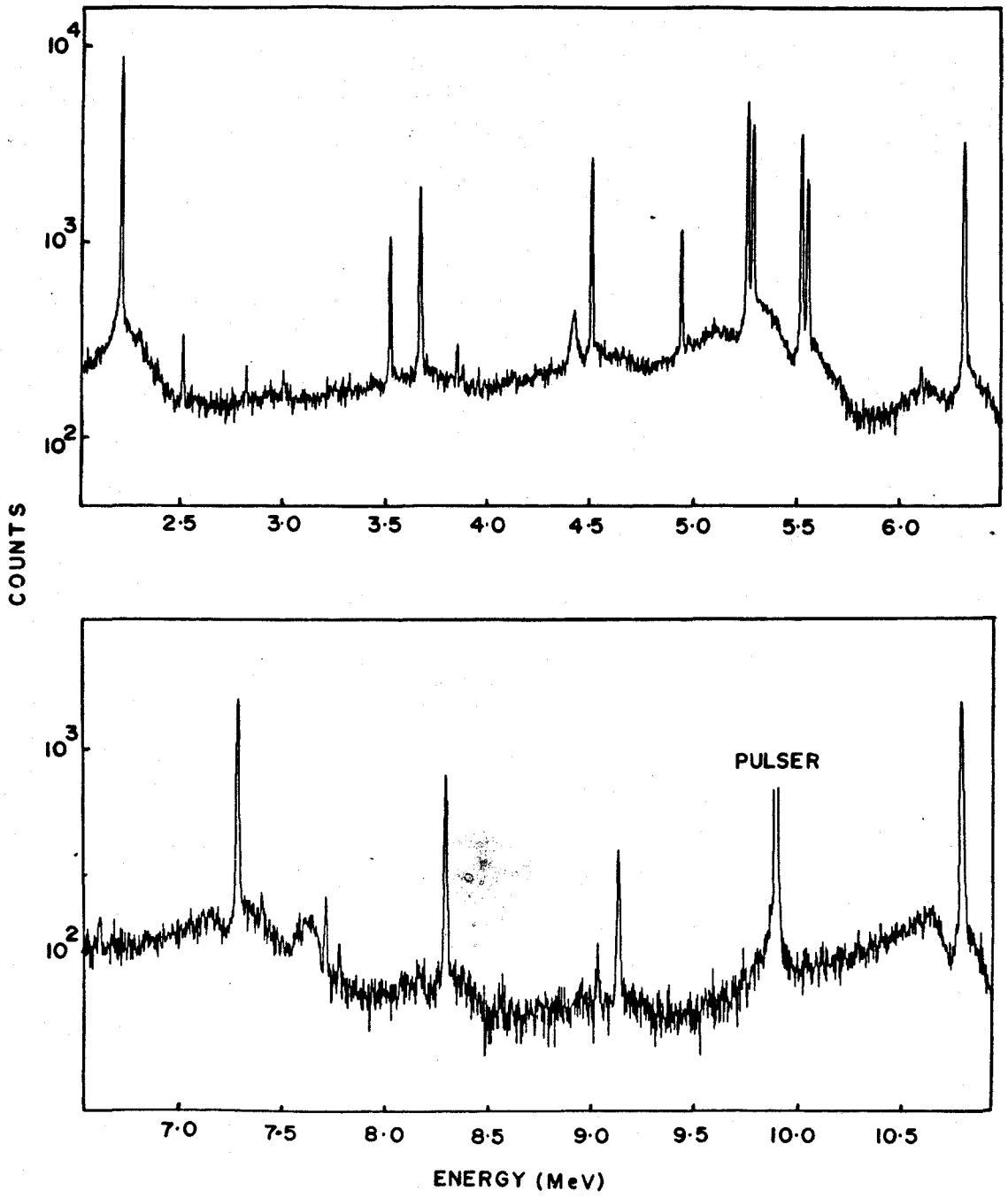

Fig. 2-3 The capture gamma ray spectrum of melamine.

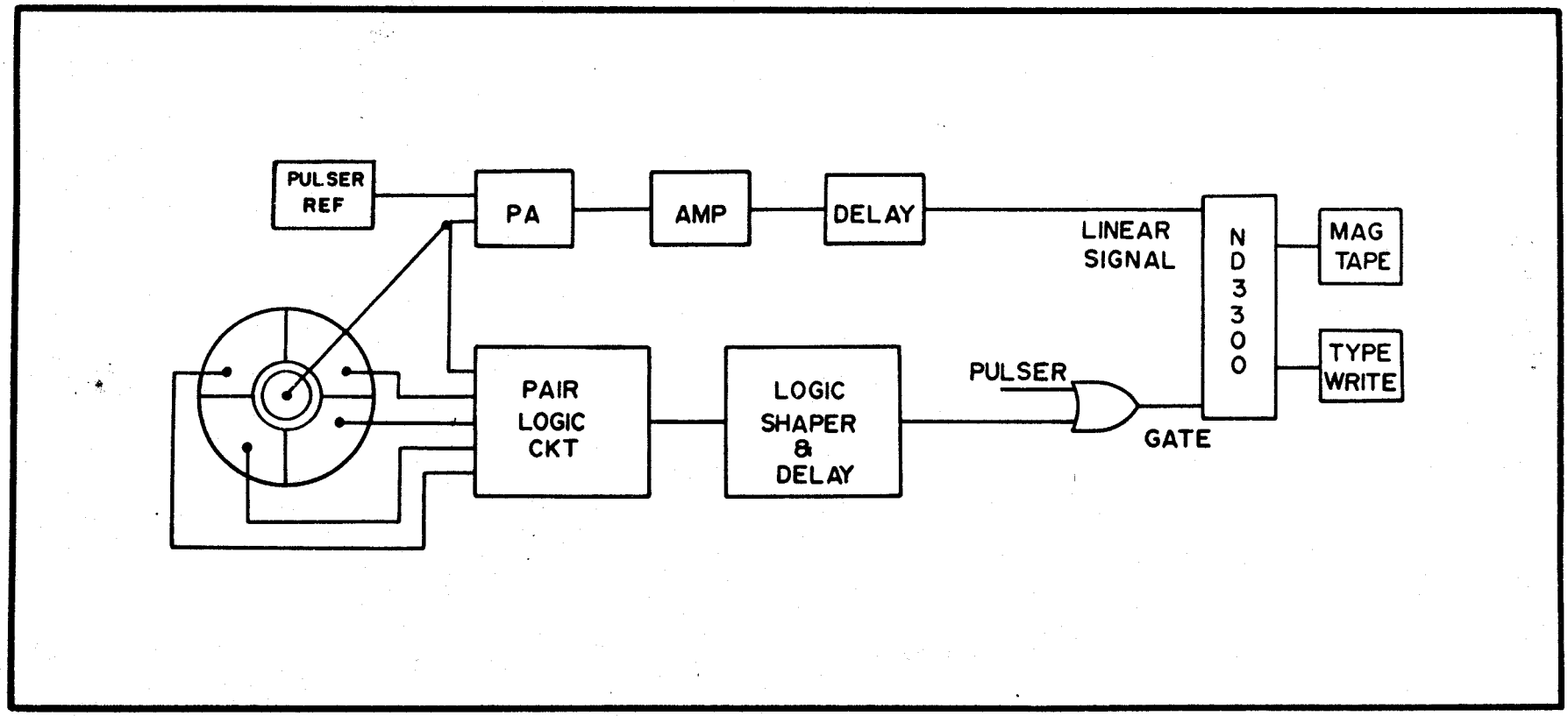

Fig. 2-4 Block diagram of the data acquisition system.

The gate pulse is generated, using integrated circuits, in the pair logic circuit module which replaces the conventional timing single channel analyzers and coincidence units. This module consists of a pair of comparators (used as upper and lower level discriminators) for each NaI channel and NAND gates used to satisfy the triple coincidence conditions.

A ^{22}Na source was used to set up the energy windows and time delays for obtaining optimum coincidence rates from each pair of diametrically opposite quadrants.

To stabilize the spectrum against gain or zero shifts, Nuclear Data digital spectrum stabilizers are used. The two outputs from the precision reference pulser are used for this stabilization.

2.4 ENERGY MEASUREMENTS

The analysis of the gamma ray spectra yield the channel numbers corresponding to peak centroids which may be converted into energies by a calibration of the system using known standards. However, an accurate measurement of energies requires a knowledge of the functional dependence of energy on channel number. In the ideal case, i.e. for a perfectly linear system, the relationship is

$$E = gC + z$$

where E is the energy, C the channel number, g the gain and z is the energy corresponding to channel zero. In the

practical systems, however, small non-linearities are present and the above relationship tends to be inaccurate. An examination of the differential linearity of the present system [Ly 68, Ly69] suggested a relationship of the form

$$\frac{\Delta E}{\Delta C} = g + 2nC$$

which upon integration yields

$$E = nC^2 + gC + z \qquad (2.1)$$

where n is the coefficient of the non-linear term.

In the work, gamma rays from thermal neutron capture in nitrogen are used as energy standards the calibration energy values employed are those due to Marion[Ma 68]. The background lines from neutron capture in carbon and hydrogen, present in all spectra, supplement the calibration where necessary. The calibration energies used are listed in Table 2-1. The energies of intense lines in each spectrum studied are obtained using a mixed source technique. The energies of the weaker components are then calculated by reference to the calibrated transitions within the spectrum. In each case, the energy scale is established by making a least squares fit to the calibration points to evaluate the three parameters in equation (2.1).

The main sources of error in the energy measurements are the uncertainty in the location of peak centroid and

TABLE 2-1

Energies of Calibration Standards

Reaction	Energy (keV)	Error (keV)	Reference
$^{1}H(n,\gamma)^{2}H$	2223.29	0.06	Pr 65
$^{12}C(n,\gamma)^{13}C$	3683.94	0.17	Pr 67
	4945.46	0.17	
$^{14}N(n,\gamma)^{15}N$	1884.6	0.2	Ma 68
	2519.9	0.5	
	3532.1	0.2	
	3677.7	0.2	
	4508.8	0.3	
	5268.5	0.2	
	5297.4	0.3	
	5533.0	0.3	
	5562.0	0.3	
	6322.1	0.4	
	7298.7	0.4	
	8310.3	0.7	
	9150.0	0.8	
	10829.2	0.4	

the error in the calibration energies. The peak centroids were obtained by inspection of the spectrum plotted on a linear scale. It was observed that centroids of isolated intense peaks could be obtained to an accuracy of a tenth of a channel. This was ascertained by testing the consistency in centroid locations in spectra recorded at same amplifier gain and by an examination of the shift in centroid as a function of channel number in two spectra accumulated at slightly different gains. The less intense transitions, peaks riding on high backgrounds and complex lines were assigned higher errors accordingly. The uncertainty in the energy scale at any point was estimated to be 0.5 keV. This estimate was arrived at by looking at the qouted errors associated with the individual calibration energies and the uncertainty involved in the location of centroids of calibration peaks. The variance in the measured energies was finally calculated by using the relation

$$\sigma^2(E) = (g\ \Delta C)^2 + 0.25\ \text{keV}^2 \qquad (2.2)$$

where ΔC is the error in the centroid location and g is the gain in keV/channel.

After the construction of a decay scheme, the capture gamma ray spectra provide much better possibilities of consistency tests than for example gamma ray spectra after beta decay. If several pairs of transitions can be identified

as two step cascades from capture to ground states then a study of the dispersion in their sums (corrected for nuclear recoil) allows one to comment on

a. The linearity of the energy scale, and

b. The errors associated with energy measurements.

If the energy scale is incorrect (i.e. the values of parameters in Equation (2.1) are in error) then the sums will show a trend in departure from the mean value as the energy of one member of the pair moves away from the value of half the mean pair sum. The mean of the pair sums which is the Q-value of the reaction can be calculated using the relation

$$Q = \frac{\sum_{i=1}^{n} \{E_n(\text{sum}/\sigma_n^2(\text{sum})\}}{\sum_{i=1}^{n} \{1/\sigma_n^2(\text{sum})\}} \qquad (2.3)$$

where n is the number of pairs and the variance in the pair sum σ_n^2 is the sum of the variances of its members. The variance in Q is given by

$$\sigma_Q^2 = 1/\{\sum_{i=1}^{n} \frac{1}{\sigma_n^2(\text{sum})}\} \qquad (2.4)$$

An analysis of the dispersion in pair sums was carried out for the cases of aluminum and chlorine where a large enough number of such pairs could be identified. No trend in the deviation from the mean could be observed in either case.

2.5 RELATIVE INTENSITY MEASUREMENTS

The Ge(Li) detector used for the study of the $^{27}Al(n,\gamma)^{28}Al$ reaction was calibrated for relative efficiency using the $^{14}N(n,\gamma)^{15}N$ reaction and the intensities of transitions given by Marion[Ma 68]. A different detector was used for the study of the other five nuclei and the efficiency calibration for this detector was carried out using the nitrogen as well as the present aluminum results. Since there are several fairly strong transitions in the aluminum spectrum below 3.5 MeV, its use gives more points on the low energy part of the efficiency curve where the efficiency is changing rather rapidly with energy.

To allow one to calculate the intensities of observed peaks using a computer program, it is desirable to have a functional relationship between energy and relative efficiency. Since it is not possible to obtain a single good fit for the entire energy range, it was decided to divide the energy region into four overlapping intervals and make a least squares fit to the data in each energy interval using the relation

$$\ln(\varepsilon) = a + bE + CE^2 \qquad (2.5)$$

where E is the energy, ε the relative efficiency in arbitrary units and a, b and c are least squares parameters. The relative efficiency of the spectrometer is shown in

Fig. 2-5. The points are the measured relative efficiencies, the solid lines show the least squares fits and the arrows mark the cross-over points from one fit to another in calculating the intensities.

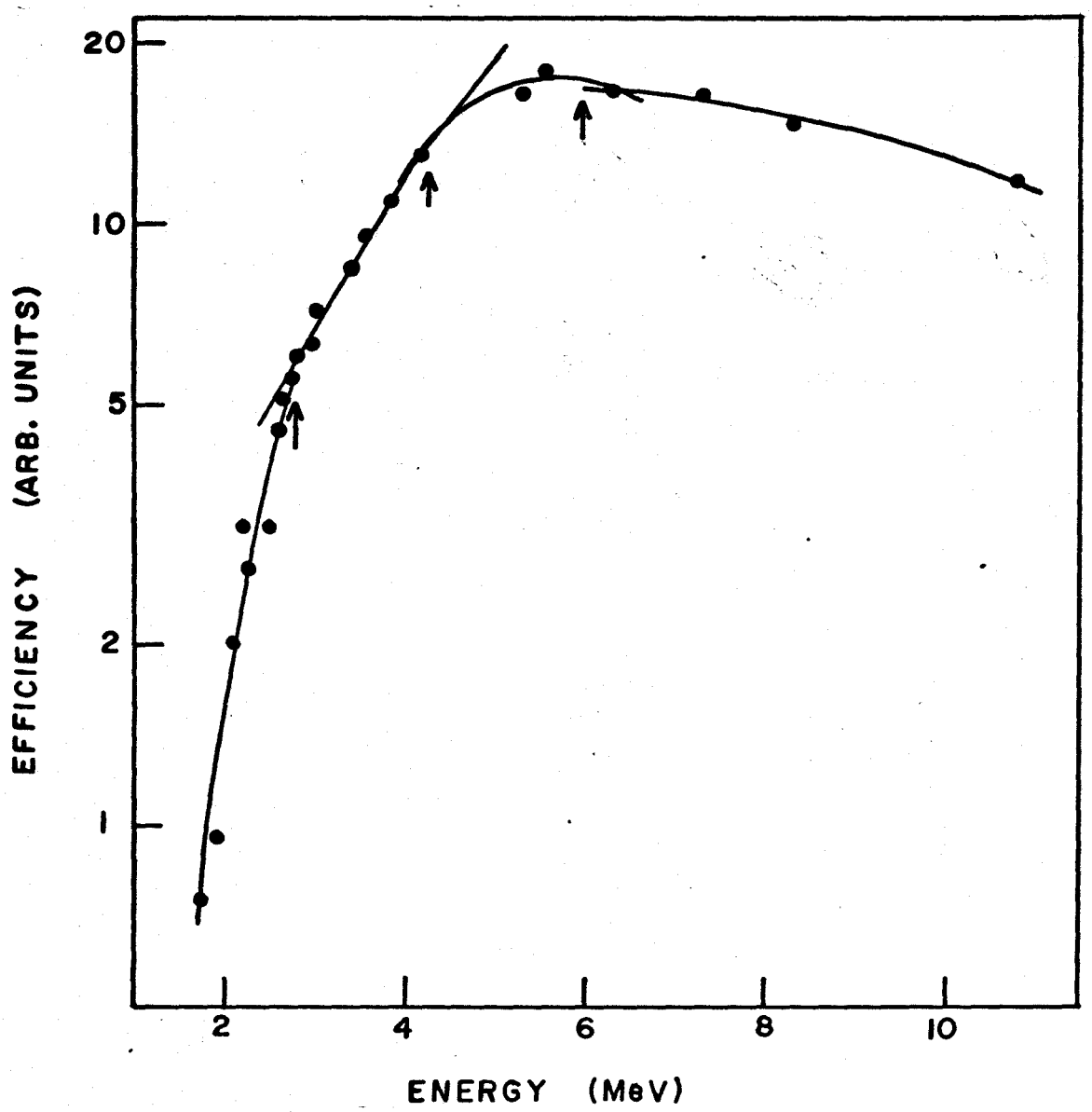

Fig. 2-5 The relative efficiency of the Ge(Li) detector. The points are experimentally obtained efficiencies, the curves are the least squares fits and the arrows mark the cross-overs from one fit to another.

CHAPTER III

THERMAL NEUTRON CAPTURE STUDIES

This chapter deals with the energy and intensity measurements, estimation of Q-values and multiplicities and the construction and discussion of decay shcemes. A brief review of previous related work is also presented for each nucleus studied.

3.1 THE $^{27}Al(n,\gamma)^{28}Al$ REACTION

3.1.1 Review of Previous Work

The (n,γ) reaction on aluminum has been studied by several authors[Ba 67], the two most recent investigations being those of Nichol et al[Ni 69] and Hardell et al[Ha 69]. The complimentary reaction, $^{27}Al(d,p)^{28}Al$, was studied by Buechner et al[Bu 56] who reported levels in ^{28}Al up to the neutron separation energy. Endt and van der Leun[En 67] have collected the data concerning levels in ^{28}Al which were available in 1967. More recently information on the low lying levels of ^{28}Al has been provided by Alburger and Harris Harris[Al 69] from their study of the beta decay of ^{28}Mg. Freeman and Gallmann[Fr 70] have reported a study of the $^{27}Al(d,p\gamma)^{28}Al$ reaction. Boerma and Smith[Bo 71] have studied the properties of levels of ^{28}Al up to an excitation energy of 2.7 MeV by means of the reactions $^{27}Al(d,p\gamma)^{28}Al$, $^{26}Mg(^{3}He, p\gamma)^{28}Al$ and $^{30}Si(d,\alpha\gamma)^{28}Al$. The (d,p) reaction

on aluminum has been recently studied by Carola and van der Baan[Ca 71] using 12 MeV deutrons. They have measured the angular distributions for 41 proton groups and carried out a DWBA analysis to determine the spectroscopic factors. They have also made some new l_n assignments.

3.1.2 Present Work

A 10 g rod of 99.99% pure aluminum served as the target for the present investigation and the total counting time was 170 hours. The principal reaction is thermal neutron capture for which the cross section is reported to be 235 $\pm$ 5 mb[St 64]. The presence of fast neutrons does result in some inelastic scattering which is manifested by a few characteristic gamma rays[Ni 72]. The Doppler broadening associated with this reaction provides a simple method to identify these components in the spectrum.

The observed gamma ray spectrum is shown in Fig. 3-1 and the energies and intensities of the transitions which have been identified, are presented in Table 3-1. All energies have been corrected for recoil losses and most of the transitions have been placed into a decay scheme. Since time-correlation studies were not done, assignments to the decay scheme were made on the basis of energy precision, intensity balance and level information from other reactions. Some assignments are tentative and are so indicated by parantheses.

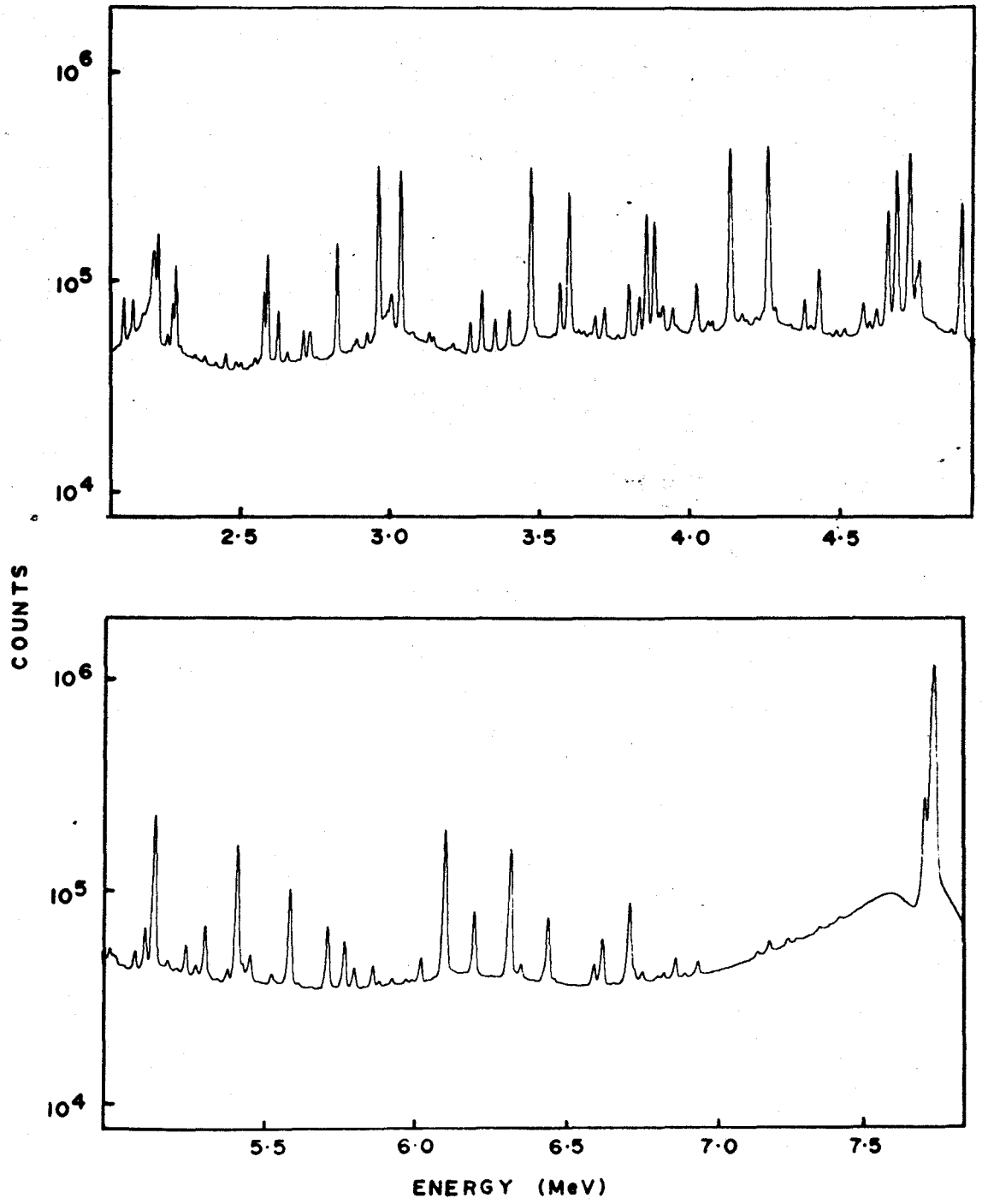

Fig. 3-1 The capture gamma ray spectrum of aluminum.

TABLE 3-1

The Observed Transitions in ^{28}Al

No.	Transition[a] energy (keV)	Error in energy (keV)	Intensity[b] (Photons/100 captures)	Assignment[c]
1	7724.9	0.5	30.5	C → 0
2	7695.3	0.6	4.06	C → 30.6
3	7342.2	0.8	0.06	7342 → 0
4	7269.2	0.9	0.04	7269 → 0
5	7238.7	0.8	0.07	7269 → 30.6
6	7176.2	0.7	0.14	7176 → 0
7	7136.1	0.8	0.05	
8	6937.3	0.7	0.13	6968 → 30.6
9	6893.8	1.1	0.03	6893 → 0
10	6861.8	0.7	0.19	6893 → 30.6
11	6822.4	0.8	0.06	6853 → 30.6
12	6800.9	0.9	0.03	6831 → 30.6
13	6751.9	0.8	0.08	(C → 972 or 6754 → 0)
14	6723.6	0.9	0.10	6754 → 30.6
15	6710.0	0.7	0.97	C → 1014
16	6619.8	0.7	0.44	6620 → 0
17	6590.8	0.7	0.17	6620 → 30.6
18	6460.0	1.1	0.02	
19	6440.0	0.7	0.70	6440 → 0
20	6388.6[d]	1.9	0.01	6419 → 30.6

TABLE 3-1 CONTINUED

No.	Transition[a] energy (keV)	Error in energy (keV)	Intensity[b] (Photons/100 captures)	Assignment[c]
21	6349.9	0.7	0.11	C → 1373
22	6315.6	0.7	2.17	6313 → 0
23	6197.1	0.7	0.73	6197 → 0
24	6101.8	0.5	2.81	C → 1623[e]
25	6018.0	0.8	0.21	6018 → 0
26	5988.3	1.9	0.02	(6018 → 30.6 or 5988 → 0)
27	5969.2	1.9	0.03	7342 → 1373
28	5923.0	0.8	0.05	6893 → 972
29	5879.3	1.1	0.04	6853 → 972
30	5859.8	0.7	0.16	5860 → 0
31	5829.3	1.9	0.01	5860 → 30.6
32	5796.8	0.7	0.15	5797 → 0
33	5765.7	0.6	0.41	(5797 → 30.6 or 5766 → 0)
34	5709.4	0.5	0.58	5740 → 30.6
35	5648.9	1.9	0.01	7269 → 1620
36	5610.9	1.1	0.02	
37	5586.1	0.5	1.17	C → 2139
38	5523.7	1.1	0.07	C → 2202
39	5452.5	0.8	0.22	C → 30.6

TABLE 3-1 CONTINUED

No.	Transition[a] energy (keV)	Error in energy (keV)	Intensity[b] (Photons/100 captures)	Assignment[c]
40	5443.9	1.9	0.11	5442 → 0
41	5424.0	1.4	0.15	6440 → 1014
42	5411.4	0.7	2.20	5442 → 30.6
43	5377.6	1.1	0.11	5378 → 0
44	5343.8	1.9	0.02	5344 → 0
45	5302.4	0.7	0.50	6316 → 1014
46	5238.7	0.9	0.27	C → 2486
47	5202.4	1.9	0.03	7342 → 2139
48	5210.5[d]	1.9	0.03	6831 → 1620
49	5176.7	0.9	0.08	5177 → 0
50	5134.4	0.5	3.16	5.34 → 0
51	5104.1	0.7	0.43	5134 → 30.6
52	5069.3	0.8	0.16	C → 2657
53	5005.4	1.1	0.05	6018 → 1014
54	4997.0	0.9	0.08	4997 → 0
55	4984.9	0.8	0.11	5016 → 30.6
56	4903.0	0.5	3.15	4903 → 0
57	4868.8	1.1	0.05	
58	4764.8	0.8	1.05	4765 → 0
59	4755.2	1.1	0.60	

TABLE 3-1 CONTINUED

No.	Transition[a] energy (keV)	Error in energy (keV)	Intensity[b] (Photons/100 captures)	Assignment[c]
60	4734.3	0.5	5.95	4765 → 30.6
61	4690.9	0.5	4.82	4691 → 0
62	4660.0	0.5	2.76	4691 → 30.6
63	4620.5	0.8	0.26	C → 3105
64	4596.5	0.9	0.10	4596 → 0
65	4575.9	0.9	0.36	6197 → 1623
66	4512.4	1.1	0.12	4512 → 0[g]
67	4485.3	1.1	0.06	5860 → 1373
68	4427.7	0.7	1.01	C → 3296
69	4397.5	1.4	0.06	(6018 → 1623)[f]
70	4378.1	0.8	0.48	(C → 3347 or 4378 → 0)
71	4331.5	1.9	0.06	5344 → 1014
72	4280.3	0.9	0.18	(4311 → 30.6)[g]
73	4259.7	0.5	7.29	C → 3465
74	4240.0	1.2	0.12	6440 → 2202
75	4215.6	0.9	0.06	5188 → 972
76	4185.4	1.1	0.06	C → 3541
77	4169.7	0.9	0.12	(6440 → 2273)[f]
78	4133.4	0.5	7.44	C → 3591
79	4101.1	1.9	0.06	

TABLE 3-1 CONTINUED

No.	Transition[a] energy (keV)	Error in energy (keV)	Intensity[b] (Photons/100 captures)	Assignment[c]
80	4069.6	0.9	0.12	5442 → 1373
81	4055.2	0.9	0.19	C → 3670
82	4016.1	0.9	0.76	C → 3709
83	4003.1	1.6	0.13	5016 → 1014
84	3950.1	1.6	0.06	
85	3935.9	0.8	0.39	3936 → 0
86	3902.3	1.1	0.39	3902 → 0
87	3890.7	1.1	0.20	4903 → 1014
88	3875.7	0.5	2.84	3876 → 0
89	3849.7	0.5	3.25	C → 3876
90	3824.2	0.7	0.61	C → 3902
91	3789.7	0.7	0.88	C → 3936
92	3754.2	1.1	0.08	5378 → 1623
93	3723.6	1.9	0.08	5344 → 1623[f]
94	3709.4	1.1	0.51	3709 → 0
95	3678.2	1.9	0.32	3709 → 30.6
96	3659.6	1.2	0.08	6316 → 2657
97	3639.8	1.1	0.08	3670 → 30.6
98	3624.4	1.6	0.08	4997 → 1373
99	3591.1	0.7	4.97	3591 → 0

TABLE 3-1 CONTINUED

No.	Transition[a] energy (keV)	Error in energy (keV)	Intensity[b] (Photons/100 captures)	Assignment[c]
100	3651.2	0.7	0.99	3591 → 30.6
101	3541.4	1.9	0.04	3541 → 0
102	3480.8	1.9	0.17	
103	3465.5	0.6	7.38	3465 → 0
104	3392.4	0.8	0.62	4765 → 1373
105	3347.3	0.8	0.50	(C → 4378 or 3347 → 0)
106	3302.2	0.7	1.15	5442 → 2139
107	3265.5	0.8	0.52	3296 → 30.6
108	3207.6	1.2	0.13	6197 → 2989
109	3192.1	1.9	0.07	
110	3142.7	1.2	0.13	4765 → 1623
111	3128.8	1.2	0.21	C → 4596
112	3074.8	1.9	0.07	3105 → 30.6
113	3034.3	0.5	7.79	C → 4691
114	2988.6	1.9	0.21	2989 → 0
115	2976.5	1.9	0.11	4596 → 1623
116	2960.4	0.5	8.73	C → 4765
117	2922.5	0.8	0.22	3963 → 1014
118	2887.6	1.1	0.23	3902 → 1014
119	2877.9	1.9	0.15	5016 → 2139

TABLE 3-1 CONTINUED

No.	Transition[a] energy (keV)	Error in energy (keV)	Intensity[b] (Photons/100 captures)	Assignment[c]
120	2821.6	0.7	3.23	C → 4903
121	2755.2	1.2	0.05	5860 → 3105
122	2710.2	0.8	0.52	C → 5016
123	2692.1	1.2	0.05	5177 → 2486
124	2657.0	1.1	0.16	2657 → 0
125	2626.1	0.5	1.09	4765 → 2139
126	2591.0	0.5	3.37	C → 5134
127	2577.7	0.5	1.74	3591 → 1014
128	2566.6	1.6	0.14	
129	2550.4	1.1	0.18	C → 5177
130	2535.3	1.6	0.06	C → 5188
131	2503.0	1.2	0.12	3876 → 1373
132	2486.5	1.2	0.16	2486 → 0
133	2451.8	0.9	0.29	3465 → 1014
134	2420.2	1.2	0.10	
135	2381.1	1.1	0.13	C → 5344
136	2347.3	1.1	0.13	C → 5378
137	2283.4	0.5	3.62	C → 5442
138	2273.4	0.5	1.51	(2273 → 0)[g]
139	2255.8	0.9	0.37	3876 → 1620

TABLE 3-1 CONTINUED

No.	Transition[a] energy (keV)	Error in energy (keV)	Intensity[b] (Photons/100 captures)	Assignment[c]
140	2172.0	1.9	0.25	2202 → 30.6
141	2139.7	0.5	1.64	2139 → 0
142	2131.1	1.1	0.35	(3105 → 972)
143	2108.8	0.7	2.08	2139 → 30.6

[a]Energies are corrected for recoil.

[b]Error in intensity measurements ranges from 10% for strong transitions to about 50% for weak lines.

[c]C stands for capture state. Assignments in parentheses are tentative.

[d]Doubtful peaks.

[e]Also contains a possible C → 1620 component.

[f]Poor energy fit.

[g]Intensity imbalance.

The Q-value for the $^{27}Al(n,\gamma)^{28}Al$ was estimated by using the twenty-two step cascades identified in the decay scheme and the ground state transition, as shown in Table 3-2. A weighted average yielded the result of 7725.3 $\pm$ 0.2 keV. However, due to possible systematic errors in the calibration energies, it is felt that a reasonable estimate of the uncertainty in the Q-value should be about 0.5 keV.

This value of 7725.3 $\pm$ 0.5 keV is in excellent agreement with the 7725.5 $\pm$ 1.0 keV value reported by Hardell et al[Ha 69] and the 7725 $\pm$ 1.5 keV result of Nichol et al[Ni 69]. The present result is at variance with the earlier value of 7723.1 $\pm$ 1.5 keV reported by Jackson et al[Ja 65]. Endt and van der Leun[En 67] have given the Q-value for this reaction as 7730.7 $\pm$ 3.4 keV based upon the mass table compilation of Mattauch et al[Ma 65]. This value is at variance with the recent (n,γ) results.

After the construction of the decay scheme, the intensities were put on an absolute scale by requiring that the sum of the primary transitions be equal to 100%. In the case of low energy primary transitions which could not be seen in this work, the yield was inferred by examining depopulation. The construction of the decay scheme also made it possible to infer the low energy part of the spectrum. The branching associated with the decay of the low lying levels was taken from the $(d,p\gamma)$ results of Freeman and Gallmann[Fr 70]. The expression $\sum_i E_i I_i/Q$ was then evaluated and found to be 99%.

TABLE 3-2

The Q-Value for the $^{27}Al(n,\gamma)^{28}Al$ Reaction

E2		E1		Sum	
5443.9	(1.9)	2283.4	(0.5)	7727.3	(2.0)
5377.6	(1.1)	2347.3	(1.1)	7724.9	(1.6)
5343.8	(1.9)	2381.1	(1.1)	7724.9	(2.2)
5134.4	(0.5)	2591.0	(0.5)	7725.4	(0.7)
4903.0	(0.5)	2821.6	(0.7)	7724.6	(0.9)
4764.8	(0.8)	2960.4	(0.5)	7725.2	(0.9)
4690.9	(0.5)	3043.3	(0.5)	7725.2	(0.7)
4596.5	(0.9)	3128.8	(1.2)	7725.3	(1.5)
3935.9	(0.8)	3789.7	(0.7)	7725.6	(1.1)
3902.3	(1.1)	3824.2	(0.7)	7726.5	(1.3)
3875.7	(0.5)	3849.7	(0.5)	7725.4	(0.7)
3709.4	(1.1)	4016.1	(0.9)	7725.5	(1.4)
3591.1	(0.7)	4133.4	(0.5)	7724.5	(0.9)
3541.4	(1.9)	4185.4	(1.1)	7726.8	(2.2)
3465.5	(0.5)	4259.7	(0.5)	7725.2	(0.7)
3347.3	(0.8)	4378.1	(0.8)	7725.4	(1.1)
2657.0	(1.1)	5069.3	(0.8)	7726.3	(1.4)
2486.5	(1.2)	5238.7	(0.9)	7725.2	(1.5)
2273.4	(0.5)	5452.5	(0.8)	7725.9	(0.9)
2139.7	(0.5)	5586.1	(0.5)	7725.8	(0.7)
0		7724.9	(0.5)	7724.9	(0.5)
		Weighted Average		7725.3 $\pm$ 0.2 keV	

TABLE 3-2 CONTINUED

All the energies are in keV. The numbers in parentheses are errors associated with the energies.

The ^{28}Al nucleus is itself radioactive and beta decays to ^{28}Si with subsequent emission of a 1778 keV gamma ray. The short half life of ^{28}Al and the 100% yield of this gamma ray provide us with another probe to test the normalization of intensities. The 1778 keV gamma ray was found to have an intensity of 94%. Thus, the three methods of normalization indicate a consistency of about 3% in the absolute intensity assignments.

The multiplicity for the $^{27}Al(n,\gamma)^{28}Al$ reaction was found to be 2.0 which is in agreement with the estimate of ~2 reported by Meulhause[Mu 50]. The low value of multiplicity is a consequence of the intense ground state transition, and if we exclude this transition, the multiplicity is found to be about 2.4 which is probably more characteristic of nuclei in this region.

The ground state transition was found to have a yield of 30.5 $\pm$ 2%. The published value to date of intensity determination for this gamma ray have been; 20%[Ba 58], 24%[Gr 58], 32%[Dr 63], 37%[Gr 65], 20.10%[Ra 69] and 28.4%[Ha 69]. The dispersion is large and it is evident that factors of two are not rare in intensity estimates.

3.1.3 Discussion of the Decay Scheme

The ground state of ^{27}Al is known to have spin 5/2 and even parity. The capture state in ^{28}Al formed by s-wave neutron capture would, in the absence of dominant resonance, most probably be a mixture of spins 2 and 3 and

would have even parity. Electric dipole transitions from the capture state would populate odd parity levels with spins 1 to 4, while magnetic dipole transitions would lead to even parity states with spins 1 to 4.

The levels of ^{28}Al observed to be populated in this work are listed in Table 3-3. Also shown in the table are the de-excitation modes of the levels with their intensities and the intensity balance, where possible. The proposed decay scheme is illustrated in Fig. 3-2. Tentative levels and transition assignments are not shown in this diagram.

The spectrum for aluminum is atypical because below the energy of the ground state doublet, there exists a gap of about an MeV which is devoid of primary transitions. This feature permits the detection of weak "inverted" transitions in which a low energy transition populates a high energy state. Several new inverted transitions have been observed in this work. Although one expects such transitions to be present, they are not observable in most cases due to interference and masking by much stronger primary gamma rays. For the population of these levels above 5700 keV, primary transitions were too low in energy to be detected in the present experiment.

The C → 4997 keV transition is presumed masked by the ^{27}Al inelastic peak at 2732 keV. No transitions populating the 4512 or 4311 keV levels were observed and these levels are tentative. The C → 2989 keV transition, if it has a

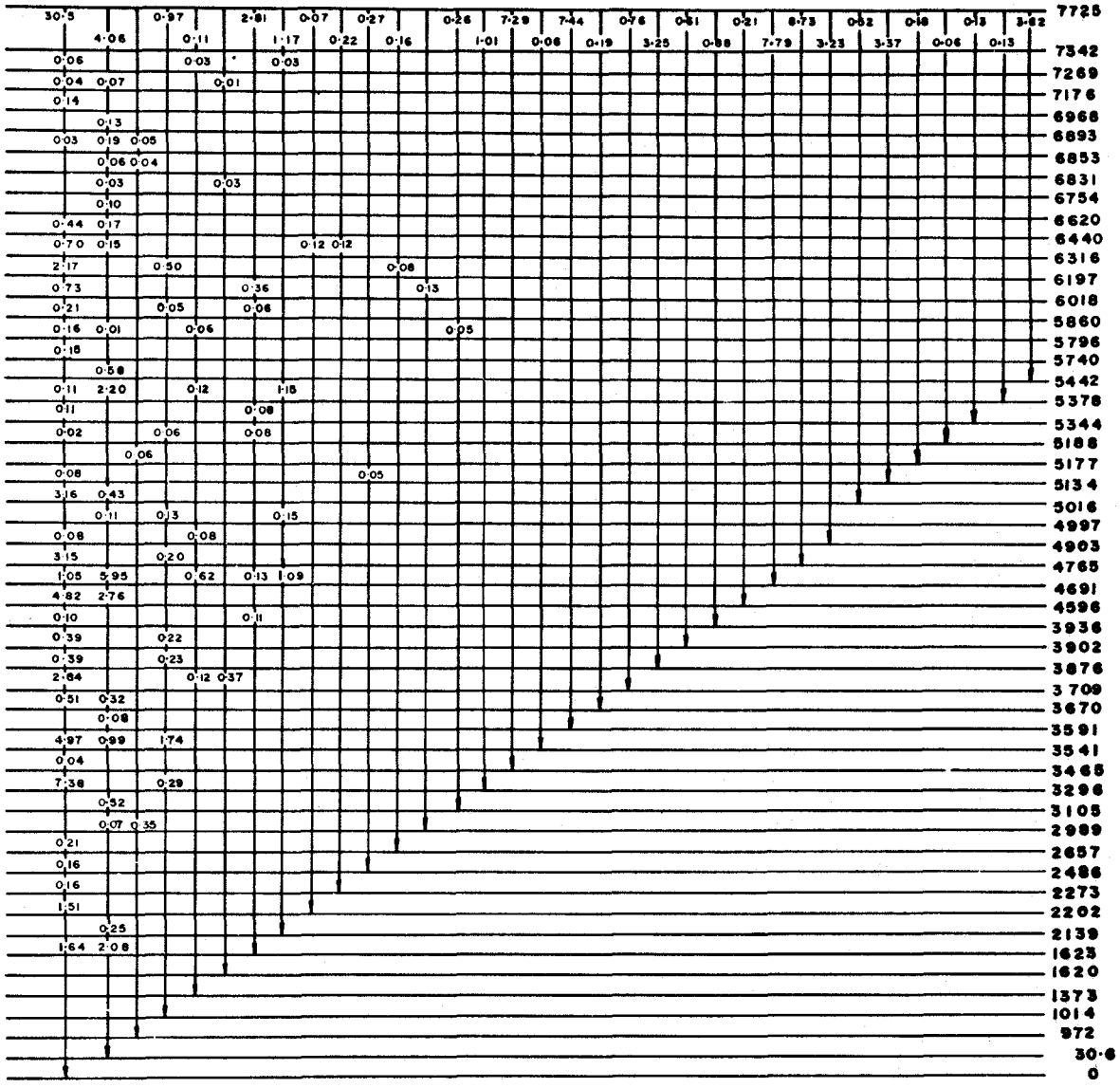

Fig. 3-2 The decay scheme of ^{28}Al.

TABLE 3-3

Decay Modes of ^{28}Al Levels

Level Energy (keV)	De-excitation modes (Intensity)	Intensity Balance I_{in}/I_{out}
7342	G(0.06), 1373(0.03), 2139(0.03	-/0.12
7269	G(0.04), 30.6(0.07), 1620(0.01)	-/0.12
7176	G(0.14)	-/0.14
6968	30.6(0.13)	-/0.13
6893	G(0.03), 30.6(0.19), 972(0.05)	-/0.27
6853	30.6(0.06), 972(0.04)	-/0.10
6831	30.6(0.03), 1620(0.03)	-/0.06
6754	G(0.08)[d], 30.6(0.10)	
6620	G(0.44), 30.6(0.17)	-/0.61
6440	G(0.70), 1014(0.15),2202(0.12), 2273(0.12)	-/1.09
(6419)	30.6(0.01)	-/0.01
6316	G(2.17), 1014(0.50), 2657(0.08)	-/8.75
6197	G(0.73), 1623(0.36), 2989(0.13)	-/1.22
6018	G(0.21), 30.6(0.02)[d], 1010(0.05), 1623(0.05)	
(5988)	G(0.02)[d]	-/0.28
5860	G(0.16), 30.6(0.01), 1373(0.06) 3105(0.05)	-/0.28
5796	G(0.15), 30.6(0.41)[d]	

TABLE 3-3 CONTINUED

Level energy (keV)	De-excitation Modes (Intensity)	Intensity Balance I_{in}/I_{out}
(5766)	G(0.41)[d]	
5740	30.6(0.58)	-/0.58
5442	G(0.11), 30.6(2.20), 1373(0.12), 2139(1.15)	3.82/3.58
5378	G(0.11), 1623(0.08)	0.13/0.19
5344	G(0.02), 1014(0.06), 1623(0.08)	0.13/0.16
5188	972(0.06)	0.06/0.06
5177	G(0.08), 2486(0.05)	0.18/0.13
5134	G(3.16), 30.6(0.43)	3.37/3.59
5016	30.6(0.11), 1014(0.13), 2139(0.15)	0.52/0.39
4997	G(0.08), 1373(0.08)	-/0.16[a]
4903	G(3.15), 1014(0.20)	3.23/3.35
4765	G(1.05), 30.6(5.95), 1373(0.62), 1623(0.13), 2139(1.09)	8.73/8.84
4691	G(4.82), 30.6(2.76)	7.79/7.56
4596	G(0.10), 1623(0.11)	0.21/0.21
(4512)	G(0.12)[d]	
(4378)	G(0.48)	0.50/0.48[b]
(4311)	30.6(0.18)[d]	
3936	G(0.39), 1014(0.22)	0.88/0.61
3902	G(0.39), 1014(0.23)	-/61/0.62

TABLE 3-3 CONTINUED

Level energy (keV)	De-excitation Modes (Intensity)	Intensity Balance I_{in}/I_{out}
3876	G(2.84), 1373(0.12), 1620(0.37)	3.25/3.33
3709	G(0.51), 30.6(0.32	0.76/0.83
3670	30.6(0.08)	0.19/0.08
3591	G(4.97), 30.6(0.99), 1014(1.74)	7.44/7.70
3541	G(0.04)	0.06/0.04
3465	G(7.38), 1014(0.29)	7.29/7.67
(3347)	G(0.50)[d]	0.48/0.50[b]
3296	30.6(0.52)	1.01/0.52
3105	30.6(0.07, 972(0.35)	0.31/0.42
2989	G(0.21)	0.13/0.21[c]
2657	G(0.16)	0.24/0.16
2486	G(0.16)	0.32/0.16
2273	G(1.51)[d]	
2202	30.6(0.25)	0.19/0.25
2139	G(1.64), 30.6(2.08)	3.59/3.72

[a]The transition populating the 4997 keV level from capture state is presumed to be masked by 2732 keV $^{27}Al(n,n'\gamma)$ peak.

[b]The 4378 keV γ-ray could be either a primary or a secondary transition with the 3347 keV γ-ray being its complement.

[c]The c → 2989 transition could not be distinguished from the strong 4765 → 30.6 transition.

[d]Tentative or ambiguous assignment.

measurable yield, could not be distinguished from the strong 4765 → 30.6 keV transition. The 2273.4 keV transition is too strong for the assignment 2273 → 0 keV. The total population of the 2273 keV level observed in this work is only 0.34 photons/100 captures, whereas, the intensity of the 2273.4 keV transition is measured to be 1.51 photons/100 captures. This latter transition probably consists of more than one component. Better low energy gamma ray measurements are required to clarify this ambiguity.

The 6751.9 keV transition could be interpreted either as C → 972 keV or 6754 → 0 keV. The spin and parity of the 972 keV level is reported to be 0^{+} (Fr 70). Thus, transitions from a 2^{+} (or a 3^{+}) capture state to the 972 keV level would have to be E2 (or M3) and therefore one tends to favour the other alternative.

The 5988.3 keV transition can be placed either as 6018 → 30.6 keV or 5988 → 0 keV. Similarly, the 5765.7 keV transition has two possible assignments, 5797 → 30.6 keV or 5766 → 0 keV. The 3347.3 and 4378.1 keV transitions form a two step cascade from the capture to the ground state. Since (d,p) measurements (En 67) show the existence of levels at 3347 and 4383 keV, it is not possible to arrive at a unique assignment for these transitions.

In their study of the beta decay of ^{28}Mg, Alburger and Harris (Al 69) observed a level at 1620.0 keV with spin

and parity 1^+ but (n,γ) studies[Ni 69, Ha 69] yielded a level around 1623 keV with spin and parity $(2,3)^+$. The problem was resolved by Freeman and Gallmann[Fr 70] who showed that the state is actually a doublet separated by 2.9 $\pm$ 0.8 keV. Any transition from the capture state to the 1620 keV level would be extremely difficult to distinguish from the strong C → 1623 keV transition. However, the intensity of any C → 1620 keV component could be isolated by studying the depopulation of 1623 and 1620 keV levels. In this work, the 1620 keV level was observed to be populated by transitions from the 7629, 6831 and 3876 keV levels.

Betts et al[Be 71] have assigned $J\pi = 1^+$ to a 2.21 MeV level seen by them in the study of $(^3He,p)$ reaction on ^{26}Mg. This can be identified as the 2202 keV level seen in the present work. A weak C → 2202 keV transition was observed and no 2202 → 0 transition could be detected, which is consistent with the 1^+ assignment for this level.

Hardy et al[Ha 70] while looking for T = 2 and T = 3 analog states in $28 \leq A \leq 40$ nuclei found a T = 2, $J^\pi = 0^+$ level in ^{28}Al at 5983 $\pm$ 25 keV. This could be either of the 5960 or 5989 keV levels seen in the (d,p) work[En 67]. However, if we identify it as the 5989 keV level then the 5988.3 keV gamma transition would have a preferred assignment of 6018 → 30.6 in the decay scheme.

3.2 THE $^{35}Cl(n,\gamma)^{36}Cl$ REACTION

3.2.1 Review of Previous Work

The (n,γ) reaction on chlorine has been studied by several investigators and the results up to 1967 have been summarized by Bartholomew et al[Ba 67]. More recently, studies of the reaction have been reported by Hughes and Kennett[Hu 70] and by Fubini et al[Fu 71]. The former used a Ge(Li) detector to measure the gamma ray spectrum and also established a coincidence surface using a Ge(Li)-NaI(Tl) system. Fubini et al[Fu 71] employed a Ge(Li) pair spectrometer to observe the high energy part of the gamma ray spectrum and used a single Ge(Li) detector to study the low energy spectrum. They also constructed a decay scheme involving 17 excited states in ^{36}Cl by applying the Ritz combination principle.

The complimentary $^{35}Cl(d,p)^{36}Cl$ reaction has been studied by several authors. Paris et al[Pa 55] identified 23 proton groups corresponding to levels in ^{36}Cl and deduced the level energies. Hoogenboom et al[Ho 62] observed levels of ^{36}Cl up to an excitation energy of 7007 keV. They also reported l_n values and spectroscopic factors for most of the observed states. Recently, Decowski[De 71] has measured the angular distribution of 15 proton groups from the $^{35}Cl(d,p)^{36}Cl$ reaction and carried out a DWBA analysis to obtain l_n values and spectroscopic factors up to an excitation energy of 3339 keV in ^{36}Cl.

Endt and van der Leun[En 67] collected all available information on the levels of ^{36}Cl up to 1967. Since then Kopecky and Warming[Ko 69] have studied the circular polarization of gamma rays following the capture of polarized thermal neutrons in chlorine and made some spin and parity assignments for the low lying levels of ^{36}Cl. Honzatko et al[Ho 71] have reported a study of the linear polarization of the low energy capture gamma rays from the $^{35}Cl(n,\gamma)^{36}Cl$ reaction.

3.2.2 Present Work

Natural chlorine consists of two isotopes ^{35}Cl and ^{37}Cl, with abundances of 75.53 and 24.4% respectively. The thermal neutron absorption cross section for ^{35}Cl is reported to 44 ± 1 b[St 64] while the thermal neutron capture cross sections for ^{37}Cl leading to ^{38m}Cl and ^{38g}Cl are 5 ± 3 mb and 430 ± 100 mb respectively[St 64]. Thus, thermal neutron capture in natural chlorine leads to the $^{35}Cl(n,\gamma)^{36}Cl$ reaction about 99.7% of the time.

A piece of Saran wrap (polyvinyl chloride), weighing about 0.2 gm served as the target for the present study and total counting time was 67 hours.

The observed gamma ray spectrum after thermal neutron capture is shown in Fig. 3-3. Of the 140 gamma rays identified, three have been tentatively assigned to the $^{37}Cl(n,\gamma)^{38}Cl$ reaction (see below) and the rest to the $^{35}Cl(n,\gamma)^{36}Cl$ reaction.

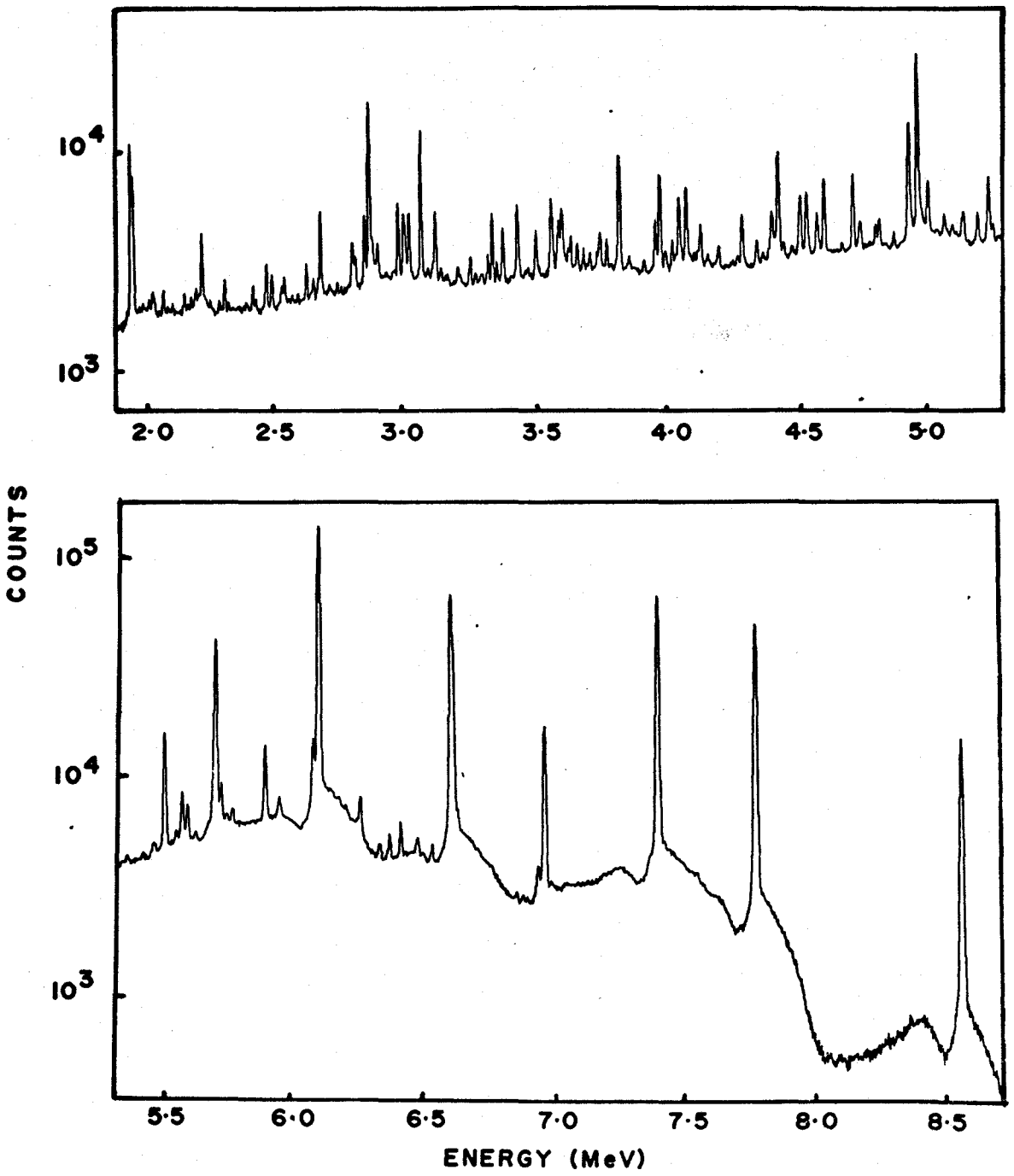

Fig. 3-3 The capture gamma ray spectrum of chlorine.

The energies of the low-lying levels of ^{38}Cl have been measured by Engelbertink and Olness[En 71, En 72] from the beta decay of ^{38}S and from the $^{37}Cl(d,p\gamma)^{38}Cl$ reaction. They have also made spin and parity assignments for several observed levels. The Q-value for the $^{37}Cl(n,\gamma)^{38}Cl$ reaction is reported to be 6110 $\pm$ 8 keV by Endt and van der Leun[En 67] based on the mass-spectroscopic results of Mattauch et al[Ma 65]. This information can be used to calculate the energies of primary electric and magnetic dipole transitions expected in ^{38}Cl. Since the ground state spin and parity of ^{37}Cl is $3/2^+$, s-wave neutron capture would populate states with spins 1 and 2 having even parity in ^{38}Cl and dipole transitions would lead to levels with spins 0 to 3. The expected and observed transitions in ^{38}Cl are shown in Table 3-4. The C $\rightarrow$ O and the C $\rightarrow$ 1692.4 keV transitions are not expected to be seen since they would be masked by strong transitions in ^{36}Cl. However three weak transitions at expected energies were observed and are tentatively assigned to ^{38}Cl. The identification of these transitions allows us to recalculate the Q-value for the $^{37}Cl(n,\gamma)^{38}Cl$ reaction. A weighted average of the three estimates presented in Table 3-7 gives a Q-value of 6107.4 $\pm$ 0.8 keV. This value is tentative since the assignment of the transitions in ^{38}Cl is not established by means of a separated isotope target or by coincidence studies.

The energies and intensities of observed transitions in ^{36}Cl are listed in Table 3-5. All the energies have been corrected for recoil losses and most transitions have

TABLE 3-4

Transitions in ^{38}Cl

Level energy (keV)	J^{π} (En 71, En 72)	Expected energy of primary dipole transition (keV)	Observed transition energy (keV)	Q-value (keV)
0	2^-	6110 ± 8		
671.27	5^-			
755.26	3^-	5355 ± 8		
1308.87	4^-			
1617.21	3^-	4493 ± 8	4490.4 ± 1.9	6107.6 ± 1.9
1672.4	1^-, 2^-, 3^-	4418 ± 8		
1745.8	0^-, 1^-	4364 ± 8		
1785.1	2^+, 3^+, 4^+	4325 ± 8		
1941.7	1^+	4168 ± 8	4165.3 ± 1.2	6107.0 ± 1.2
1981.1	2^-, 3^-	4129 ± 8	4126.6 ± 1.2	6107.7 ± 1.2
2743.1	3^-	3367 ± 8		

TABLE 3-5

The Observed Transitions in ^{36}Cl

No.	Transition[a] energy (keV)	Error in energy (keV)	Intensity[b] (Photons/100 captures)	Assignment[c]
1	8578.9	0.5	3.39	C → 0
2	7790.9	0.5	10.22	C → 787
3	7414.4	0.5	11.58	C → 1165
4	6978.0	0.5	2.74	C → 1602
5	6951.9	1.2	0.22	
6	6892.8	2.3	0.03	
7	6767.6	2.3	0.03	
8	6642.6	2.3	0.47	
9	6627.9	1.2	5.89	C → 1951
10	6620.6	0.9	11.20	C → 1958
11	6543.3	0.9	0.14	6543 → 0
12	6488.0	1.2	0.15	
13	6479.8	1.2	0.08	
14	6422.1	2.3	0.33	
15	6379.3	0.9	0.21	
16	6340.8	1.7	0.13	
17	6267.7	1.4	0.47	
18	6111.4	0.5	21.66	C → 2469
19	6087.5	0.9	1.34	C → 2491[d]

TABLE 3-5 CONTINUED

No.	Transition[a] energy (keV)	Error in energy (keV)	Intensity[b] (Photons/100 captures)	Assignment[c]
20	5955.2	1.2	0.25	5955 → 0
21	5903.0	0.7	1.30	C → 2676[d]
22	5777.8	0.6	0.22	
23	5755.2	1.7	0.17	C → 2824
24	5733.9	0.9	0.59	
25	5714.5	0.5	5.89	C → 2864
26	5633.0	0.6	0.07	
27	5603.9	1.4	0.42	5604 → 0[e]
28	5584.7	0.9	0.59	C → 2995[d]
29	5560.9	0.7	0.11	
30	5517.6	0.5	1.93	5518 → 0
31	5474.9	0.7	0.09	C → 3106
32	5464.5	2.3	0.03	(5461 → 0)[f]
33	5372.5	1.4	0.04	
34	5262.1	1.7	0.10	5262 → 0
35	5247.2	0.9	0.61	C → 3333
36	5204.0	0.7	0.24	5204 → 0
37	5149.5	0.9	0.25	5150 → 0
38	5108.9	1.2	0.08	
39	5079.3	1.1	0.15	

TABLE 3-5 CONTINUED

No.	Transition[a] energy (keV)	Error in energy (keV)	Intensity[b] (Photons/100 captures)	Assignment[c]
40	5017.9	0.7	0.51	5018 → 0
41	4979.9	0.5	4.11	C → 3600
42	4945		1.38	C → 3635
43	4884.8	1.4	0.11	(4885 → 0)[g]
44	4824.9	1.1	0.21	4829 → 0
45	4815.3	1.1	0.17	
46	4756.5	1.1	0.19	4756 → 0
47	4749.0	2.3	0.12	C → 3830
48	4728.6	0.7	0.71	5518 → 787
49	4683.1	1.9	0.06	
50	4616.8	0.6	0.73	C → 3962
51	4587.4	0.9	0.32	C → 3992
52	4548.3	0.7	0.56	6506 → 1958
53	4524.5	0.9	0.53	(5311 → 787)[g]
54	4457.7	1.1	0.11	
55	4440.6	0.6	1.29	C → 4139
56	4415.0	0.7	0.42	5204 → 787
57	4376.9	1.2	0.07	
58	4354.7	0.9	0.19	5518 → 1165,
59	4298.2	0.6	0.45	5461 → 1165
				4299 → 0

TABLE 3-5 CONTINUED

No.	Transition[a] energy (keV)	Error in energy (keV)	Intensity[b] (Photons/100 captures)	Assignment[c]
60	4279.7	1.4	0.07	C → 4299
61	4205.4	1.1	0.13	
62	4138.6	0.7	0.35	4139 → 0
63	4111.2	1.2	0.07	
64	4083.1	0.5	0.89	C → 4496
65	4054.7	0.5	0.70	
66	4026.2	1.1	0.19	C → 4553
67	3999.3	1.2	0.12	6676 → 2676
68	3981.4	0.7	1.09	C → 4598
69	3862.6	0.7	0.50	3962 → 0
70	3916.3	1.2	0.09	5518 → 1602
71	3860.9	0.9	0.11	5461 → 1602
72	3823.2	0.7	1.63	C → 4756
73	3790.9	1.2	0.04	
74	3775.3	1.1	0.27	
75	3749.3	1.2	0.35	C → 4829
76	3736.4	0.9	0.15	(3736 → 0)[g]
77	3708.6	0.9	0.13	4496 → 787
78	3660.7	0.9	0.24	5262 → 1602
79	3634.7	0.9	0.36	3635 → 0

TABLE 3-5 CONTINUED

No.	Transition[a] energy (keV)	Error in energy (keV)	Intensity[b] (Photons/100 captures)	Assignment[c]
80	3624.9	1.2	0.20	
81	3601.1	1.1	0.74	3600 → 0
82	3589.1	0.9	0.55	4756 → 1165
83	3561.5	0.7	0.99	C → 5018
84	3501.7	0.9	0.52	5461 → 1958
85	3428.4	0.5	1.07	C → 5150
86	3375.4	0.7	0.66	C → 5204
87	3350.2	0.9	0.21	4139 → 787
88	3333.0	0.7	0.99	3333 → 0
89	3315.7	0.9	0.34	C → 5262
90	3292.6	2.3	0.18	
91	3269.7	1.2	0.11	C → 5311
92	3249.7	0.9	0.35	
93	3200.8	0.9	0.19	5150 → 1951
94	3162.3	1.2	0.11	5839 → 2676
95	3152.9	1.1	0.09	4756 → 1602
96	3135.8	1.1	0.11	5627 → 2491
97	3116.3	0.9	1.08	C → 5461
98	3106.9	1.2	0.20	3106 → 0
99	3086.5	1.4	0.12	

TABLE 3-5 CONTINUED

No.	Transition[a] energy (keV)	Error in energy (keV)	Intensity[b] (Photons/100 captures)	Assignment[c]
100	3061.4	0.5	3.93	C → 5518
101	3015.5	0.7	1.03	
102	3001.3	1.2	0.77	
103	2995.3	1.2	1.04	2995 → 0
104	2975.2	0.7	1.41	4139 → 1165, C → 5605
105	2952.4	2.3	0.12	C → 5627
106	2927.6	1.7	0.12	(4885 → 1958)[g]
107	2895.7	0.9	0.66	2896 → 0
108	2876.1	1.2	0.86	(C → 5703)[g]
109	2864.0	0.5	6.21	2864 → 0
110	2845.2	0.7	1.44	3635 → 787[f]
111	2810.5	1.1	0.45	3600 → 787
112	2799.8	0.9	0.79	4756 → 1958
113	2740.0	1.1	0.17	C → 5839
114	2710.2	1.2	0.11	5703 → 2995
115	2676.2	0.7	2.01	2676 → 0
116	2647.7	1.1	0.26	4598 → 1951
117	2622.6	0.7	0.64	C → 5955
118	2591.0	1.1	0.13	
119	2567.7	0.9	0.15	5461 → 2896

TABLE 3-5 CONTINUED

No.	Transition[a] energy (keV)	Error in energy (keV)	Intensity[b] (Photons/100 captures)	Assignment[c]
120	2537.2	1.1	0.56	4496 → 1958
121	2527.7	1.1	0.39	5204 → 2676
122	2490.8	0.9	0.70	2491 → 0
123	2469.2	0.7	0.98	2469 → 0
124	2429.2	1.1	0.16	
125	2418.3	0.9	0.53	
126	2340.9	1.2	0.09	5204 → 2864
127	2324.9	1.1	0.23	5150 → 2824
128	2310.7	0.7	0.74	
129	2289.1	1.1	0.35	
130	2199.3	1.1	0.60	
131	2180.7	0.9	0.40	4139 → 1958
132	2155.3	1.1	0.51	5150 → 2996
				4829 → 2676
133	2074.6	1.1	0.63	C → 6505
134	2036.0	1.1	0.68	2824 → 787,
				C → 6543
135	2020.9	1.1	0.39	5018 → 2995
136	1958.1	0.5	14.27	1958 → 0
137	1950.1	0.5	22.74	1951 → 0

TABLE 3-5 CONTINUED

[a]Energies are corrected for recoil.

[b]Error in intensity measurement ranges from 10% for strong transitions to about 50% for weak lines.

[c]C stands for capture state. Assignments in parentheses are tentative.

[d]May have possible secondary component.

[e]Level not seen in (d,p) work.

[f]Poor energy fit.

[g]Intensity imbalance.

been placed into a proposed decay scheme. No time-correlation studies were made in the present work but some coincidence results obtained by Hughes and Kennett[Hu 70] have been used in arriving at the decay scheme along with level information from the $^{35}Cl(n,\gamma)^{36}Cl$ reaction. The energy precision and intensity balance provided further constraints for assignment of transitions in the decay scheme. After the construction of the decay scheme, the intensities where put on an absolute scale by requiring that the sum of intensities of the transitions assigned as primary be equal to 100%.

The identification of 19 two step cascades in the gamma ray spectrum allows us to estimate the Q-value for the $^{35}Cl(n,\gamma)^{36}Cl$ reaction. This is shown in Table 3-6. A weighted average of all estimates of the Q-value yielded the result 8579.1 $\pm$ 0.2 keV. Again, to account for possible systematic error in calibration energies, the error is enlarged to 0.5 keV. The present estimate of 8579.1 $\pm$ 0.5 keV for the Q-value is in agreement with the 8580.6 $\pm$ 1.0 keV value given by Hughes and Kennett[Hu 70] but deviates from the 8581.5 $\pm$ 0.2 keV value of Fubini et al[Fu 71]. Endt and van der Leun[En 67] give the Q-value for the reaction as 8576.9 $\pm$ 3.9 keV based on the mass spectroscopic results of Mattauch et al[Ma 65]. This value is in agreement with the present estimate.

The proposed decay scheme is illustrated in Fig. 3-4. The levels of ^{36}Cl observed in this work are listed in Table

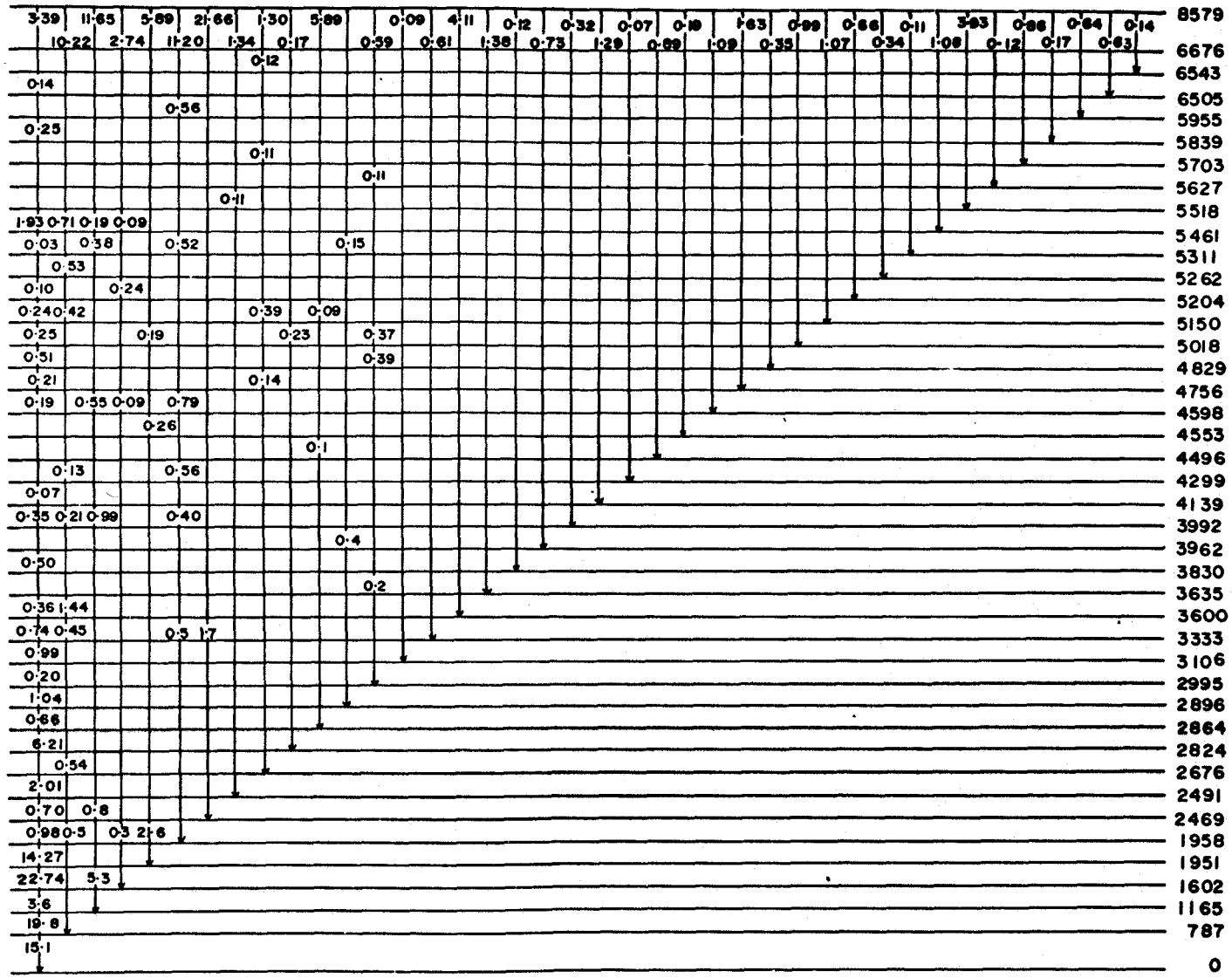

Fig. 3-4 The decay scheme of ^{36}Cl.

TABLE 3-6

The Q-Value for the $^{35}Cl(n,\gamma)^{36}Cl$ Reaction

E_1		E_2		Sum	
2622.6	(0.7)	5955.2	(1.2)	8577.8	(1.4)
3061.4	(0.5)	5517.6	(0.5)	8579.0	(0.7)
3315.7	(0.9)	5262.1	(1.7)	8577.8	(1.9)
3375.4	(0.7)	5204.0	(0.7)	8579.4	(1.0)
3428.4	(0.5)	5149.5	(0.9)	8577.9	(1.0)
3561.5	(0.7)	5017.9	(0.7)	8579.4	(1.0)
3749.3	(1.2)	4828.9	(1.1)	8578.2	(1.6)
3823.2	(0.7)	4756.5	(1.1)	8579.7	(1.3)
4440.6	(0.6)	4138.6	(0.7)	8579.2	(0.9)
4616.8	(0.6)	3962.6	(0.7)	8579.4	(0.9)
5247.2	(0.9)	3333.0	(0.7)	8580.2	(1.1)
5474.9	(0.7)	3106.9	(1.2)	8581.8	(1.4)
5584.7	(0.9)	2995.3	(1.2)	8580.0	(1.5)
5714.5	(0.5)	2864.0	(0.5)	8578.5	(0.7)
5903.0	(0.7)	2676.2	(0.7)	8579.2	(1.0)
6087.5	(0.9)	2490.8	(0.9)	8578.3	(1.3)
6111.4	(0.5)	2469.2	(0.7)	8580.6	(0.8)
6620.6	(0.9)	1958.1	(0.5)	8578.7	(1.0)
6627.9	(1.2)	1950.1	(0.5)	8578.0	(1.3)
8578.9	(0.5)	0		8578.9	(0.5)

Weighted average = 8579.1 $\pm$ 0.2 keV

All the energies are in keV. The numbers in parentheses are errors associated with the energies.

TABLE 3-7

Decay Modes of ^{36}Cl Levels

Level energy (keV)	De-excitation Modes (Intensity)	Intensity Balance I_{in}/I_{out}
6676	2676(0.12	-/0.12
6543	G(0.14)	0.14/0.14[c]
6505	1958(0.56)	0.63/0.56
5955	G(0.25)	0.64/0.25
5839	2676(0.11)	0.17/0.11
5703	2995(0.11	0.86/0.11
5627	2491(0.11)	0.12/0.11
(5604)	G(0.42)	0.42/0.42[c]
5518	G(1.93, 787(0.71), 1165(0.19), 1602(0.09)	3.93/2.92
5461	G(0.03), 1165(0.38)[a], 1602(0.11), 1958(0.52) 2896(0.15)	1.08/1.19
5311	787(0.53)	0.53/0.11
5262	G(0.10), 1602(0.24)	0.34/0.34
5204	G(0.24), 787(0.42), 2676(0.39), 2864(0.09)	0.66/1.14
5150	G(0.25), 1951(0.19), 2824(0.23), 2995(0.37)[a]	1.07/1.04
5018	G(0.51), 2995(0.39)	0.99/0.90

TABLE 3-7 CONTINUED

Level energy (keV)	De-excitation Modes (Intensity)	Intensity Balance I_{in}/I_{out}
(4885)	G(0.11), 1958(0.12)	
4829	G(0.21), 2676(0.14)[a]	0.35/0.35[c]
4756	G(0.19), 1165(0.55), 1602(0.09), 1958(0.79)	1.63/1.62
4598	1951(0.26)	1.09/0.26
4553	2864(0.1)[b]	0.19/0.1
4496	787(0.13), 1958(0.56)	0.89/0.69
4299	G(0.07)[a]	0.07/0.07[c]
4139	G(0.35), 787(0.21), 1165(0.99)[a], 1958(0.40)	1.29/1.95
3992	2895(0.4)[b]	0.32/0.4
3962	G(0.50)	0.73/0.50
3830	2995(0.2)[b]	0.12/0.2
(3736)	G(0.15)	
3635	G(0.36), 787(1.44)	1.38/1.80
3600	G(0.74), 787(0.45), 1958(0.5)[b], 2469(1.7)[b]	4.11/3.4
3333	G(0.99)	0.61/0.99
3106	G(0.20)	0.09/0.20
2995	G(1.04)	1.66/1.04
2906	G(0.66)	0.55/0.66

TABLE 3-7 CONTINUED

Level energy (keV)	De-excitation Modes (Intensity)	Intensity Balance I_{in}/I_{out}
2864	G(6.21)	6.18/6.21
2824	787(0.54)[a]	0.40/0.54
2676	G(2.01)	2.06/2.01
2491	G(0.80, 1165(0.8)[d]	
2469	G(0.98), 787(0.5)[b], 1602(0.3)[b], 1951(21.6)[d]	
1958	G(14.27)	14.65/14.27
1951	G(22.74), 1165(5.3)[d]	
1602	G(3.6)[d]	
1165	G(19.8)[d]	
787	G(15.1)[d]	

[a]Transition interpreted as having more than one component. Intensity divided to balance simpler cascade. A balance obtained like this is marked with c.

[b]Transition observed by Huges and Kennett (Hu70).

[c]Artifical balance; see note a above.

[d]Intensity calculated by balance.

3-7 along with their modes of decay and intensity balance, where possible. Some low energy transitions observed by Hughes and Kennett[Hu 70] were used in constructing the decay scheme and the intensities of strong low-energy transitions were calculated using intensity balance. The expression $\Sigma E_i I_i/Q$ was then evaluated and found to be 103% thus providing a check on the normalization of intensities. The multiplicity of the reaction was estimated to be 2.5.

In constructing the decay scheme, several transitions were interpreted as consisting of more than one component. In such cases the intensity was divided so as to balance the simpler cascade. An intensity balance, within experimental accuracy, is obtained for most levels but some levels do show an obvious imbalance. This could be due to a total or partial misinterpretation of the transitions concerned. In Table 3-8, the intensities of strong low energy transitions as deduced from this work are compared with the measurements of Hughes and Kennett[Hu 70] and Fubini et al[Fu 71]. It can be seen that the agreement is very good.

All the levels seen in this work have been observed in the $^{35}Cl(d,p)^{36}Cl$ measurements[En 67] except for the 5604 keV level which is, therefore, tentative.

The 6087.5, 5903.0 and 5584.7 keV transitions have been interpreted as primary transitions to the 2491, 2676 and 2995 keV levels respectively. The $^{35}Cl(d,p)^{36}Cl$ work of Hoogenboom et al[Ho 62] shows levels at 6090, 5906 and 5584 keV. Thus, there is a possibility that the above transitions have a secondary component depopulating these levels.

TABLE 3-8

Intensities of Low Energy Transitions in ^{36}Cl

Transition	Intensity		
	Present	Fubini et al (Fu 71)	Hughes and Kennett (Hu 70)
1469 → 1951	21.6	21.9	18.0
1951 → 1165	5.3	13.0	20.6
787 → 0	15.1	10.8	
1165 → 0	19.8	23.9	22.2
1602 → 0	3.6	3.0	3.9

Hughes and Kennett[Hu 70] observed that the 1951 keV level cascaded down through a 1165-787 or 787-1165 keV pair with an intensity of about 5 times per hundred neutron captures. Fubini et al[Fu 71] observed a doublet structure for the 787 keV gamma ray. The lower energy component can be interpreted as the 1951 → 1165 keV transition and the higher energy component as the 787 → 0 transition. While the total intensity for the two transitions observed by them agrees with the present deduced values and the masurements of Hughes and Kennett[Hu 70], the intensity of the lower component found by them is 13% which is much higher than what we expect.

The energy and intensity of the 4945 keV transition was difficult to measure accurately due to interference from the 4945.2 keV transition arising from the $^{12}C(n,\gamma)^{13}C$ reaction in the graphite sample holder. The contribution of the $^{12}C(n,\gamma)^{13}C$ reaction to this transition was calculated by measuring the intensity of the 3683.7 keV transition arising from the same reaction and using the branching ratios reported by Spilling et al[Sp 68].

3.3 THE $^{31}P(n,\gamma)^{32}P$ REACTION

3.3.1 Review of Previous Work

The $^{31}P(n,\gamma)^{32}P$ reaction has been investigated by several authors[Ba 67]. Van Middelkoop and Spilling[Va 65] studied the gamma radiation following thermal neutron capture in phosphorus using scintillation detectors. They measured singles and coincidence spectra and also performed some angular correlation measurements which yielded several spin assignments in ^{32}P. Two more recent investigations of the reactions using Ge(Li) detectors have been reported by van Middelkoop[Va 67] and Lycklama and Kennett[Ly 67]. The (d,p) reaction on phosphorus has been studied by Piraino et al[Pi 60] and by Holtebekk[Ho 62a]. The former reported the energies of ^{32}P levels up to an excitation energy of 6.2 MeV and the latter measured the reduced widths and l_n values for some of the st states. A summary of the available data on the levels of ^{32}P up to 1967 can be found in the review paper by Endt and van der Leun[En 67].

3.3.2 Present Work

In the present investigation, the target consisted of 2.4 g of red phosphorus and the total counting time was 74 hours. The thermal neutron capture cross section for phosphorus is reported to be 190 $\pm$ 10 mb[St 64].

The observed gamma ray spectrum after thermal neutron capture in phosphorus is shown in Fig. 3.5. The energies and intensities of identified transitions are listed in Table 3-9. Most of the observed transitions have been placed in a decay scheme. After the construction of the decay scheme, the intensities were put on an absolute scale by requiring the sum of the intensities of primary transitions equal 100%.

The identification of 7 two step cascades in the decay scheme allowed an accurate estimation of the Q-value for the $^{31}P(n,\gamma)^{32}P$ reaction to be made. This is shown in Table 3-10. The Q-value is obtained as 7935.5 $\pm$ 0.3 keV. As in the previous cases, the error is enlarged to 0.5 keV to account for any possible systematic errors in the calibration energies. The present estimate of 7935 $\pm$ 0.5 keV for the Q-value is in agreement with the 7936 $\pm$ 1 keV result of Lycklama and Kennett[Ly 70] and the 7936.8 $\pm$ 0.8 keV value of van Middlekoop[Va 67]. The present result is also in agreement with the 7936.6 $\pm$ 2.4 keV value given by Endt and van der Leun[En 67] based upon the mass-spectrometric data of Mattauch et al[Ma 65].

The transitions observed by Lycklama and Kennett[Ly 67] below an energy of 1.8 MeV were utilized to complete the decay scheme. The expression $\Sigma E_i I_i/Q$ was then evaluated and found to be 99%. This is in excellent agreement with the normalization of intensities. The multiplicity of the reaction was estimated to be 2.9.

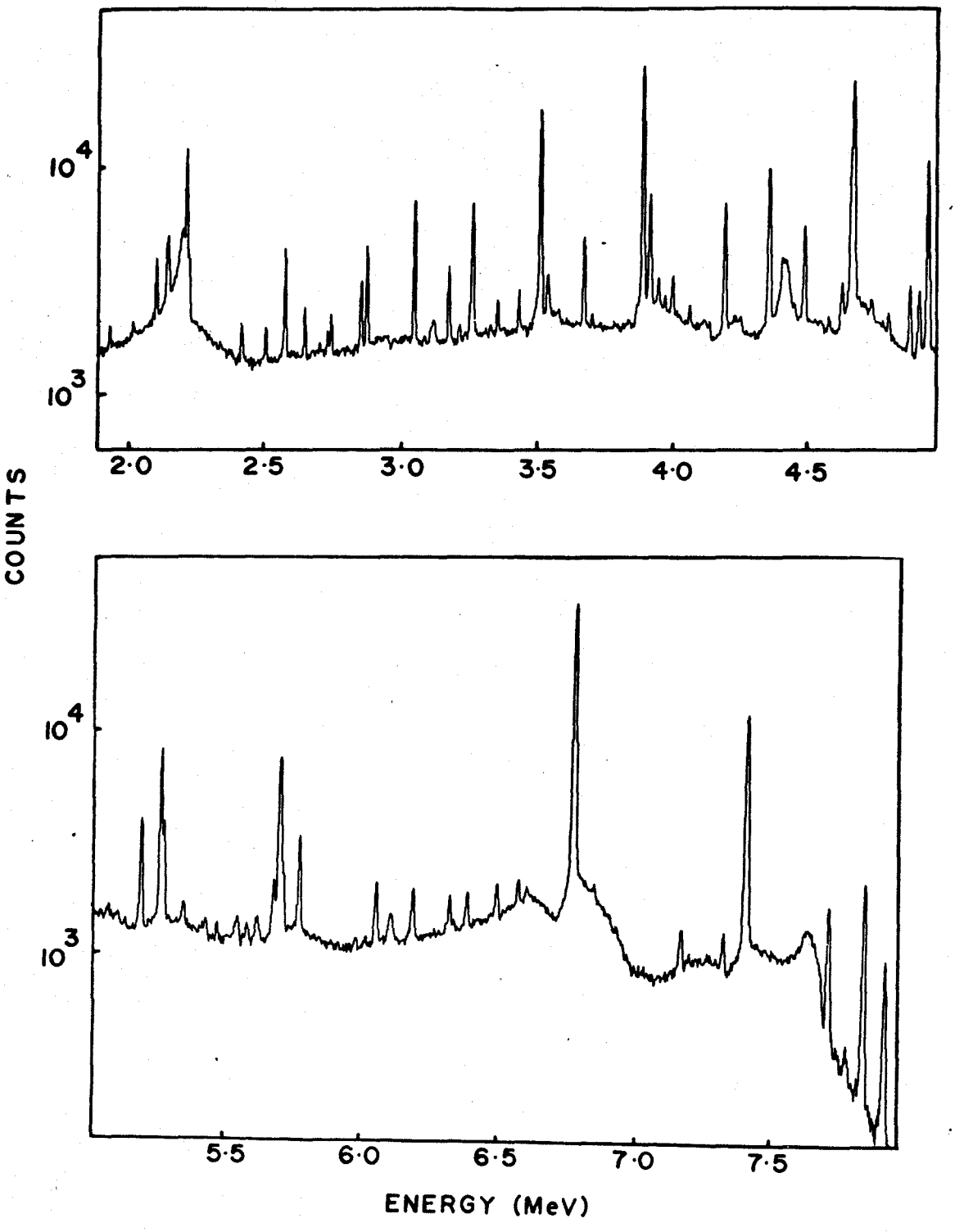

Fig. 3-5 The capture gamma ray spectrum of phosphorus.

TABLE 3- 9

The Observed Transitions in ^{32}P

No.	Transition[a] Energy (keV)	Error in energy (keV)	Intensity[b] (Photons/100 captures)	Assignment[c]
1	7935.7	0.5	0.45	C → 0
2	7857.0	0.5	1.06	C → 78
3	7423.0	0.5	5.71	C → 513
4	7337.2)	0.7	0.20	
5	7179.4	1.0	0.23	
6	6786.0	0.5	17.52	C → 1149
7	6614.5	2.3	0.09	C → 1322
8	6581.8	1.2	0.23	6582 → 0
9	6503.6	0.8	0.29	6582 → 75
10	5346.1	1.2	0.06	
11	6332.9	0.8	0.27	6333 → 0
12	6196.8	0.8	0.40	6198 → 0
13	6121.8	2.3	0.09	6198 → 78
14	6062.3	0.5	0.50	6062 → 0
15	5778.4	0.7	1.05	5778 → 0
16	5716.9	2.3	0.46	(C → 2219)[d]
17	5705.7	0.5	3.04	C → 2229
18	5683.5	0.7	0.43	6198 → 513
19	5585.3	1.2	0.08	

TABLE 3-9 CONTINUED

No.	Transition[a] energy (keV)	Error in energy (keV)	Intensity[b] (Photons/100 captures)	Assignment[c]
20	5549.2	1.2	0.14	6062 → 513
21	5536.6	2.3	0.04	
22	5474.9	0.8	0.10	
23	5432.1	1.6	0.12	5510 → 78
24	5349.1	1.2	0.16	5349 → 0
25	5277.4	0.8	1.18	C → 2657
26	5266.3	0.5	3.35	5778 → 513
27	5195.0	0.7	1.34	C → 2940
28	4913.5	0.8	0.70	6062 → 1149
29	4877.4	0.7	0.80	4877 → 0
30	4799.3	1.8	0.20	4877 → 78
31	4737.6	1.4	0.18	(6062 → 1322)[e]
32	4672.0	0.7	12.58	C → 3264
33	4660.9	1.2	3.15	4661 → 0
34	4630.4	0.8	0.70	5778 → 1149
35	4580.7	2.3	0.10	(4661 → 78)[e]
36	4491.7	0.5	2.07	C → 3445
37	4364.2	0.5	5.02	4877 → 51338
38	4200.3	0.5	3.46	5349 → 1149
39	4072.6	1.2	0.32	

TABLE 3-9 CONTINUED

No.	Transition[a] energy (keV)	Error in energy (keV)	Intensity[b] (Photons/100 captures)	Assignment[c]
40	4009.2	0.7	0.62	4009 → 0
41	3957.8	0.8	0.64	4036 → 78
42	3926.0		4.17	C → 4009, 5072 → 1149, 4009 → 78
43	3900.4	0.5	20.44	C → 4036
44	3550.7	0.8	1.20	5778 → 2229
45	3523.2	0.5	15.08	4036 → 513
46	3444.9	0.8	0.87	3445 → 0
47	3366.6	0.7	0.77	3445 → 78
48	3275.0	0.6	5.58	C → 4661
49	3225.2	1.2	0.32	
50	3186.3	0.6	2.26	3264 → 78
51	3130.2	1.2	0.55	
52	3.20.5	1.6	0.36	5349 → 2229
53	3058.9	0.5	6.87	C → 4877
54	2887.0	0.5	4.10	4036 → 1149
55	2863.9	0.6	2.19	C → 5072
56	2740.1	1.0	0.54	2740 → 0
57	2712.1	1.0	0.32	4036 → 1322
58	2657.4	0.5	1.58	2657 → 0
59	2586/2	0.5	5.41	C → 5349

TABLE 3-9 CONTINUED

No.	Transition[a] energy (keV)	Error in energy (keV)	Intensity[b] (Photons/100 captures)	Assignment[c]
60	2515.6	0.7	1.13	5778 → 3264
61	2426.9	0.7	1.48	C → 5510
62	2157.0	1.2	8.60	C → 5778
63	2151.9	1.2	7.81	2229 → 78
64	2114.6	0.5	7.91	3264 → 1149
65	2028.4	1.2	1.16	(5349 → 3321)[g]
66	1941.3	0.8	2.68	3264 → 1322
67	1872.4	1.0	1.80	C → 6062

[a]Energies are corrected for recoil.

[b]Error in intensity measurements ranges from 10% to strong lines to about 50% for weak transitions.

[c]C stands for capture state. Assignments in parentheses are tentative.

[d]Tentative level.

[e]Poor energy fit.

[f]Intensity imbalance

TABLE 3-10

The Q-Value for the $^{31}P(n,\gamma)^{32}P$ Reaction

E_1	E_2	Sum
1872.4 (1.0)	6062.3 (0.5)	7934.7 (1.1)
2157.0 (1.2)	5778.4 (0.7)	7935.4 (1.4)
2586.2 (0.5)	5349.1 (1.2)	7935.3 (1.3)
3275.0 (0.6)	4660.9 (1.2)	7935.9 (1.3)
4491.7 (0.5)	3444.9 (0.8)	7936.6 (0.9)
5195.0 (0.7)	2740.1 (1.0)	7935.1 (1.2)
5277.4 (0.8)	2657.4 (0.5)	7934.8 (0.9)
7935.7 (0.5)	0	7935.7 (0.5)

Weighted average = 7935.5 $\pm$ 0.3 keV

All the energies are in keV and the numbers in parantheses are errors in the energies.

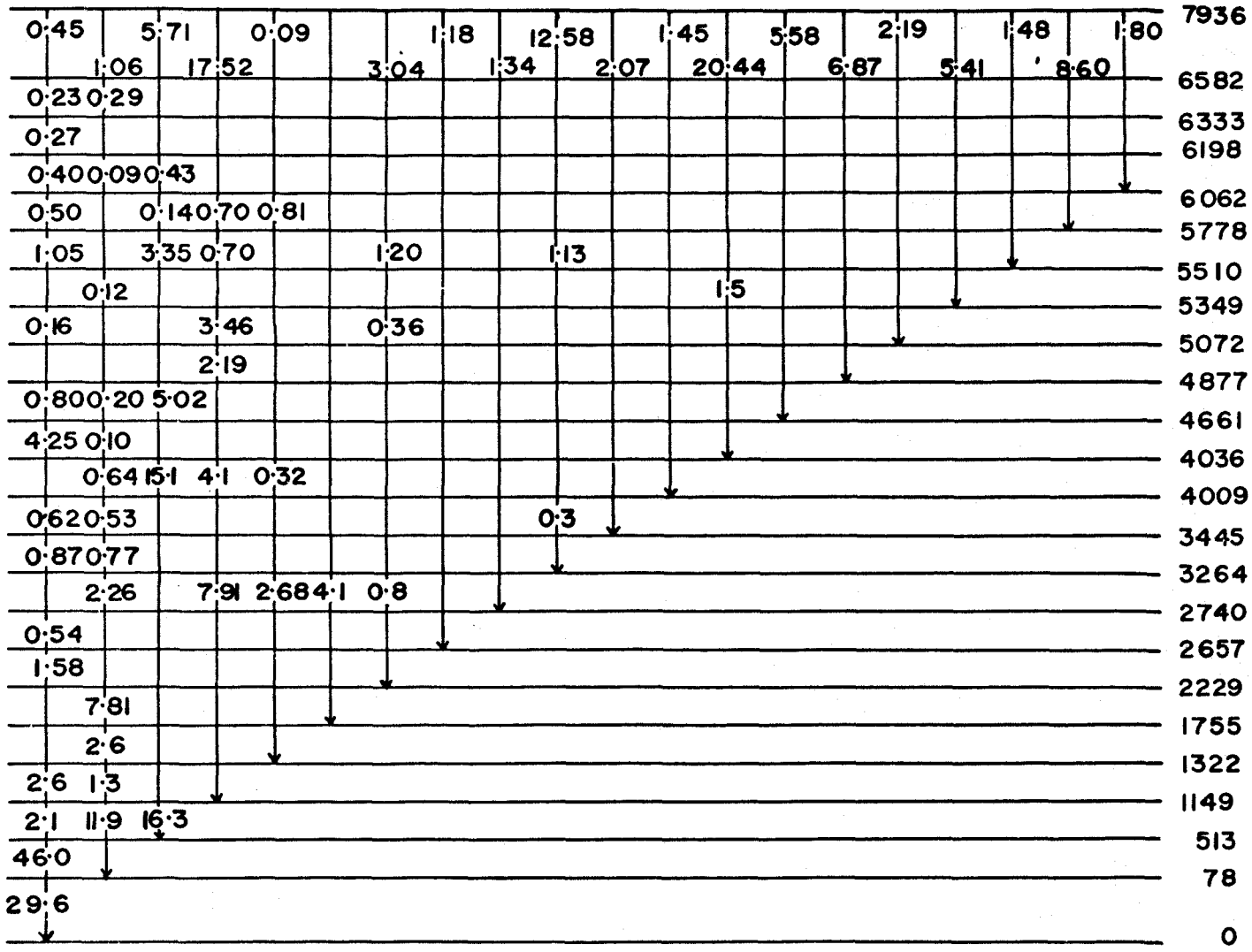

^{32}P

Fig. 3-6 The decay scheme of ^{32}P.

3.3.3. Discussion of the Decay Scheme

The proposed decay scheme is illustrated in Fig. 3.6. The levels of ^{32}P observed to be excited are listed in Table 3-11 along with their de-excitation modes and intensity balance, where possible.

In the present work, no evidence could be found for the excitation of the 6599 keV level observed by van Middelkoop[Va 67] or the 6708 and 5700 keV levels seen by Lycklama and Kennett[Ly 67]. The 4944 keV gamma ray seen by the previous investigators[Va 67, Ly67], and assigned as 4944 → 0 keV transition, would be masked in the present work by the 4945 keV transition from $^{12}C(n,\gamma)^{13}C$ reaction in the graphite sample holder. However, no primary transition to the 4944 keV level could be observed in this work.

Following the arguments of Lycklama and Kennett[Ly 67], the 5716.9 keV transition has been assigned as a primary transition to a tentative level at 2219 keV. No gamma ray de-exciting this level could be observed, but a 2219 → 0 keV transition would be masked by intense background radiation at 2223 keV arising from the $^{1}H(n,\gamma)^{2}H$ reaction.

Several new transitions are observed in the present work most of which are interpreted as second members of three step cascades. However, a weak primary transition to the 1322 keV level is seen for the first time. Also observed is a 2740 → 0 keV transition which accounts, in part, for the de-excitation of the level.

TABLE 3-11

The Decay Modes of ^{32}P Levels

Level energy (keV)	De-excitation Modes (Intensity)	Intensity balance I_{in}/I_{out}
6582	G(0.23), 78(0.29)	-/0.52
6333	G(0.27)	-/0.27
6198	G(0.40), 78(0.09), 513(0.43)	-/0.92
6092	G(0.50), 513(0.14), 1149(0.70),	1.80/1.52
5778	G(1.05), 513(3.35), 1149(0.70	8.60/7.43
	2229(1.20),3264(1.13)	
5510	78(0.12), 4036(1.5)[a]	1.48/1.62
5349	G(0.16),1149(3.46), 2229(0.36),	5.41/5.14
	3321(1.16)	
5072	1149(2.19)	2.19/2.19[b]
4877	G(0.80), 78(0.20), 513(5.02)	6.87/6.02
4661	G(4.25), 78(0.10)	5.58/4.35
4036	78(0.64),513(15.08), 1149(4.10)	21.94/20.14
	1322(0.32)	
4009	G(0.62), 78(0.53), 3264(0.3)[a]	1.45/1.45[b]
3445	G(0.87), 78(0.77)	2.07/1.64
3264	78(2.26), 1149(791), 1322(2.68),	14.01/17.75
	1755(4.1)[a], 2229(0.8)[a]	
2740	G(0.54)	1.34/0.54
2657	G(1.58)	1.18/1.58

TABLE 3-11 CONTINUED

Level energy (keV)	De-excitation Modes (Intensity)	Intensity balance I_{in}/I_{out}
2229	78(7.81)	5.40/7.81
1755	78(2.6)[a]	4.1 /2.6
1322	G(2.6)[a], 78(1.3)[a]	3.27/3.9
1149	G(2.1)[a], 78(11.9)[a], 513(16.3)[a]	36.58/30.3
513	G(46.0)[c]	
78	G(29.6)[c]	

[a]Transitions taken from the work of Lycklama and Kennett (Ly 67).

[b]Balance obtained by suitable division of intensity of transtion interpreted as having more than one component.

[c]Intensity calculated by balance.

Hardy et al[Ha 70] identified a 5071 ± 40 keV level in ^{32}P as the first T = 2 state with $J^{\pi} = 0^{+}$. Recently, Adelberger and Balamuth[Ad 71] have studied the decay of this state using $^{30}Si(^{3}He,p\gamma)^{32}P$ reaction. They concluded that this is the 5072 keV level seen in neutron capture studies and found the branching associated with the decay of this level to be 6.6, 85.6 and 7.8% to the 0, 1149 and 2229 keV levels respectively. In the present work only the strongest decay branch could be observed.

3.4 THE $^{19}F(n,\gamma)^{20}F$ REACTION

3.4.1 Review of Previous Work

The gamma radiation following thermal neutron capture in fluorine has been studied by several authors[Ba 67]. Nadjakov[Na 63] studied the reaction using a three crystal pair spectrometer and observed about 20 gamma rays. Recently, the reaction has been studied by Hardell and Hasselgren[Ha 68] and by Spilling et al[Sp 68] using Ge(Li) detectors.

The complimentary (d,p) reaction has also been extensively studied. Ajzenberg-Selove and Lauritsen[Aj 59] have summarized the information then available regarding the levels of ^{20}F. Several investigations of the $^{19}F(d,p)^{20}F$ reaction have been reported since then. Rout et al[Ro 63] studied the angular distribution of 21 proton groups upto an excitation energy of 4.3 MeV in ^{20}F. They obtained some new l_n values and modified some previous assignments. De Lopez[de 64]

studied the ground state and fourteen excited states of ^{20}F through the (d,p) reaction and found stripping patterns for twelve of the angular distributions. El-Behay et al(El 64) also studied the angular distribution of proton groups from $^{19}F(d,p)^{20}F$ reaction for a deutron energy range of 0.8 to 2.5 MeV. Recently, Rollefson et al(RO 70) have reported accurate excitation energies of ^{20}F levels from their study of $^{19}F(d,p)^{20}F$ and $^{18}O(He^3,p)^{20}F$ reactions. The angular distribution of protons from the $^{19}F(d,p)^{20}F$ reaction has been studied by Fortune et al(Fo 70, Fo 72) using 16 MeV deutrons. They have carried out a DWBA analysis and modified several previous l_n assignments.

The $^{19}F(d,p\gamma)^{20}F$ reaction has been recently studied by Holtebekk et al(Ho 69) using a Ge(Li) detector. They have studied single gamma ray spectra as well as proton-gamma coincidences and obtained accurate level energies upto an excitation energy of 4083 keV in ^{20}F.

Quin et al(Bi 67, Qu 67, Qu 70) have studied the directional correlation of gamma rays with protons in the $^{18}O(^3He, p\gamma)^{20}F$ reaction for several levels of ^{20}F upto 3 MeV in excitation. Finally, Fortune et al(Fo 71) have made some spin assignments in ^{20}F using the results of $^{18}O(^3He,p)^{20}F$, $^{19}F(d,p)^{20}F$ and $^{22}Ne(d,\alpha)^{20}F$ reactions.

3.4.2 Present Work

The recommended value for the thermal neutron capture cross-section for fluorine is 9.8 ± 0.7 mb[St 64]. The material used as target in the present study was teflon, $(C_2F_4)_n$. To get a maximum amount of teflon in the target position, the lower part of the sample holder was made out of teflon with no cavity. The total amount of teflon present in the irradiation position was about 16 g but only a fraction of it could be seen by the detector due to collimation. The total counting time for this experiment was 90 hours.

The observed gamma ray spectrum after thermal neutron capture in fluorine is shown in Fig. 3-7. The energies and intensities of identified transitions are listed in Table 3-12. The observed transition energies are in excellent agreement with the measurements of Spilling et al[Sp 68]. The intensities were put on an absolute scale by normalizing to the absolute intensities given by Spilling et al[Sp 68]. To do this the intensities of eight strong transitions were compared and the average of the ratios was used as the normalization factor. A decay scheme for ^{20}F was constructed using the present results and the measurements of Spilling et al[Sp 68] below 2.2 MeV.

The cascades C → 3587 → 0 and C → 3488 → 0 are the only two step ones for which both the members lie in the present range of energy measurement. Using these and the C → 0 transition, the Q-value for the $^{19}F(n,\gamma)^{20}F$ reaction was estimated to be 6601.2 ± 0.3 keV. Again, the error is enlarged

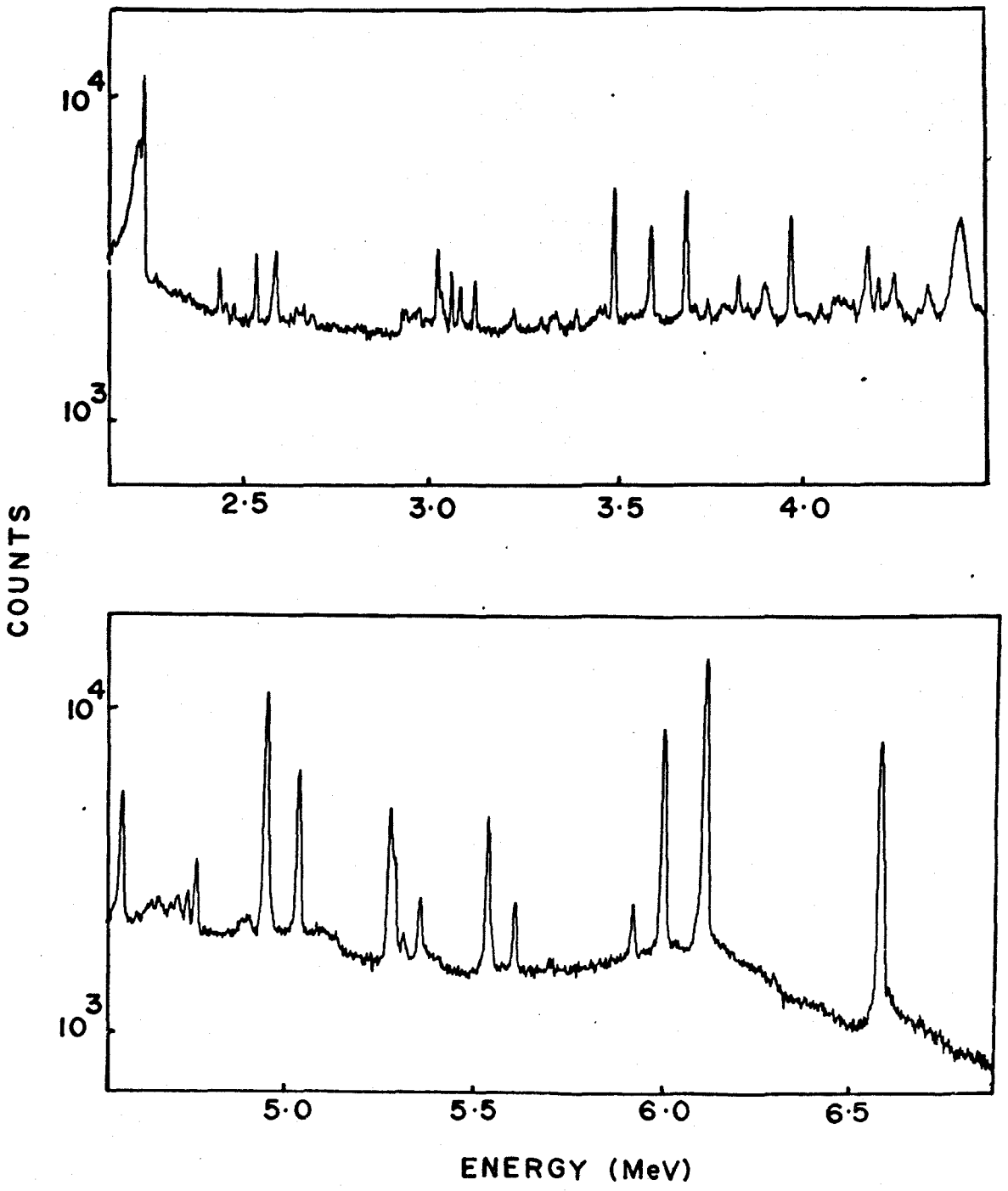

Fig. 3-7 The capture gamma ray spectrum of fluorine.

TABLE 3-12

The Observed Transitions in ^{20}F

No.	Transition[a] energy (keV)	Error in energy (keV)	Intensity[b] (Photons/100 captures)	Assignment[c]
1	6600.9	0.6	8.94	C → 0
2	6017.2	0.6	8.81	6017 → 0
3	5935.0	0.8	0.92	5436 → 0
4	5616.9	0.7	1.17	C → 984
5	5544.0	0.6	3.85	C → 1057
6	5362.1	0.8	1.12	6017 → 656
7	5317.8	1.1	0.41	5318 → 0
8	5291.9	0.9	2.05	C → 1309
9	5280.4	0.6	4.15	5936 → 656
10	5033.9	0.6	5.68	6017 → 984
11	4756.7	0.9	1.75	C → 1843
12	4734.6	0.9	0.74	6044 → 1309
13	4709.3	1.1	0.58	6017 → 1309
14	4657.9	0.9	0.49	(5715 → 1057)
15	4637.8	0.9	0.42	
16	4557.1	0.6	4.87	C → 2044
17	4538.2	1.1	0.39	
18	4342.9	1.4	0.45	
19	4333.0	1.1	0.72	

TABLE 3-12CONTINUED

No.	Transition[a] energy (keV)	Error in energy (keV)	Intensity[b] (Photons/100 captures)	Assignment[c]
20	4313.1	1.1	0.22	(4313 → 0)
21	4245.3	0.8	1.13	(5555 → 1309)
22	4236.6	1.3	0.50	
23	4201.2	0.7	0.90	6044 → 1843
24	4173.7	0.8	2.09	6017 → 1843
25	4163.7	1.1	0.49	
26	3965.0	1.0	4.24	5936 → 1971
27	3904.9	1.4	0.70	
28	3893.8	0.9	1.09	5936 → 2044
29	3823.5	0.8	1.13	6017 → 2195
30	3740.2	0.8	0.46	5936 → 2195
31	3587.3	0.6	4.55	3587 → 0
32	3488.0	0.6	7.89	3488 → 0
33	3448.5	1.9	0.62	
34	3387.5	1.3	0.64	
35	3332.2	1.3	0.50	
36	3321.3	1.3	0.50	
37	3292.8	1.4	0.37	(4277 → 984
38	3218.9	1.1	0.76	(4277 → 1057)
39	3112.7	0.6	2.35	C → 3488

TABLE 3-12 CONTINUED

NO.	Transition[a] energy (keV)	Error in energy (keV)	Intensity[b] (Photons/100 captures)	Assignment[c]
40	3074.9	0.8	2.00	C → 3526
41	3051.4	0.8	2.84	6017 → 2966
42	3025.4	1.3	1.43	3680 → 656
43	3015.1	0.6	4.50	C → 3587
44	2993.6	1.9	0.55	
45	2982.6	1.9	0.59	3965 → 984
46	2965.6	1.9	1.11	2966 → 0
47	2954.4	1.9	0.79	
48	2944.0	1.9	0.63	
49	2931.5	1.9	0.97	3587 → 656
50	2921.6	1.9	0.94	C → 3680
51	2684.8	1.9	0.57	
52	2678.1	1.9	0.61	
53	2656.2	1.9	0.92	3965 → 1309
54	2637.6	1.6	0.77	C → 3965
55	2529.3	0.6	6.34	6017 → 3488
56	2468.8	1.1	1.19	3526 → 1057
57	2447.1	1.4	1.06	5936 → 3488
58	2430.0	0.6	4.83	6017 → 3587, 3488 → 1057
59	2257.0	1.9	1.27	5936 → 3680

TABLE 3-12CONTINUED

[a]Energies are corrected for recoil losses.

[b]Error in intensity measurements ranges from 10% for strong lines to about 50% for weak transitions. See text for possible error in normalization.

[c]C stands for capture state. The assignments in parantheses are tentative.

to 0.5 keV to account for any possible systematic error in the calibration energies. The present estimate of 6601.2 ± 0.5 keV is in excellent agreement with the 6601.1 ± 0.3 keV value given by Spilling et al[Sp 68] and the 6602.0 ± 0.6 keV result of Hardell and Hasselgren[Ha 68]. The following results were then obtained:

$$\sum_i I_i(\text{Primary}) = 88\%$$

$$\sum_i E_i I_i / Q = 91\%$$

and

$$\sum_i I_i = 255\%$$

The first two expressions have an expected value of 100% if the intensity normalization is correct and all the components in the spectrum have been identified. Since the spectrum of ^{20}F is not very complicated, it can be assumed that the contribution of undetected components would be small. This suggests that the normalization is off by about 10%. Correcting for this, the multiplicity for the reaction is found to be 2.8.

3.4.3 Discussion of the Decay Scheme

The ground state spin and parity of ^{19}F are known to be $1/2^+$, therefore, dipole radiation after s-wave neutron capture would populate levels with spins 0, 1 and 2 in ^{20}F. The levels of ^{20}F observed to be excited by the

$^{19}F(n,\gamma)^{20}F$ reaction are listed in Table 3-13 alongwith their modes of decay and intensity balance.

The 5715 and 5555 keV levels have not been observed by Rollefson et al[Ro 70] but a 5.72 $\pm$ 0.02 MeV has been reported in previous (d,p) work[Aj 59]. No transitions populating the 5715 or 4313 keV levels could be observed. These three levels are, therefore, tentative.

The unassigned 1281.5 keV transition observed by Spilling et al[Sp 68] may be interpreted as the primary transition to 5318 keV level, which de-excites entirely by a single transition to the ground state.

It can be seen that about 50% of the transitions from the capture state lead to the highly excited states at 6017 and 5936 keV. The 5936 keV level is known to have negative parity on the basis of l_n assignment[Aj 59]. The 6017 keV level is also believed[Ha 68, Sp 68] to have negative parity because of the strong primary transition which is assumed to be E1 in character. This restricts the spin and parity assignments for these levels to 0^-, 1^- and 2^-. Both the levels decay to the first excited state at 656 keV which is known to have $J^\pi = 3^+$[Fo 71, Qu 70]. This would limit the spin and parity assignment for the 5936 and 6017 keV levels to 2^-, since a 1^- (or 0^-) assignment would require the 6017 $\rightarrow$ 656 and 5936 $\rightarrow$ 656 transitions to be M2 (or E3). The 2^- assignment for these levels is supported by the fact that both decay to the 2195 keV state which has been tentatively assigned

TABLE 3-13

The Decay Modes of ^{20}F Levels

Level energy (keV)	De-excitation Modes (Intensity)	Intensity balance I_{in}/I_{out}
6044	1309(0.74), 1843(0.90)	1.8/1.6
6017	G(8.81), 656(1.12), 984(5.68), 1309(0.58), 1843(2.09), 2195(1.13), 2966(2.84), 3488(6.34), 3587(3.96), 4082(1.1)[a]	34.0/33.7
5936	G(0.92), 656(4.15), 1971(4.24), 2044(1.09), 2195(0.46), 3488(1.06), 3680(1.27)	15.4/13.2
(5715)	1057(0.49)	-/10.5
(5555)	1309(1.13)	2.5/1.1
5318	G(0.41)	0.4/0.4
(4313)	G(0.22)	-/0.2
4277	984(0.37), 1057(0.76)	1.0/1.1
4082	2195(0.5)[a]	1.1/0.5
3965	984(0.59), 1309(0.92)	0.8/1.5
3680	656(1.43)	2.2/1.4
3587	G(4.55), 656(0.97), 2044(2.3)[a]	8.5/7.8
3526	1057(1.19)	2.0/1.2
3488	G(7.38), 1057(0.87), 1309(1.5)[a]	9.8/9.8[b]
2966	G(1.11), 823(2.0)[a]	2.8/3.1

TABLE 3-13CONTINUED

Level energy (keV)	De-excitation Modes (Intensity)	Intensity balance I_{in}/I_{out}
2195	G(0.7)[a], 823(1.3)[a]	2.1/2.0
2044	G(0.5)[a], 656(9.0)[a]	8.3/9.5
1971	G(1.0)[a], 823(2.3)[a], 1309(1.7)[a]	4.2/5.0
1843	G(6.5)[a]	4.7/6.5
1309	G(8.6)[a]	6.3/8.6
1057	G(9.1)[a]	6.6/9.1
984	G(12.8)[a]	9.0/12.8
823	G(2.0)[a], 656(3.7)[a]	5.6/5.7
656	G(20.4)[a]	20.4/20.4

[a]Transitions taken from the work of Spilling et al (Sp 68).

[b]Balance obtained by suitable division of intensity of transition interpreted as having more than one component.

$J^{\pi} = (3^+)$ (Fo 72) and that neither has a decay branch to the 3526 keV state which has $J^{\pi} = 0^+$ (Fo 71). The 6017 keV level also decays to 2966 keV state which has been tentatively assigned $J^{\pi} = (3^+)$ (Fo 72).

The (n,γ) results are not in disagreement with the $J^{\pi} = (3^+)$ assignment for 2195 and 2966 keV levels since no primary transition to these levels is observed.

3.5 THE $^{23}Na(n,\gamma)^{24}Na$ REACTION

3.5.1 Review of Previous Work

The $^{23}Na(n,\gamma)^{24}Na$ reaction has been investigated by several authors (Ba 67). Greenwood (quoted as private communication in Ba 67, En 67) studied the gamma ray spectrum using a Ge(Li) detector and proposed a decay scheme. Nichol et al (Ni 69) have also reported the energies and intensities of transitions, following thermal neutron capture in ^{23}Na, observed with a Ge(Li) detector.

The $^{23}Na(d,p)^{24}Na$ reaction has been studied by Sperduto and Buechner (Sp 52) who reported the excitation energies in ^{24}Na. Daum (Da 63) studied the angular distribution of proton groups from the (d,p) reaction on sodium. He was able to assign some l_n values and extract spectroscopic factors for some levels. The information on the energy levels of ^{24}Na, available at the time has been summarized in the review work of Endt and van der Leun (En 67). Since then, three new low-lying levels have been reported to be observed in ^{24}Na. A

level at 1.50 MeV was reported by Teterin et al[Te 68] from their study of $^{26}Mg(d,\alpha)^{24}Na$ reaction. At about the same time Jahr et al[Ja 67] reported observing a level at 1508 ± 10 keV using the same reaction. Two new levels have been recently observed by Keverling Buisman et al[Ke 71] at 1344.4 ± 0.3 keV and 2905 ± 15 keV from their study of the $^{26}Mg(d,\alpha\gamma)^{21}Na$ reaction.

McDonald et al[Mc 69] assigned $J^{\pi} = 1^{+}$ to the 1347 keV level from the results of the study of the beta decay of ^{24}Na. Several spin and parity assignments have been made by Keverling Buisman et al[Ke 71] for the low lying levels of ^{24}Na.

3.5.2 Present Work

In this investigation, 2.8 g of reagent grade Na_2CO_3 served as the target and the total counting time was about 54 hours. The thermal neutron capture cross section for ^{23}Na is reported to be 534 ± 5 mb[St 64].

The observed gamma ray spectrum after thermal neutron capture in sodium is shown in Fig. 3.8. The energies and intensities of identified transitions are listed in Table 3-14. Most of the observed transitions have been placed in a decay scheme constructed on the basis of level information from other reactions, energy precision and intensity balance.

The normalization of intensities was carried out using the 2754 keV gamma ray from ^{24}Mg after the beta decay of ^{24}Na. The contribution of the C → 4207 keV transition to this line

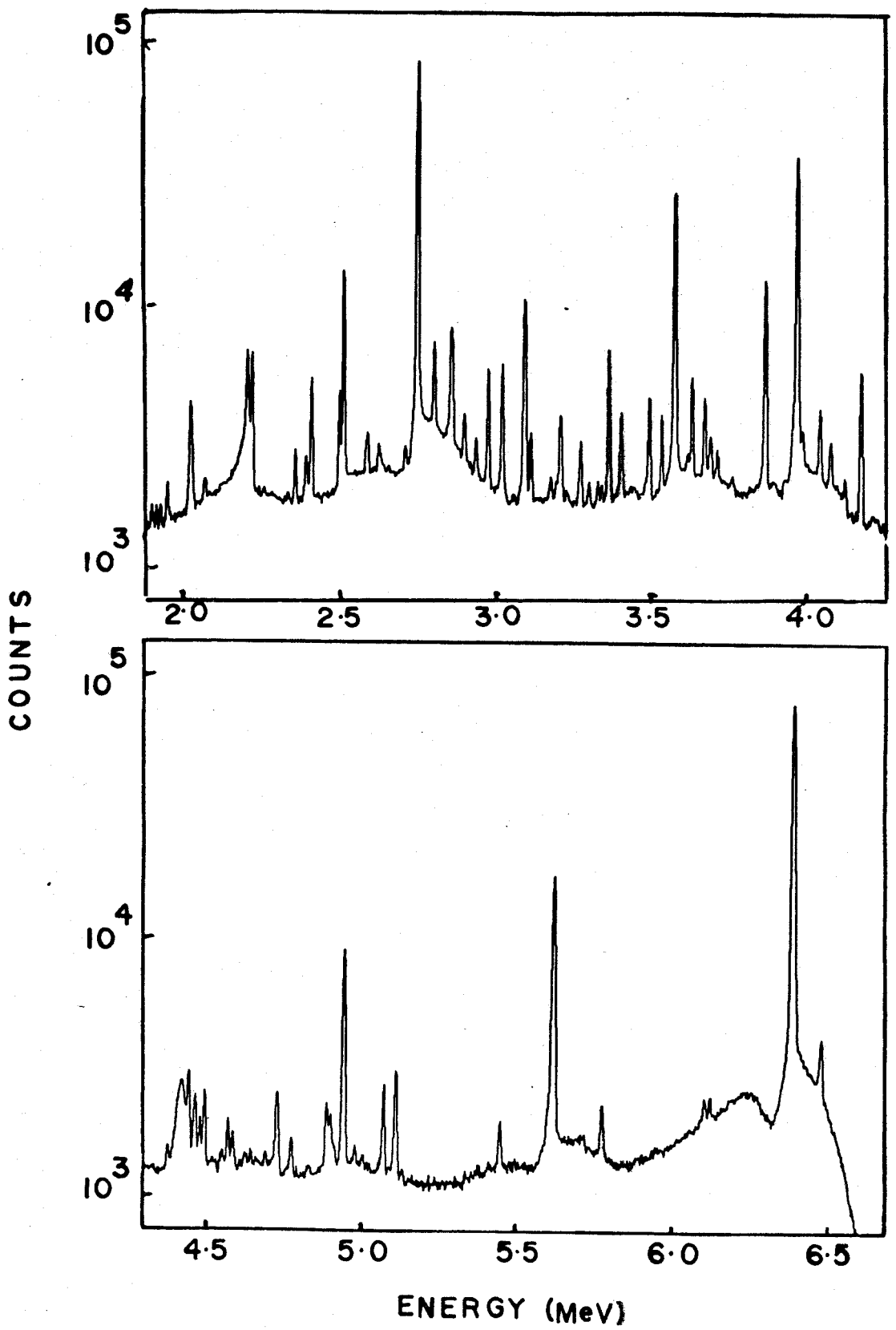

Fig. 3-8 The capture gamma ray spectrum of sodium.

TABLE 3-14

The Observed Transitions in ^{24}Na

No.	Transition[a] energy (keV)	Error in energy (keV)	Intensity[b] (Photons/100 captures)	Assignment[c]
1	6486.5	0.7	0.46	C → 472
2	6395.8	0.5	21.85	C → 563
3	6128.9	0.8	0.13	
4	5774.6	0.8	0.24	
5	5617.8	0.5	4.44	C → 1341
6	5600.0	1.0	0.24	
7	5446.4	0.7	0.17	C → 1513
8	5113.3	0.5	0.55	C → 1846
9	5073.7	0.5	0.44	C → 1885
10	5007.1	1.2	0.04	(5481 → 472
11	4903.6	0.8	0.22	
12	4891.6	1.0	0.31	
13	4775.4	0.8	0.16	(5247 → 472)
14	4731.4	1.2	0.33	(6072 → 1341)
15	4725.0	2.3	0.11	(6072 → 1347)
16	4585.4	0.8	0.17	(5060 → 472)[d]
17	4571.8	0.8	0.34	5045 → 472
18	4553.1	1.2	0.09	
19	4496.2	0.7	0.44	5060 → 563

TABLE 3-14 CONTINUED

No.	Transition[a] energy (keV)	Error in energy (keV)	Intensity[b] (Photons/100 captures)	Assignment[c]
20	4481.7	0.8	0.26	5045 → 563
21	4464.8[m]		0.40	
22	4445.9	1.2	0.61	C → 2514
23	4376.2	0.8	0.12	
24	4187.8	0.5	1.62	4751 → 563
25	4136.6	0.8	0.18	(5481 → 1344
26	4109.3	1.2	0.04	
27	4089.9	1.0	0.40	4561 → 472
28	4056.1	0.8	0.72	C → 2904
29	3998.1	0.8	0.43	4561 → 563
30	3982.0	0.5	15.10	C → 2978
31	3905.3	2.3	0.08	(5247 → 1341)
32	3878.6	0.5	4.92	4442 → 563
33	3771.9	2.3	0.09	
34	3723.4	1.6	0.27	
35	3702.5	1.2	0.50	3045 → 1341, 1344
36	3644.0	0.7	1.63	4207 → 563
37	3630.0	2.3	0.38	
38	3588.4	0.5	13.37	C → 3372
39	3546.6	0.5	1.03	C → 3413

TABLE 3-14 CONTINUED

No.	Transition[a] energy (keV)	Error in energy (keV)	Intensity[b] (Photons/100 captures)	Assignment[c]
40	3505.2	0.8	1.53	3977 → 472
41	3414.0	1.0	0.99	3977 → 563
42	3408.8	1.6	0.59	4751 → 1341, 1344
43	3370.3	0.7	2.99	C → 3589
44	3344.7	1.2	0.19	
45	3331.8	1.2	0.24	
46	3304.0	1.2	0.23	
47	3278.2	0.8	0.84	
48	3213.1	1.8	1.03	5060 → 1846
49	3117.5	0.7	1.01	3589 → 472
50	3099.4	1.0	5.10	4442 → 1341,1344
51	3094.8	1.6	3.19	4442 → 1347
52	3026.3	0.5	3.07	3589 → 563
53	2982.5	0.5	2.83	C → 3977
54	2941.6	0.7	0.75	3413 → 472
55	2905.0	0.7	1.10	4751 → 1846 , 2904 → 0
56	2862.1[m]		5.53	4207 → 1344, 1347
57	2808.5	0.5	2.96	3372 → 563
58	2753		10.82	C → 4207
59	2716.3	0.8	0.59	

TABLE 3-14CONTINUED

No.	Transition[a] energy (keV)	Error in energy (keV)	Intensity[b] (Photons/100 captures)	Assignment[c]
60	2637.4	2.3	0.29	3977 → 1341
61	2630.7	1.2	0.69	3977 → 1347
62	2595.6	1.2	1.02	4442 → 1846
63	2588.7	1.6	0.42	
64	2518.3	0.5	13.53	C → 4442
65	2505.8	0.7	3.41	2978 → 472
66	2414.9	0.5	4.78	2972 → 563
67	2399.2	1.0	1.12	C → 4561
68	2392.9	1.8	0.50	
69	2361.6	0.7	1.66	4207 → 1846
70	2338.5	1.2	0.32	
71	2071.2	0.8	1.60	
72	2030.5	1.0	3.13	3372 → 1341
73	2025.8	1.0	7.67	3372 → 1347
74	1950.4	0.7	2.36	2514 → 563
75	1928.6	0.8	0.98	4442 → 2514
76	1914.2	0.8	1.20	C → 5045
77	1899.1	1.0	1.48	C → 5060

TABLE 3-14 CONTINUED

[a]Energies are corrected for recoil losses.

[b]Error in intensity measurements ranges from 10% for strong lines to about 50% for weak transitions.

[c]C stands for capture state. The assignments in parentheses are tentative.

[d]Poor energy fit.

[m]Unresolved multiplet.

was estimated by looking at the depopulation of the 4207 keV level. After subtraction of the C → 4207 keV transition component, the remaining intensity was normalized to the expected value after correction for half-life.

To estimate the Q-value for the $^{23}Na(n,\gamma)^{24}Na$ reaction, the excitation energies of levels in ^{24}Na were taken from the review work of Endt and van der Leun[En 67]. A weighted average of the ten cascade pair sums (Table 3-15) yielded a result of 6959.4 ± 0.2 keV. As in the previous cases the error is enlarged to 0.5 keV to account for any possible systematic errors in the calibration energies. The present estimate of 6959.4 ± 0.5 keV is in excellent agreement with the 6959.3 ± 0.4 keV value of Greenwood[Gr 66] and 6960.3 ± 1.5 keV result of Nichol et al[Ni 69]. The present result is also in agreement with the 6961.5 ± 3.0 keV value reported by Endt and van der Leun[En 67] based on the nuclear mass compilations of Mattauch et al[Ma 65].

As a check on intensity normalization, the sum of intensities of the primary transitions and the expression $\sum_i E_i I_i/Q$ were evaluated. These were found to be 96% and 103% respectively, showing good agreement. The multiplicity of the $^{23}Na(n,\gamma)^{24}Na$ reaction was estimated to be 3.8.

3.5.3 Discussion of the Decay Scheme

The ground state spin and parity of ^{23}Na are known to be $3/2^+$. Thus s-wave capture would populate levels

TABLE 3-15

The Q-Value for the $^{23}Na(n,\gamma)^{24}Na$ Reaction

E_1		E_2		Sum	
6486.5	(0.7)	472.31	(0.15)	6958.8	(0.7)
6395.8	(0.5)	563.31	(0.15)	6959.1	(0.5)
5113.3	(0.5)	1846.1	(0.3)	6959.4	(0.6)
5073.7	(0.5)	1885.4	(0.3)	6959.1	(0.6)
3982.0	(0.5)	2977.6	(0.3)	6959.6	(0.6)
3588.4	(0.5)	3371.7	(0.3)	6960.1	(0.6)
3370.3	(0.7)	3589.1	(0.3)	6959.4	(0.8)
2982.5	(0.5)	3977.2	(0.3)	6959.7	(0.6)
2518.3	(0.5)	4441.6	(0.3)	6959.9	(0.6)
1914.2	(0.8)	5044.7	(0.4)	6958.9	(0.9)

Weighted average = 6959.4 $\pm$ 0.2

All the energies are in keV and the figures in bracket are the errors associated with the energies.

with spins 1 and 2 in ^{24}Na and dipole radiation from capture state would lead to final states with spins 0 to 3. The levels of ^{24}Na observed to be populated are listed in Table 3-16 alongwith their modes of decay and intensity balance where possible.

Several transitions have been assigned as populating more than one members of the triplet at 1.34 MeV because on the basis of present energy precision a unique assignment was not possible. It can be seen in Table 3-16 that a good combined intensity balance is obtained for the 1341, 1344 and 1347 keV levels. However, if the 780.9 and 1344.5 keV transitions observed by Greenwood (En 67) are not interpreted as 1344 → 563 and 1344 → 0 keV transitions, an obvious intensity imbalance would result. This supports the existence of the 1344 keV level.

The 5446.4 keV transition has been interpreted as C → 1513 keV. Keverling Buisman et al (Ke 71) have assigned $J^{\pi} = (3,5)^{+}$ to the 1510 ± 10 keV state. If the present assignment of 5446.4 keV transition is valid, it would rule out spin 5 for the final state.

The 2514 keV level is observed to be populated from capture and 4442 keV states and the only decay mode observed leads to 563 keV, which is in agreement with the results of Keverling Buisman et al (Ke 71).

The C → 4751 keV transition could not be isolated in the observed spectrum due to interference by the radiation arising from neutron capture in hydrogen.

TABLE 3-16

The Decay Modes of ^{24}Na Levels

Level energy (keV)	De-excitation Modes (Intensity)	Intensity balance I_{in}/I_{out}
(6072)	1341(0.33), 1347(0.11)	-/0.44
(5481)	472(0.04), 1344(0.18)	-/0.22
(5247)	472(0.16), 1341(0.08)	-/0.24
5060	472(0.18), 563(0.44), 1846(1.03)	1.48/1.65
5045	472(0.34), 563(0.26), 1341-44(0.50	1.20/1.10
4751	563(1.62, 1846(1.0)	-/2.62
4561	472(0.40), 563(0.43), 1341-44(0.59)	1.12/1.42
4442	563(4.92), 1341-44(5.10), 1347(3.19), 1846(1.02), 2514(0.98)	13.53/15.21
4207	563(1.63), 1344-47(5.53), 1846(1.66) 3372(2.0)[a]	-/10.82
3977	472(1.53), 563(0.99), 1341(0.29), 1347(0.69)	2.83/3.50
3589	472(1.01), 563(3.07)	2.99/4.08
3413	472(0.75)	1.03/0.75
3372	563(2.96), 1341(3.13), 1347(7.67)	13.37/13.76
2978	472(3.41), 563(4.78), 1341(6.3)[a]	15.10/14.49
2904	G(0.10)[c]	

TABLE 3-16CONTINUED

Level energy (keV)	De-excitation Modes (Intensity)	Intensity balance I_{in}/I_{out}
2514	563(2.36)	1.59/2.36
1885	563(1.9)[a]	0.44/1.9
1846	472(4.0)[a], 563(1.5)[a], 1347(2.2)[a]	5.26/7.7
1513	G(0.17)[c]	
1347	472(14)[a]	40.0/41.8[b]
1344	G(4.0)[a], 563(3.8)[a]	
1341	472(20)[a]	
563	G(1.1)[a], 472(51.4)[c]	
472	G(97.7)[c]	

[a]Transitions observed by Greenwood (En 67).

[b]Combined intensity balance for 1341, 1344 and 1347 keV levels.

[c]Intensity calculated by balance.

3.6 THE $^{39}K(n,\gamma)^{40}K$ REACTION

3.6.1 Reciew of Previous Work

The $^{39}K(n,\gamma)^{40}K$ reaction has been the subject of several investigations[Ba 67]. Recently, studies of the reaction have been reported by Johnson and Kennett[Jo 70] and by Op den Kamp and Spits[Op 72]. The latter used natural as well as enriched ^{39}K targets.

The $^{39}K(d,p)^{40}K$ reaction has been studied by Enge et al[En 59] and the information on the levels of ^{40}K available at the time has been summarized by Endt and van der Leun[En 67] Main et al[Ma 68a] measured the lifetime of the 1644 kev level in ^{40}K to be 0.49 ± 0.01 μs and concluded that the level was most likely to have $J^{\pi} = 0^{+}$. Twin et al[Tw 69, Tw 70], from their study of the $^{40}Ar(p,n\gamma)^{40}K$ reaction, confirmed the above assignment and made some other spin and parity assignments for the low lying levels of ^{40}K. The $^{39}K(d,p\gamma)^{40}K$ reaction has recently been studied by Freeman and Gallmann[Fr 70].

The $^{40}K(n,\gamma)^{41}K$ and $^{41}K(n,\gamma)^{42}K$ reactions have been studied by Beckstrand and Shera[Be 71a] and by Skeppstedt[Sk 69] respectively.

3.6.2 Present Work

Natural potassium consists of three isotopes, ^{39}K, ^{40}K and ^{41}K, having abundances of 93.1%, 0.1% and 6.9% respectively. The thermal neutron capture cross sections for

these isotopes are reported to be 1.94 ± 0.15 b, 70 ± 20 b and 1.24 ± 0.10 b respectively[Ba 67]. The contributions of the $^{39}K(n,\gamma)^{40}K$, $^{40}K(n,\gamma)^{41}K$ and $^{41}K(n,\gamma)^{41}K$ reactions in a natural target are 95%, 0.4% and 4.6% respectively.

In this experiment, 2.9 g of reagent grade K_2CO_3 served as the target and the total counting time was 53 hours. The observed gamma ray spectrum after thermal neutron capture in potassium is shown in Fig. 3-9. Among the identified transitions, some could be attributed to the $^{41}K(n,\gamma)^{42}K$ reaction[Sk 64]. These are listed in Table 3-17. No contribution from the $^{40}K(n,\gamma)^{41}K$ reaction[Be 71a] could be found in the observed spectrum. The remaining transitions have, therefore, been assigned to the $^{39}K(n,\gamma)^{40}K$ reaction. These are listed in Table 3-18.

While the analysis of the present data was in progress, the results of Op den Kamp and Spits[Op 72] became available in print. No attempt has been made here to construct a new decay scheme. Most of the assignment in Table 4-10 are from their work, although a few assignments made by Johnson and Kennett[Jo 70] have been retained. It will be shown later that some changes in the decay scheme may be necessary.

The Q-value for the $^{39}K(n,\gamma)^{40}K$ reaction was calculated using the cascade sums shown in Table 3-19. The result obtained is 7799.5 ± 0.4 keV but the error would be quoted as 0.5 keV, as in the previous cases. The present result is in agreement with the 7799.7 ± 0.8 keV value of Op den Kamp and

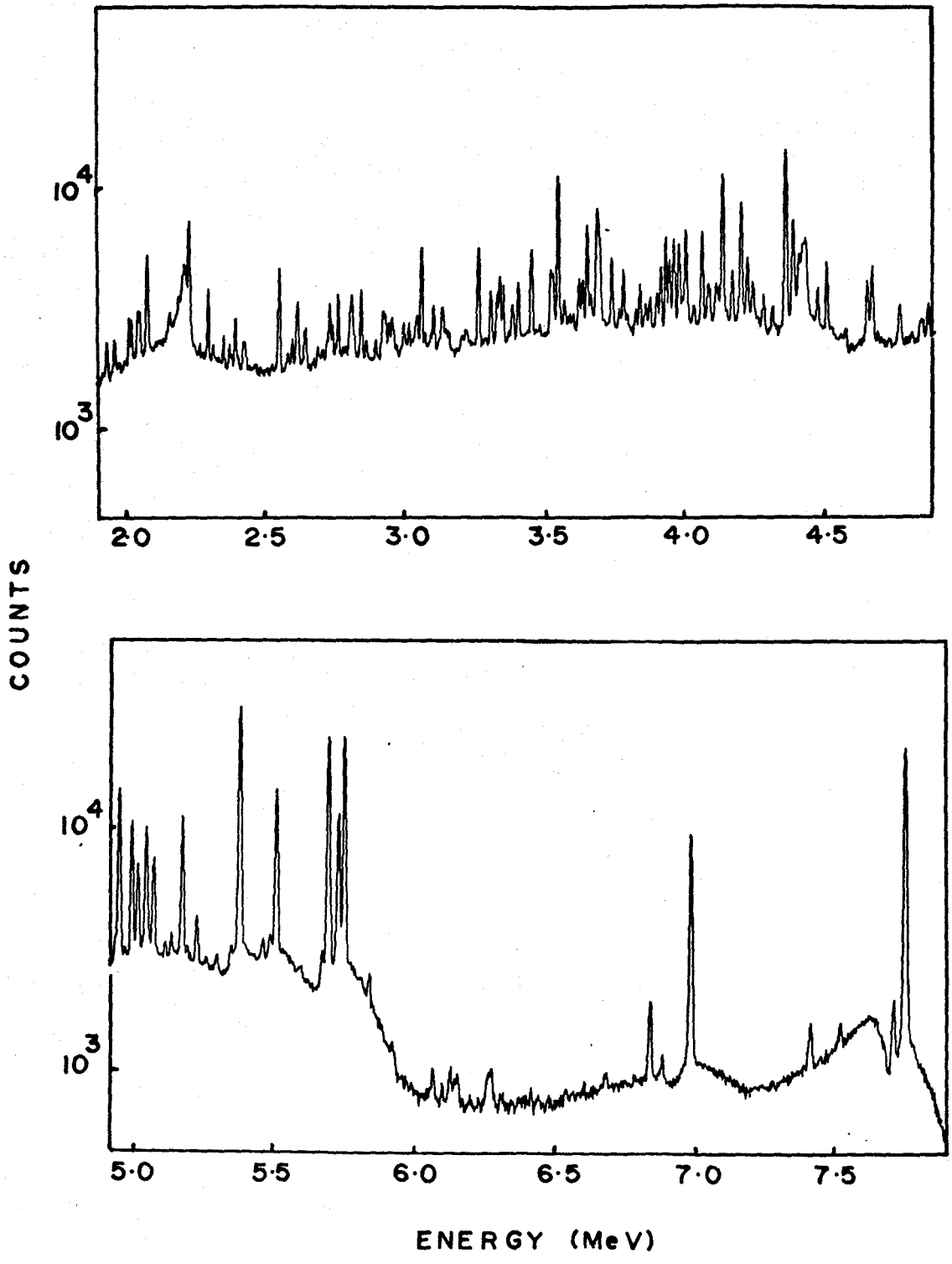

Fig. 3-9 The capture gamma ray spectrum of potassium.

TABLE 3-17

The Transitions Attributed to ^{42}K

No.	Gamma ray energy (keV)	Error in energy (keV)	Relative intensity
1	7534.3	0.8	0.9
2	7427.3	0.8	1.7
3	6853.7	1.0	3.1
4	6690.3	2.3	0.4
5	6278.7	0.8	1.0
6	6267.8	1.2	0.8
7	6156.9	0.8	0.7
8	5672.2	0.7	3.0
9	5488.1	1.2	1.9
10	5459.8	1.2	1.4
11	5295.2	0.7	1.3
12	5132.9	0.8	1.9
13	5109.8	1.0	0.9
14	4905.5	1.2	0.7

TABLE 3-18

The Observed Transitions in ^{40}K

No.	Transition[a] energy (keV)	Error in energy (keV)	Intensity[b] (Photons/100 captures)	Assignment[c]
1	7770.2	0.5	6.88	C → 30
2	6999.9	0.5	2.73	C → 800
3	6894.0	1.0	0.08	
4	6846.1	1.2	0.16	
5	6144.0	0.8	0.05	
6	6129.7	1.0	0.08	
7	6099.9	1.0	0.03	
8	6068.4	1.0	0.08	
9	5921.2	1.0	0.08	
10	5839.0	1.0	0.16	C → 1960
11	5752.4	0.5	6.68	C → 2048
12	5730.1	0.5	2.83	C → 2070
13	5696.3	0.5	6.68	C → 2104
14	5510.1	0.5	3.70	C → 2290
15	5380.3	0.5	9.14	C → 2419
16	5345.1	0.8	0.18	
17	5257.6	1.0	0.07	
18	5224.0	0.5	0.47	C → 2576
19	5173.5	0.5	2.73	C → 2626

TABLE 3-18 CONTINUED

No.	Transition[a] energy (keV)	Error in energy (keV)	Intensity[b] (Photons/100 captures)	Assignment[c]
20	5068.6	0.7	1.51	C → 2731
21	5043.0	0.5	2.31	C → 2757
22	5013.2	0.5	1.36	C → 2787
23	4991.8	0.5	2.57	C → 2808
24	4963.3	0.8	0.10	
25	4930.4	1.6	0.24	
26	4873.2	0.7	0.31	
27	4852.9	2.3	0.17	C → 2948
28	4843.6	2.3	0.14	
29	4769.7	0.5	0.39	
30	4671.1	0.5	0.91	C → 3129
31	4654.0	0.5	0.66	C → 3146
32	4507.8	0.7	0.89	4538 → 30
33	4474.2	0.5	0.47	
34	4405.6	0.8	0.83	C → 3394
35	4385.8	0.5	1.96	C → 3414
36	4360.9	0.5	4.87	C → 3439
37	4313.7	0.7	0.29	C → 3486
38	4280.6	0.7	0.35	(4281 → 0)
39	4243.0	0.5	0.59	(4273 → 30)

TABLE 3-18 CONTINUED

No.	Transition[a] energy (keV)	Error in energy (keV)	Intensity[b] (Photons/100 captures)	Assignment[c]
40	4224.1	0.5	1.07	4253 → 30
41	4200.5	0.5	2.64	C → 3599
42	4169.8	0.5	0.84	C → 3630
43	4136.2	0.5	3.89	C → 3664
44	4112.2	0.7	0.59	
45	4085.0[m]		1.00	
46	4061.7	0.5	1.74	C → 3738
47	4031.9	0.7	0.23	
48	4002.5	0.5	1.88	C → 3797
49	3978.3	0.5	1.51	C → 3822
50	3960.3	0.5	1.69	C → 3840
51	3744.2	0.5	1.06	4744 → 800
52	3931.6	0.5	1.76	C → 3868
53	3912.0	0.5	1.01	C → 3888
54	3898.4	0.5	0.51	C → 3902
55	3875.3	1.6	0.42	C → 3923
56	3868.2	2.3	0.10	3868 → 0
57	3858.2	0.7	0.34	3888 → 30
58	3838.6	0.5	0.70	3868 → 30
59	3821.9	0.7	0.23	3822 → 0

TABLE 3-18 CONTINUED

No.	Transition[a] energy (keV)	Error in energy (keV)	Intensity[b] (Photons/100 captures)	Assignment[c]
60	3792.6	0.8	0.20	3822 → 30
61	3779.2	0.5	1.03	C → 4020
62	3764.8	0.8	0.24	
63	3737.6	0.5	1.40	4538 → 800
64	3696.5	1.0	1.43	C → 4104
65	3664.0	0.7	0.52	(3664 → 0, 4465 → 800)
66	3650.5	0.5	2.52	C → 4149
67	3635.1	2.3	0.74	
68	3630.9	1.8	0.72	3630 → 0
69	3620.0	0.5	0.93	
70	3599.5	0.8	0.18	(3599 → 0, 3630 → 30)
71	3586.4	1.0	0.22	
72	3569.5	0.5	0.50	3599 → 30
73	3546.6	0.5	5.37	C → 4253
74	3527.0	0.8	1.21	(C → 4273)
75	3519.5	0.8	1.21	(C → 4281)
76	3452.6	0.5	1.94	4253 → 800
77	3403.9	0.5	1.10	C → 4396
78	3383.2	0.8	0.60	3414 → 30
79	3349.4	0.5	1.17	4149 → 800

TABLE 3-18 CONTINUED

No.	Transition[a] energy (keV)	Error in energy (keV)	Intensity[b] (Photons/100 captures)	Assignment[c]
80	3336.7	0.7	1.35	C → 4465
81	3326.7	0.7	0.93	
82	3304.7	0.5	1.00	4104 → 800
83	3262.5	0.5	2.48	C → 4538
84	3216.7[m]		0.24	
85	3201.5[m]		0.23	
86	3153.3	0.7	0.31	
87	3144.2	0.7	0.33	
88	3130.4[m]		0.82	(3129 → 0, C → 4666)
89	3099.5	0.5	0.89	4744 → 1644
90	3089.7	0.7	0.25	3888 → 800
91	3069.1	0.7	0.32	
92	3055.9	0.5	2.92	C → 4744
93	3039.3	0.8	0.69	
94	3029.3	0.8	0.23	
95	3011.0	0.7	0.52	C → 4789
96	2993.3	0.5	0.54	C → 4807
97	2955.7	1.0	0.46	
98	2949.5	0.8	0.73	4908 → 1959
99	2938.8	0.7	0.65	

TABLE 3-18 CONTINUED

No.	Transition[a] energy (keV)	Error in energy (keV)	Intensity[b] (Photons/100 captures)	Assignment[c]
100	2926.6	0.8	0.90	
101	2918.8	0.8	0.96	2948 → 30
102	2892.6	0.5	0.33	C → 4908
103	2857.5	0.7	0.36	
104	2839.9	0.5	1.72	4909 → 2070
105	2813.7	1.2	0.61	
106	2805.9	0.8	1.58	
107	2799.2	1.0	0.79	3599 → 800
108	2785.7	0.8	0.24	2787 → 0
109	2775.2	0.8	0.24	
110	2757.0	0.5	1.64	2787 → 30
111	2736.6	0.5	0.74	4807 → 2070
112	2726.6	0.7	1.41	2757 → 30
113	2718.8	0.8	0.46	4789 → 2070
114	2702.5	0.7	0.26	(2731 → 30, 4807 → 2804)
115	2685.4	0.8	0.31	3486 → 800
116	2640.3	0.7	0.92	3439 → 800
117	2611.9	0.5	1.83	(3414 → 800, 4253 → 1644)
118	2594.1	0.5	0.73	3394 → 800
119	2576.8	0.8	0.39	(4538 → 1960, 2576 → 30)

TABLE 3-18 CONTINUED

No.	Transition[a] energy (keV)	Error in energy (keV)	Intensity[b] (Photons/100 captures)	Assignment[c]
120	2570.3	1.0	0.15	
121	2546.3	0.5	3.70	(2576 → 30, 3439 → 892)
122	2521.4	1.2	0.17	3414 → 892
123	2461.5	2.3	0.21	
124	2425.9	1.6	0.73	
125	2418.6	0.8	0.92	2419 → 0
126	2389.7	0.5	1.85	2419 → 30
127	2375.2	0.8	0.46	4666 → 2290
128	2368.8	0.7	0.80	2397 → 30
129	2347.7	0.5	1.13	(3146 → 800, 4744 → 2397)
130	2310.8	0.7	0.63	3110 → 800
131	2291.3	0.5	3.78	(4253 → 1960, 2290 → 0)
132	2271.5	1.0	0.40	(4666 → 2397)
133	2261.0	1.2	0.71	2290 → 30
134	2185.5	1.2	1.07	(2986 → 800, 4253 → 2070, 4744 → 2558)
135	2153.1	1.2	1.28	(3797 → 1644, 4908 → 2756)

TABLE 3-18 CONTINUED

No.	Transition[a] energy (keV)	Error in energy (keV)	Intensity[b] (Photons/100 captures)	Assignment[c]
136	2073.6	0.5	10.69	(2104 → 30, 2070 → 0)
137	2047.6	1.0	3.80	2048 → 0
138	2040.5	0.8	3.87	2070 → 30
139	2017.8	0.8	3.78	2048 → 30
140	2008.3	0.7	3.95	2808 → 800
141	1992.3	1.6	0.55	4253 → 2261
142	1973.8	1.6	0.71	4020 → 2047
143	1956.3	0.8	3.16	2756 → 800
144	1929.2	0.7	3.42	1960 → 30

[a] Energies are corrected for recoil losses.

[b] Error in intensity measurements ranges from 10% for strong lines to about 50% for weak transitions. See text for possible error in normalization.

[c] C denotes the capture state. The assignments in parantheses are tentative.

[m] Unresolved multiplet.

TABLE 3-19

The Q-Value for the $^{39}K(n,\gamma)^{40}K$ Reaction

5380.3	(0.5)	2418.6	(0.8)	7798.9	(0.9)
5013.2	(0.5)	2785.7	(0.8)	7798.9	(0.9)
4200.5	(0.5)	3599.5	(0.8)	7800.0	(0.9)
3978.3	(0.5)	3821.9	(0.7)	7800.2	(0.9)
3931.6	(0.5)	3868.2	(2.3)	7799.8	(2.4)

Weighted Average 7799.5 ± 0.4 keV

All the energies are in keV and the numbers in parantheses are the errors in the energies.

Spits[Op 72] but varies from the 7800.5 ± 0.2 keV result of Johnson and Kennett[Jo 70]. The present result is also in agreement with the 7801.5 ± 2.7 keV value given by Endt and van der Leun[En 67] based on the mass table compilation of Mattauch et al[Ma 65].

The intensities were put on an absolute scale by requiring that the sum of intensities of primary transitions equal 100%. The expression $\Sigma E_i I_i/Q$ was then evaluated using the results of Op den Kamp and Spits[Op 72] below 1.9 MeV. It was found to be 111%. The evaluation of the expression $\Sigma E_i I_i/Q$ for all the transitions reported by Op den Kamp and Spits[Op 72] gave a result of 112%. If it is assumed that no bias is introduced by the efficiency calibration curve and that all the transitions are due to $^{39}K(n,\gamma)^{40}K$ reaction, then this would indicate that all the primary transitions have not been identified. The present normalization is tentatively retained in Table 3-18.

The multiplicity of the $^{39}K(n,\gamma)^{40}K$ is estimated to be 3.9. This estimate is corrected for the assumed bias in the normalization of intensities.

Several new weak transitions have been observed between 5.9 and 6.9 MeV. These could be interpreted as "inverted transitions", i.e. transitions depopulating high excited states An extension of the (d,p) work in this excitation region would throw more light on this, since it would be almost impossible to detect the weak primaries associated with these transitions due to poorer signal to noise ratio at the low end of the gamma ray spectrum.

CHAPTER IV

TRANSITION STRENGTHS

The data regarding the primary transitions, in the nuclei studied, are presented in this chapter. A simple model is developed to estimate the bias introduced in the observed mean reduced intensities of these transitions due to branching. The average transition strengths are calculated for the E1 and M1 transitions for the nuclei studied.

4.1 Composite Capture State

If no resonance is present at thermal energies, then the capture cross-section is made up of contributions from neighboring resonances. In this case there is no well defined capture state and both spins ($I \pm 1/2$, where I is the spin of the target nucleus) are expected to contribute. In the case of zero target spin nuclei, the s-wave capture state can only be formed with spin 1/2 but again, more than one resonance may contribute. It has been correctly pointed out by previous authors (Ba 61, Mo 65) that if the capture state is composite then there is no real sense to partial radiation widths for individual primary transitions since they are not originating from a single level. The partial radiation widths could also be affected by interference between resonances and are expected to provide only an order of magnitude estimate for the

transition strength. However, an average over several individual radiation widths should still yield a realistic estimate of the mean reduced width for primary transitions.

It can be shown (Bo 70) that the interference between two resonances would be prominent only when the quantity,

$$\Gamma_{1f}\Gamma_{2f}\Gamma_{n1}\Gamma_{n2}\ (E_1E_2)^{-1}(E_2-E_1)^{-4}$$

is large. In this expression the subscripts 1 and 2 refer to the two resonances, Γ_f is the partial radiation width for the final state f and Γ_n and E are the neutron width and the energy of a resonance. It is evident that this quantity would be large only when the resonances are very closely spaced. Since the level density is low in the mass region of the present work, it can be assumed that the interference effects will be small. Also, the interference can be either constructive or destructive, therefore, the expectation value of the interference term will be zero if an average is taken over a large enough sample to obtain the mean reduced width.

If one can identify several M1 or E1 transitions, the corresponding mean reduced width can be calculated. However, the mean reduced width obtained in this manner, will be smaller than its true value because some of the observed transitions will be proceeding from only one of the possible capture spin states. More specifically, the final states with spins $I-\frac{3}{2}$ and $I+\frac{3}{2}$ can be populated by only one of the two capture spin states via dipole radiation, while final states with spins $I-\frac{1}{2}$ and $I+\frac{1}{2}$ can be reached from both the capture

spin states by dipole radiation. To estimate this lowering in the mean, one requires a knowledge of,

a. the relative populations of the two capture spin states, and

b. the relative level density for states with spin J (for $I-\frac{3}{2} \leq J \leq I+\frac{3}{2}$) in the final nucleus.

For the calculation of the lowering bias, it can be assumed that the two capture spin states have equal cross-sections. This is because the final result is not very sensitive to the relative populations and a change from 50-50 to 80-20 for relative populations changes it by only a few percent.

The relative level density for different spin values may be obtained using equation (1.20) and normalized such that

$$\sum_J R(J) = 1 \qquad (4.1)$$

where R(J) is the relative level density for spin J and the summation extends from $J = I-\frac{3}{2}$ to $J = I+\frac{3}{2}$. The relative strengths, S(J), of transitions to levels with spin J will (under the assumption of equal cross-sections for capture spin states) be 1 for $J = I\pm\frac{1}{2}$ and 0.5 for $J = I\pm\frac{3}{2}$.

The mean transition intensity, or the bias in the observed mean, is then given by,

$$\bar{S} = \sum_J S(J)\ R(J) \qquad (4.2)$$

where the summation extends again from $J = I-\frac{3}{2}$ to $J = I+\frac{3}{2}$. The observed mean should be divided by $\bar{S}$ to obtain the true mean.

In the above discussion it has been implicitly assumed that $I \geq 3/2$. If this is not the case, then one or more of the branches will disappear but the treatment will be similar.

The variance in the observed mean relative width may be calculated using the usual formula for a sample variance,

$$\sigma_x^2 = \frac{1}{N-1} \sum_{i=1}^{N} (x-x_i)^2 \qquad (4.3)$$

where $\bar{x}$ is the average of N estimates denoted by X_i. One can also estimate the expected variance in the mean reduced width. The total expected variance would be the sum of the variance of the distribution and the contribution of the branching. The contribution due to branching is given by:

$$\sigma_{Br}^2 = \{\sum_J (\bar{S}-S(J))R(J)\} / \bar{S}^2 \qquad (4.4)$$

for a mean of unity. The variance of to the distribution (assumed to be chi-squared with ν degrees of freedom) would be $\frac{2}{\nu}$ for a mean of unity. The total expected variance would then be,

$$\sigma_{Exp}^2 = \sigma_{Br}^2 + \frac{2}{\nu} \qquad (4.5)$$

For a single channel process, ν is expected to be unity. In the case of a composite capture state ν will be greater than one due to branching. The value of ν will be quite sensitive to the relative populations of the two capture spin states, being a maximum for equal population. Since ν will always be greater than one, and the contribution of σ_{Br}^2 is very small, we can safely assume that the upper

limit on the variance in the mean is 2. This gives the usual estimate of error of $(2/N)^{1/2}$ for N measurements.

For an infinite sample, the observed variance (eq. 4.3) will be equal to the expected variance (eq. 4.5). Thus, if a large enough sample is available, one can estimate the ν for the distribution from the sample variance.

To obtain an estimate of the average transition strength from the observed mean reduced intensity, $\langle I/E^3 \rangle$, one requires a knowledge of D and Γ_γ. In the absence of a dominating resonance, the value of Γ_γ used should be a mean over the resonances which are expected to contribute. Since the value of Γ_γ is knwon for very few resonances, one may have to assume a value of the expected order of magnitude. It was noted in Chapter I that the value of Γ_γ is not expected to vary too much from resonance to resonance or from nucleus to nucleus, and since one is only interested in an order of magnitude estimation of transition strength, the uncertainty in Γ_γ is not expected to alter the inference. The average spacing of s-wave neutron resonances near the neutron separation energy may be used for D. However, in the presence of a dominating resonance (e.g. ^{36}Cl), the spacing between s-wave resonances having the same spin is to be used.

4.2 Average Transition Strengths

For all the nuclei studied, the spins and parities of a few low-lying levels are known and for the levels of higher excitation, the (d,p) results have yielded some l_n values.

This information allows one to asses the nature of some of the observed primary transitions assuming that only dipole transitions are significant.

In the following part of this section the data concerning the identified M1 and E1 transitions for each nucleus are presented and the average transition strengths are calculated using equations (1.3) and (1.4) with Wilkinson's[Wi 60] recommended valued for D_o. The errors are calculated using the limiting value of 2 for the variance for a mean of unity.

4.2.1 The ^{20}F Nucleus

The ground state spin and parity of ^{19}F are known to be $1/2^+$. The capture state can have possible spin values of 0 and 1 after s-wave neutron capture and subsequent emission of dipole radiation will populate states with spins 0, 1 and 2 in ^{20}F.

To estimate the lowering bias in the observedmmean it will be assumed that the two capture spin states have equal probability of population. (If the $J^\pi = 2^-$ assignments for the 5936 and 6017 keV levels are valid, then this assumption is unrealistic but will not produce too large a change in the bias estimate). Assuming a value of 2[Gi 65a] for δ_m for ^{20}F and proceeding as shown in last section, one finds $\bar{S} = 0.71$.

The data on eight transitions identified as M1 are summarized in Table 4-1. The transition intensities have been enhanced by 10% to account for a possible error in the normalization (see Section 3.4.3). An average of the eight partial relative widths, after an adjustment for the lowering bias, yields the result

$$\langle I/E^3 \rangle_{M1} = 0.056 \pm 0.028 \qquad (\%/MeV^3)$$

The first two neutron resonances in ^{19}F are reported to have radiation widths of 0.7 and 1.6 eV[St 64]. Assuming a value of 1 eV for mean Γ_γ and 0.11 MeV for D[Ca 58], the average transition strength for primary M1 transitions is found to be,

$$T(M1) = 2.46 \pm 1.23$$

which is consistent with the theoretical estimate.

The only two primary transitions identified to be E1 in nature are the C → 5936 keV and the C → 6017 keV transitions. This is not a large enough sample to allow one to estimate $\langle I/E^3 \rangle_{E1}$, but averaging over the two transitions, we find,

$$I/E^3 \approx 0.17 \times 10^3 \qquad (\%/MeV^3)$$

and

$$T(E1) \approx 370$$

which shows that the two E1 transitions are highly enhanced.

TABLE 4-1

The Primary M1 Transitions in ^{20}F

Level energy (keV)	Intensity (%)	I/E^3 (%/MeV^3)
0	9.83	0.34×10^{-1}
984	1.29	0.73×10^{-2}
1057	4.24	0.25×10^{-1}
1309	2.26	0.15×10^{-1}
1843	1.93	0.18×10^{-1}
2044	5.36	0.57×10^{-1}
3488	2.59	0.86×10^{-1}
3526	2.20	0.76×10^{-1}

4.2.2 The ^{21}Na Nucleus

The ground state spin and parity of ^{23}Na are known to be $3/2^+$. Therefore, dipole radiation after s-wave neutron capture will populate states with spins 0, 1, 2 and 3 in ^{24}Na. Using a value of 2.2 for σ_m (Gi 65) and equal cross-section for the capture in the two possible spin states, one finds $\overline{S} = 0.81$.

The data concerning the primary M1 and E1 transitions are presented in Tables 4-2 and 4-3. After correcting for the lowering bias, the mean reduced intensities are found to be,

$$\langle I/E^3 \rangle_{M1} = 0.059 \pm 0.028 \quad (\%/MeV^3),$$

and

$$\langle I/E^3 \rangle_{E1} = 0.46 \pm 0.29 \quad (\%/MeV^3)$$

Using Hibdon's (Hi 60) data on the neutron resonances in ^{23}Na one finds a value of 0.04 MeV for D. Assuming a value of 1 eV for mean Γ_γ, we get,

$$T(M1) = 7.1 \pm 3.3,$$

and

$$T(E1) = 2.46 \pm 1.52.$$

It can be seen that average reduced width for E1 transitions agrees with the theoretical estimates, and in the case of M1 transitions, an order of magnitude agreement is possible within the observed error.

TABLE 4-2

The Primary M1 Transitions in ^{24}Na

Level energy (keV)	Intensity (%)	I/E^3 (%/MeV^3)
472	0.46	0.16×10^{-2}
563	21.85	0.83×10^{-1}
1513	0.17	0.11×10^{-2}
1846	0.55	0.41×10^{-2}
1885	0.44	0.34×10^{-2}
2904	0.72	0.11×10^{-1}
2978	15.10	0.24
3413	1.03	0.23×10^{-1}
3589	2.99	0.65×10^{-1}

TABLE 4-3

The Primary El Transitions in ^{24}Na

Level energy (keV)	Intensity (%)	I/E^3 (%/MeV^3)
3372	13.37	0.29
3977	2.83	0.11
4207	10.82	0.52
4442	13.53	0.85
4561	1.12	0.08

4.2.3 The ^{28}Al Nucleus

The ground state of ^{27}Al is known to have $J^{\pi} = 5/2^{+}$. Therefore levels with spin values of 1, 2, 3, and 4 in ^{28}Al will be excited by dipole radiation after s-wave n neutron capture in ^{27}Al. Again, using the assumption that the two possible capture state spins have equal cross-sections and a value of 2.2 for $\sigma\sigma_m$ (Gi 65) for ^{28}Al, we find $\overline{S} = 0.79$.

Of the observed primary transitions, 19 could be identified as being M1 and 7 as having E1 nature. These data are presented in Tables 4-4 and 4-5. The mean reduced intensities, after removing the bias, are found to be,

$$\langle I/E^3 \rangle_{M1} = 0.013 \pm 0.004 \qquad (\%/MeV^3)$$

and

$$\langle I/E^3 \rangle_{E1} = 0.21 \pm 0.11 \qquad (\%/MeV^3)$$

An examination of Hibdon's (Hi 59) data on the neutron resonances in ^{27}Al cross-section provides a value of 0.06 MeV for D for this case. The total radiative widths for the first three neutron resonances in ^{27}Al are known to be about 1 eV, 0.9 eV and 0.6 eV (Be 67). Using a value of 1eV for the mean Γ_γ, one finds for the primary transitions in ^{28}Al

$$T(E1) = 0.68 \pm 0.36,$$

and

$$T(M1) = 1.05 \pm 0.34$$

Both the results show consistency with the theoretical estimates.

TABLE 4-4

The Primary M1 Transitions in ^{28}Al

Level energy (keV)	J^{π} (Fr 70)	l_n (En 67)	I (Photons/100 captures)	I/E^3 (%/MeV^3)
0	3^+	0	30.5	0.66×10^{-1}
30.6	2^+	0	4.06	0.89×10^{-2}
1014	$(3)^+$	2 + 0	0.97	0.32×10^{-2}
1373	1^+	2	0.11	0.43×10^{-3}
1623	$(2,3)^+$	0	2.81	0.12×10^{-1}
2139	$(2,3)^+$		1.17	0.67×10^{-2}
2202	$(1)^+$	2	0.07	0.42×10^{-3}
2273		2	0.22	0.14×10^{-2}
2486	2^+	0 + (2)	0.27	0.19×10^{-2}
2657		2	0.16	0.12×10^{-2}
3105		2	0.26	0.26×10^{-2}
3296		0 + (2)	1.01	0.12×10^{-1}
3670		0	0.19	0.28×10^{-2}
3709		0	0.76	0.12×10^{-1}
3902		(2)	0.61	0.11×10^{-1}
3936		0 + 2	0.88	0.16×10^{-1}
4596		(0)	0.21	0.68×10^{-2}
4997		2	0.16	0.79×10^{-2}
5016		0	0.52	0.26×10^{-1}

TABLE 4-5

The Primary E1 Transitions in ^{28}Al

Level energy (keV)	l_n (En 67)	I (Photons/100 ¢aptures)	I/E^3 (%/MeV^3)
3465	1 + (3)	7.29	0.94×10^{-1}
3591	1 + (3)	7.44	0.11
3876	1	3.25	0.57×10^{-1}
4691	1	7.79	0.28
4765	1 + (3)	8.73	0.34
4903	1	3.23	0.14
5134	1	3.37	0.19

4.2.4 The ^{32}P Nucleus

The spin and parity of the ground state of ^{31}P are known to be $1/2^+$. The situation is analogous to that of ^{20}F and using $\sigma_m = 2.0$ (Gi 65) we get the result, $\bar{S} = 0.71$.

The data concerning transitions identified as M1 or E1 are presented in Tables 4-6 and 4-7. After adjusting the means for the anticipated lowering bias, one finds,

$$\langle I/E^3 \rangle_{M1} = 0.038 \pm 0.020 \qquad (\%/MeV^3)$$

and

$$\langle I/E^3 \rangle_{E1} = 0.37 \pm 0.17 \qquad (\%/MeV^3)$$

Again, assuming a mean Γ_γ of 1 eV and using the value of 0.05 for D (Ca 58), the average transition strengths are found to be,

$$T(M1) = 3.68 \pm 1.96,$$

and

$$T(E1) = 1.30 \pm 0.62.$$

It can be seen that both the results show reasonable consistency with the theoretical estimates.

4.2.5 The ^{36}Cl Nucleus

The high thermal nuetron capture cross-section for ^{35}Cl suggests the presence of a resonance. Brugger et al (Br 56) showed that the negative energy resonance in ^{35}Cl

TABLE 4-6

The Primary M1 Transitions in ^{32}P

Level energy (keV)	l_n (En 67)	I (%)	I/E^3 (%/MeV^3)
0	0 + 2	0.45	0.90×10^{-3}
78	2	1.06	0.22×10^{-2}
513	0	5.71	0.14×10^{-1}
1149	0	17.52	0.56×10^{-1}
2229		3.04	0.16×10^{-1}
2740	2	1.34	0.96×10^{-2}
5072		2.19	0.93×10^{-1}

TABLE 4-7

The Primary El Transitions in ^{32}P

Level energy (keV)	l_n (En 69)	I (%)	I/E^3 (%/MeV^3)
3264	1	12.58	0.12
3445	(2), 3	2.07	0.23×10^{-1}
4036	1, (2)	20.44	0.34
4661	1, (2)	5.58	0.16
4877	1, (2)	6.87	0.24
5349	1, (2)	5.41	0.31
5510	1, (2)	1.48	0.10
5778	1, (2)	8.60	0.86
6062	1, (2)	1.80	0.27
6198	1, (2)	0.92	0.18

accounts for the observed thermal cross-section. They carried out a shape analysis of the cross section to obtain a consistent set of parameters and arrived at the choice of J = 2 and $\Gamma_\gamma = 0.48 \pm 0.02$ eV. The present recommended value of radiation width for this resonance is 0.50 ± 0.02 eV[St 64]. The M1 and E1 data are presented in Tables 4-8 and 4-9 respectively. In all, six M1 and twenty-six E1 transitions could be identified. In this case, a variance of 2 is expected for a mean of unity for the distribution of individual widths. Using this to estimate the errors, one finds,

$$\langle I/E^3 \rangle_{M1} = 0.014 \pm 0.008 \quad (\%/MeV^3),$$

and

$$\langle I/E^3 \rangle_{E1} = 0.019 \pm 0.005 \quad (\%/MeV^3)$$

Taking a value of 0.02 MeV for D for ^{36}Cl[Fu 71], the average transition strengths are found to be,

$$T(E1) = 0.077 \pm 0.0022,$$

and

$$T(M1) = 1.67 \pm 0.97.$$

It can be seen that while the observed mean reduced width for M1 radiation is consistent with the theoretical estimate, the observed mean reduced width for E1 radiation seems to be an order of magnitude smaller then the theoretical expectation.

TABLE 4-8

The Primary M1 Transitions in ^{36}Cl

Level energy (keV)	l_n (En 67)	Intensity (%)	I/E^3 $(\%/MeV)^3$
0	2(+0)	3.39	0.54×10^{-2}
787	2	10.22	0.22×10^{-1}
1165	0(+2)	11.58	0.28×10^{-1}
1951		5.89	0.20×10^{-1}
2491	0	1.34	0.59×10^{-2}
4553	0	0.19	0.29×10^{-2}

TABLE 4-9

The Primary E1 Transitions in ^{36}Cl

Level energy (keV)	l_n (En 67)	Intensity (%)	I/E^3 (%/MeV^3)
1959		11.20	0.38×10^{-1}
2469	1	21.66	0.95×10^{-1}
2864	3	0.17	0.89×10^{-3}
2864	3	55.89	0.32×10^{-1}
2995	1	0.59	0.34×10^{-2}
3106	1 + 3	0.09	0.55×10^{-3}
3333	1	0.61	0.42×10^{-2}
3600	1	4.11	0.33×10^{-1}
3635	1	1.38	0.11×10^{-1}
3692	1	0.73	0.74×10^{-2}
3992	1	0.32	0.33×10^{-2}
4139	1	1.29	0.15×10^{-1}
4496	1	0.89	0.13×10^{-1}
4598	1	1.09	0.17×10^{-1}
4756	1	1.63	0.29×10^{-1}
5018	1	0.99	0.22×10^{-1}
5150	1	1.07	0.27×10^{-1}
5204	1	0.60	0.16×10^{-1}
5262	1	0.34	0.93×10^{-2}

TABLE 4-9 CONTINUED

Level energy (keV)	l_n (En 67)	Intensity (%)	I/E^3 (%/MeV^3)
5311	1	0.11	0.31×10^{-2}
5461	1	1.08	0.36×10^{-1}
5627	1	0.12	0.47×10^{-2}
5703	1	0.86	0.36×10^{-1}
5839	1	0.17	0.83×10^{-2}
6676	1	0.12	0.17×10^{-1}

4.2.6 The ^{40}K Nucleus

The ground state of ^{39}K is known to have $J = 3/2^+$. As int the case of ^{24}Na, we find $\bar{S} = 0.81$ using a value of 2.2 for σ_m (Gi 65).

The data concerning primary M1 and E1 transitions in ^{40}K are presented in Tables 4-10 and 4-11. One finds, after correcting for the anticipated bias,

$$\langle I/E^3 \rangle_{M1} = 0.021 \pm 0.015 \qquad (\%/MeV^3),$$

and

$$\langle I/E^3 \rangle_{E1} = 0.035 \pm 0.010 \qquad (\%/MeV^3)$$

Bowman et al (Bo 62) have reported D = 0.01 MeV for the s-wave neutron resonances for ^{39}K. Using this and assuming a value of 1 eV for mean Γ_γ, one obtains,

$$T(M1) = 10.1 \pm 7.1$$

and

$$T(E1) = 0.53 \pm 0.16.$$

It is seen that while the observed average reduced w width for E1 transitions shows reasonable consistency with the theoretical result, the corresponding result for M1 transitions appears to be larger than the expected value. Again, an order of magnitude agreement is possible within the large error.

TABLE 4-10

The Primary M1 Transitions in ^{40}K

Level energy (keV)	Intensity (%)	I/E^3 (%/MeV^3)
1960	0.14	0.70×10^{-3}
2290	3.33	0.20×10^{-1}
3414	1.77	0.21×10^{-1}
3797	1.69	0.26×10^{-1}

TABLE 4-11

The Primary E1 Transitions in ^{40}K

Level energy (keV)	l_n (En 67)	Intensity (%)	I/E^3 (%/MeV^3)
30	3	6.20	0.13×10^{-1}
800	3	2.46	0.72×10^{-2}
2048	1	6.02	0.32×10^{-1}
2070	1	2.55	0.14×10^{-1}
2104	1	6.02	0.33×10^{-1}
2419	1	8.23	0.53×10^{-1}
2626	1	2.46	0.18×10^{-1}
2808	1	2.32	0.19×10^{-1}
3486	1	0.26	0.32×10^{-2}
3599	1	2.38	0.32×10^{-1}
3630	1	0.76	0.10×10^{-1}
3868	1	1.59	0.26×10^{-1}
4020	1	0.93	0.17×10^{-1}
4104	1	1.29	0.26×10^{-1}
4253	1	4.84	0.11
4396	1	0.99	0.25×10^{-1}
4465	1	1.22	0.33×10^{-1}
4538	1	2.23	0.64×10^{-1}
4789	1	0.47	0.17×10^{-1}
4807	1	0.49	0.18×10^{-1}
4908	1	0.30	0.12×10^{-1}

4.3 Conclusions and Discussion

The estimates of transition strengths obtained in the last section indicate that the observed average reduced widths for M1 transitions are reasonably consistent with the Weisskopf estimates as used by Wilkinson[Wi 60]. The average reduced width for E1 transitions also shows consistency except for the cases of ^{20}F and ^{36}Cl.

4.3.1 Choice of Values for D_o

In the above calculations Wilkinson's[Wi 60] recommended values for D_o (3 MeV for M1 and 10 MeV for E1 radiation) have been used. In more recent studies, a value of 15 MeV has been used for D_o for both the E1 and the M1 radiation. One can treat D_o as a parameter and find the best value to get agreement with the experimental average reduced widths.

Taking the T(M1) values for the six nuclei and normalizing their weighted average to unity, one finds a value of 7.6 MeV for D_o for M1 transitions. A similar treatment of T(E1) values (excluding the cases of ^{20}F and ^{36}Cl) yields a value of 4.8 MeV for D_o for E1 radiation. These values for D_o are tentative because of the uncertainties in the values of Γ_γ used to arrive at the estimates of transition strengths. The estimates of transition strengths with the modified D_o values are presented in Table 4-12.

TABLE 4-12

SUMMARY OF TRANSITION STRENGTHS

Nucleus	T(E1) D_o = 4.8 MeV	T(M1) D_o = 7.6 MeV
^{20}F	~ 590	1.9 ± 0.9
^{24}Na	3.9 ± 2.4	5.4 ± 2.5
^{28}Al	1.1 ± 0.6	0.8 ± 0.3
^{32}P	2.1 ± 1.0	2.8 ± 1.5
^{36}Cl	0.12 ± 0.04	1.3 ± 0.7
^{40}K	0.9 ± 0.3	7.7 ± 5.4

4.3.2 Assessment of Nature of Transitions

If for a given nucleus the mean reduced intensities differs substantially for M1 and E1 transitions, then one may be able to assess the nature of other primary transitions to levels with unknown parity. However, it is not possible to make any firm assignments due to the wide distribution of individual lifetimes and also the possibility of these being affected by interference between resonances.

This method can be applied to the case of ^{28}Al. The data regarding these primary transitions are presented in Table 4-13. For some transitions, it is possible to assign the likely multipole-type. It can be seen that there is some fairly strong evidence that the "inverted" transitions are E1 in nature. Such identification if valid, yields a negative parity for the states in question.

4.3.3 Energy Dependence of Transition Probability

It was discussed in Chapter I that the Weisskopf single particle estimate yields an E^3 dependence for the transition probability of E1 transitions but the approach of using the giant dipole resonance yields a higher energy dependence - E^4 or E^5, depending upon the proximity of the giant resonance. If a large enough number of E1 transitions can be identified in a nucleus, then one can determine the energy dependence of the transition probability. To obtain a reasonably precise estimate one must average over several

TABLE 4-13

The Other Primary Transitions in ^{28}Al

Level energy (keV)	I (Photons/100 Captures)	I/E^3 (%/MeV^3)	Likely Nature
3541	0.06	0.82×10^{-3}	M1
5177	0.18	0.11×10^{-1}	
5188	0.06	0.37×10^{-2}	M1
5344	0.13	0.96×10^{-2}	
5378	0.13	0.10×10^{-1}	
5442	3.62	0.31	E1
5740	0.58	0.73×10^{-1}	
5860	0.28	0.43×10^{-1}	
6197	1.22	0.34	E1
6316	2.75	0.09	E1
6419	0.01	0.44×10^{-2}	M1
6440	1.09	0.51	E1
6620	0.61	0.45	E1
6831	0.06	0.85×10^{-1}	
6853	0.10	0.15	E1
6893	0.27	0.47	E1
6968	0.13	0.30	E1
7176	0.14	0.84	E1
7269	0.12	0.12×10^{1}	E1
7342	0.12	0.22×10^{1}	E1

transitions in each energy interval because of the inherent dispersion.

The case of ^{36}Cl appears most attractive for this purpose. In all 25 primary transitions have been identified as having E1 character and also the uncertainties introduced by branching are absent since the capture is dominated by a single resonance. The reduced intensities are plotted as a function of energy in Fig. 4.1. To test the energy dependence, the sample may be assembled into four groups of 6, 6, 6, and 7 transitions respectively. The group averages are shown in Fig. 4-1 as X's and the dotted line shows the reduced intensity averaged over the whole sample.

Using the average energies and reduced intensities of the four groups of transitions a non-linear fit was made to obtain the energy dependence, E^n, of the transition probability. This yielded a value of $n = 3.6 \pm 0.5$.

One may try a similar evaluation of n for the 21 primary transitions identified as having E1 character in ^{40}K, although the uncertainties are expected to be higher in this case because of branching and also due to the possible contribution of direct capture (La 60). The sample of 21 transitions was divided into three groups of seven transitions each (Fig. 4-2), and a similar treatment yielded $n = 2.6 \pm 0.6$.

It is seen that the primary E1 transition in ^{36}Cl and ^{40}K show consistency with E^3 dependence of transition probability but within the error of present estimation, an E^4 dependence is possible for ^{36}Cl.

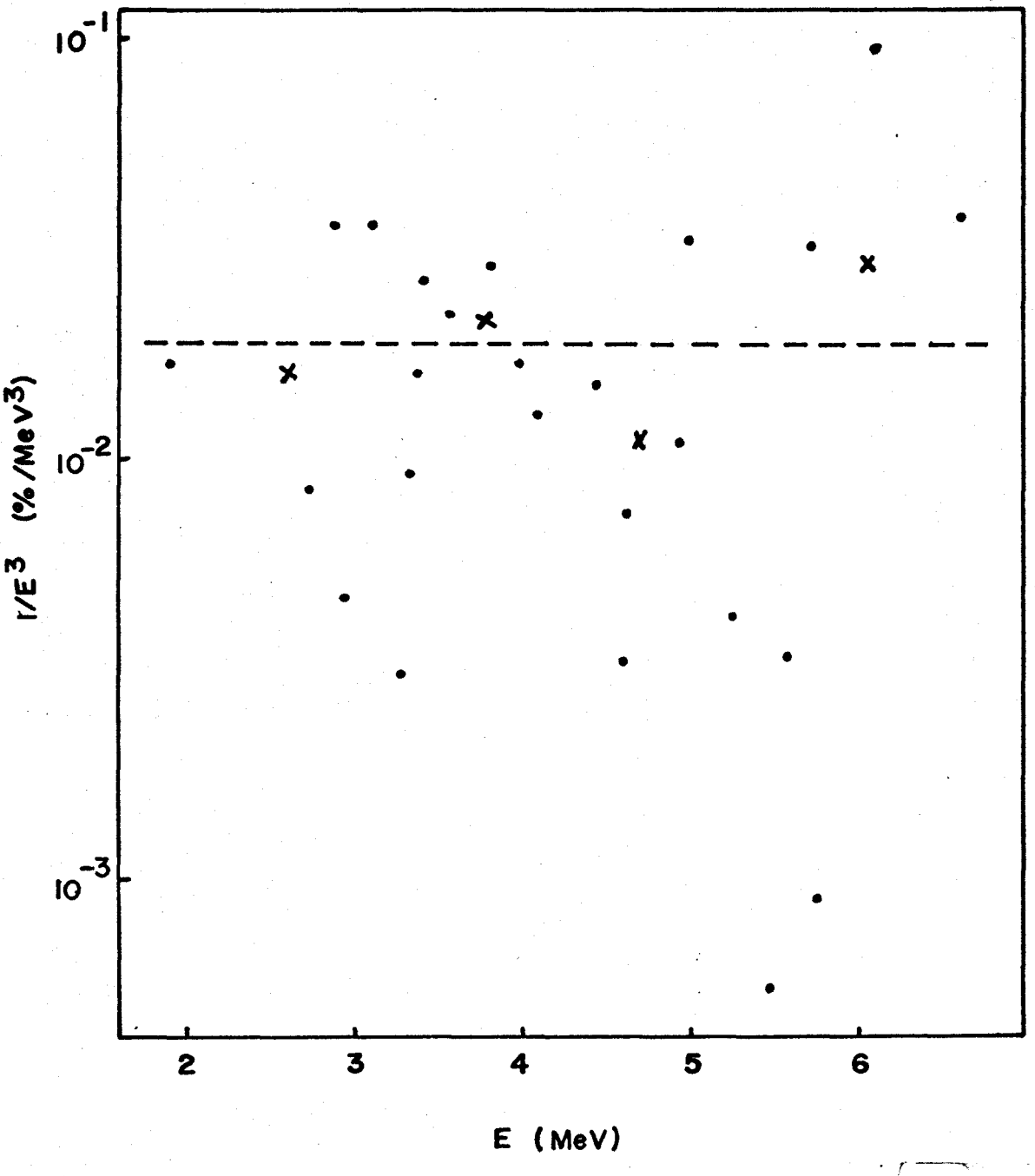

Fig. 4-1 The reduced intensities of the primary E1 transitions in ^{36}Cl. The x's mark the group averages and the dotted line is the average of the whole sample.

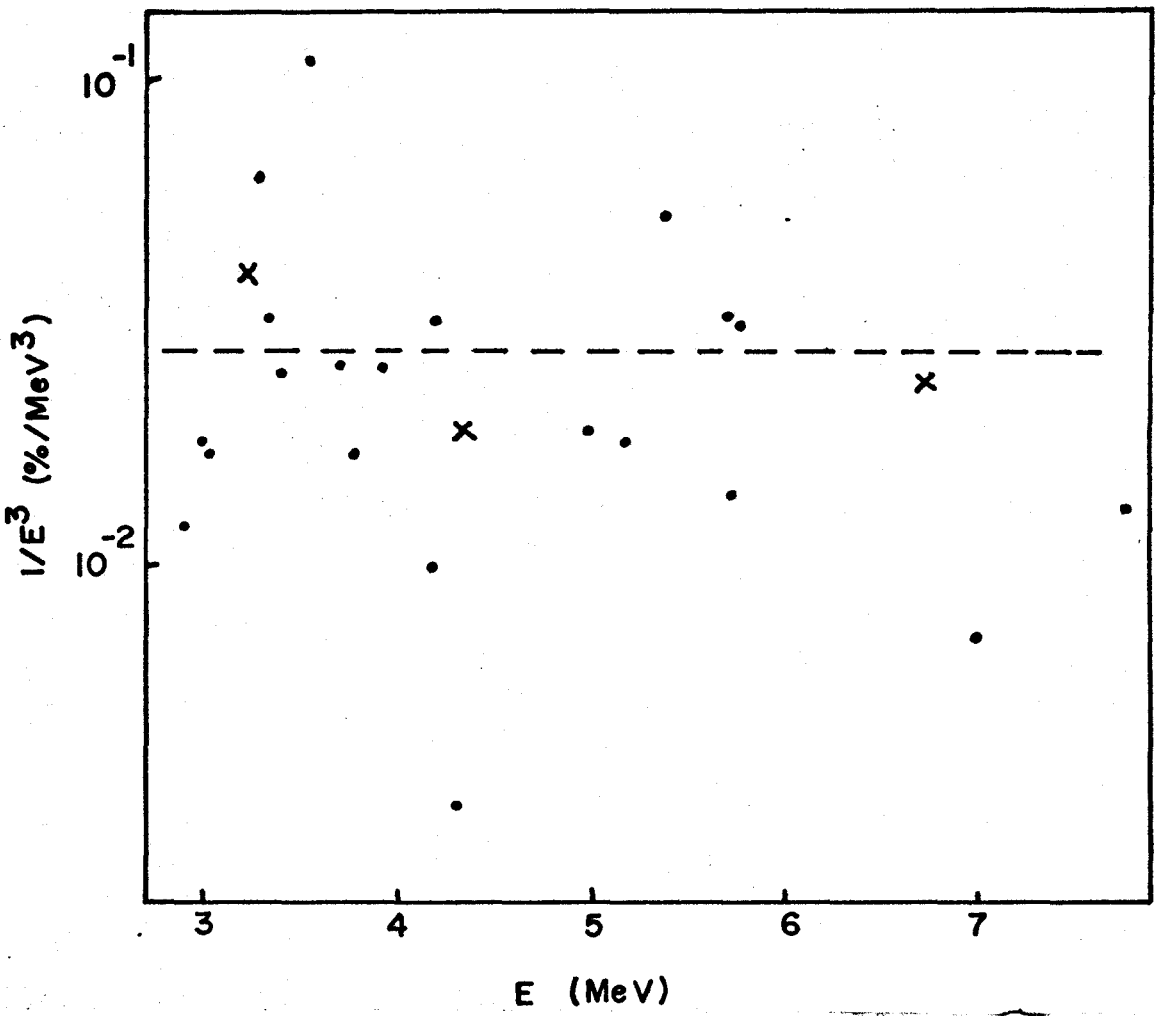

Fig. 4-2 The reduced intensities of the primary E1 transitions in ^{40}K. The x's mark the group averages and the dotted line is the average of the whole sample.

A similar treatment may be applied to the 19 primary M1 transition in ^{28}Al. Dividing the sample in three groups of 6, 6 and 7 transitions respectively (Fig. 4-3) and proceed-as before, one finds $n = 3.4 \pm 0.8$. This is consistent with the E^3 dependence predicted by the Weisskopf single particle estimates.

4.3.4 Estimate of Degrees of Freedom

It was noted in Section 4.1 that the sample variance can actually be used to obtain an estimate of the number of degrees of freedom, ν, associated with the distribution, provided a large enough sample is available.

One can combine the E1 and M1 data (after correcting for the difference in their means) to obtain a single larger sample for the computation of ν. This is justified if only s-wave resonances are contributing.

If the contribution of σ^2_{Br} is neglected, then one obtains the relation,

$$\gamma = 2/\sigma^2_{obs} \qquad (4.6)$$

where σ^2_{obs} is the sample variance defined by equation (4.3) with $\bar{x}$ normalized to unity. The error in the estimate of σ^2_{obs} is given by,

$$\Delta(\sigma^2_{obs}) = \left(\frac{4\ \sigma^2_{obs}}{N-1}\right)^{1/2} \qquad (4.7)$$

where N is the sample size.

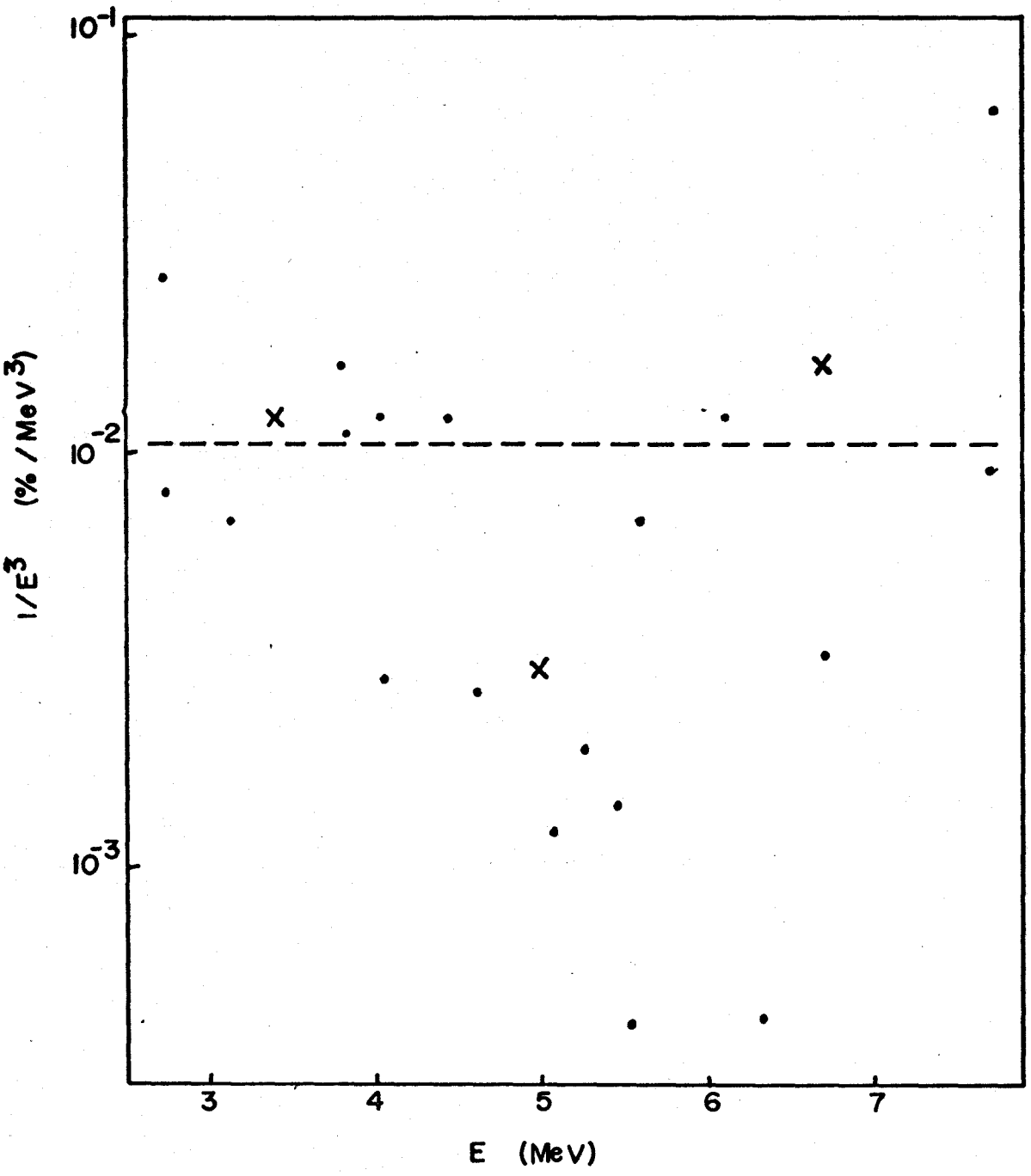

Fig. 4-3 The reduced intensities of the primary M1 transitions in ^{28}Al. The x's mark the group averages and the dotted line is the average of the whole sample

These data are presented in Table 4-14. The uncertainties in ν are high as expected because of the small sample sizes. The value of ν obtained in this manner is known to be biased to a higher value[Ly 69a] but for most cases the bias would be small.

Is is seen that in the case of ^{36}Cl, where a ν of unity expected, the lower limit of the present estimate is 1.5.

A value of ν close to unity, in the absence of a resonance at thermal energies, would indicate that the compound nucleus is formed dominantly with one of the two possible spins. This appears to be true for ^{24}Na and ^{28}Al, but the errors are high and no definite conclusions can be reached.

The high value of ν in the case of ^{40}K could be due to the possible contribution of direct capture[La 60].

TABLE 4-14

The Estimates of Degrees of Freedom

Nucleus	N	σ^2_{obs}	$\Delta(\sigma^2_{obs})$	ν
^{24}Na	14	1.85	0.75	$0.8 < \nu < 1.7$
^{28}Al	26	1.54	0.50	$1.0 < \nu < 1.9$
^{32}P	17	1.04	0.50	$1.3 < \nu < 3.8$
^{36}Cl	31	0.95	0.36	$1.5 < \nu < 3.2$
^{40}K	25	0.67	0.33	$2.0 < \nu < 5.9$

CHAPTER V

SPECTRAL FEATURES

A summary of the Q-value and multiplicity results is presented in this Chapter. The features of the total and primary capture gamma ray spectra are discussed. It is observed that the total intensity contained in the spectrum above an energy of 0.3 times the Q-value is almost the same (about 1.4 photons/capture) for the six nuclei studied.

5.1 The Q-values and Multiplicities

The results of Q-value estimations are summarized in Table 5-1. It was mentioned in Capter I that in the case of thermal neutron capture, the Q-value gives the binding energy of the last neutron in the product nucleus since the kinetic energy of the incident neutrons is negligibly small.

It can be seen in Table 5-1, that the binding energy increases steadily upto ^{36}Cl and then drops in the case of ^{40}K. This can be attributed to the neutron shell closure at N=20.

The estimates of the gamma ray multiplicities, for the reactions studied, are reported in Table 5-2. Also shown in the Table are the spins and parities of the capture and the ground states for the nuclei. The multiplicities associated with the $^{23}Na(n,\gamma)^{24}Na$ and the $^{39}K(n,\gamma)^{40}K$ are rather high probably because of the large spin difference between the

TABLE 5-1

Summary of Q-value Measurements

Reaction	Q-Value
$^{19}F(n,\gamma)^{20}F$	6601.2 ± 0.5
$^{23}Na(n,\gamma)^{24}Na$	6959.4 ± 0.5
$^{27}Al(n,\gamma)^{28}Al$	7725.3 ± 0.5
$^{31}P(n,\gamma)^{32}P$	7935.5 ± 0.5
$^{35}Cl(n,\gamma)^{36}Cl$	8579.1 ± 0.5
$^{39}K(n,\gamma)^{40}K$	7799.5 ± 0.5

TABLE 5-2

The Gamma Rays Multiplicities

Nucleus	J Capture State	J Ground State	Multiplicity
^{20}F	$0^+, 1^+$	2^+	2.8
^{24}Na	$1^+, 2^+$	4^+	3.8
^{28}Al	$2^+, 3^+$	3^+	2.0
^{32}P	$0^+, 1^+$	1^+	2.9
^{36}Cl	2^+	2^+	2.5
^{40}K	$1^+, 2^+$	4^-	3.9

capture and the ground states for the nuclei. The multiplicities for the other four nuclei are fairly close to each other.

5.2 Spectral Features

It was noted in Chapter I that if the level density is sufficiently high, then one may treat the gamma decay of the compound nucleus as a statistical process. Using Equation (1.21) and the exponential level density form, one can write for the primary component of the gamma ray spectrum,

$$S(E)dE = C\ E^3\ e^{(Q-E)/T}\ dE \qquad (5.1)$$

where C is a constant which may be evaluated by integrating the expression from 0 to Q and normalizing to 100%. In the above expression it has been assumed that only dipole radiations are important and their transition probabilities have an E^3 dependence.

One may write down similar expressions for secondary, tertiary etc. components of the gamma ray spectrum but one cannot really expect the lower part of the cascades to be statistical in nature. This part will depend upon the properties of the individual excited states.

Although the level densities in the nuclei studied here are not sufficiently high for a statistical treatment to be very reliable, one may try comparing the observed

average energy of primary transitions to the result expected from equation (5.1). The expected average primary transition energy may be defined by

$$\bar{E}_p(\text{exp}) = \frac{\int_o^Q E\, S(E)\, dE}{\int_o^Q S(E)\, dE} \qquad (5.2)$$

Once the primary transitions in the observed spectrum are identified, the observed average energy is given by,

$$\bar{E}_p(\text{obs}) = \frac{\sum_i E_{P_i} I_{P_i}}{\sum_i I_{P_i}} \qquad (5.3)$$

The construction of a decay scheme allows one to extract the primary component from the observed capture gamma ray spectrum. A comparison of the observed and expected values is made in Table 5-3. The expected values were obtained using Equations (5.1) and (5.2) with the values of T given by Gilbert and Cameron[Gi 65]. It is seen that reasonable agreement is obtained in the cases of ^{24}Na, ^{28}Al and ^{40}K. For ^{32}P and ^{36}Cl, the observed average primary transition energies are respectively lower and higher than the expected values.

The gross shapes of the total and the primary spectra for the nuclei studied are presented in Figs. 5-1 to 5-6. It can be seen that the total spectra for ^{28}Al and ^{36}Cl are rather flat. The other four spectra show high intensities at low energies. In the cases of ^{24}Na, ^{32}P and ^{40}K, this is due to the strong transitions from the first excited states to the

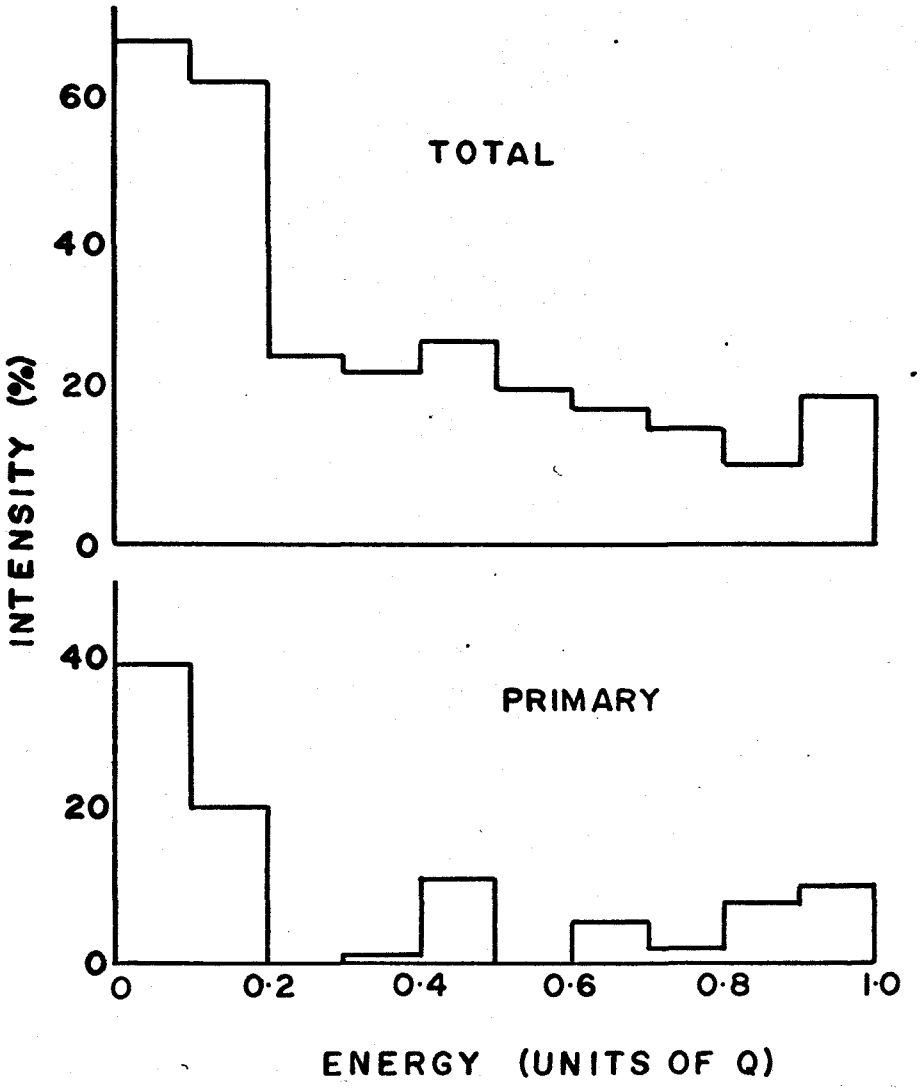

Fig. 5-1 The spectral distribution of the radiation from the $^{19}F(n,\gamma)^{20}F$ reaction.

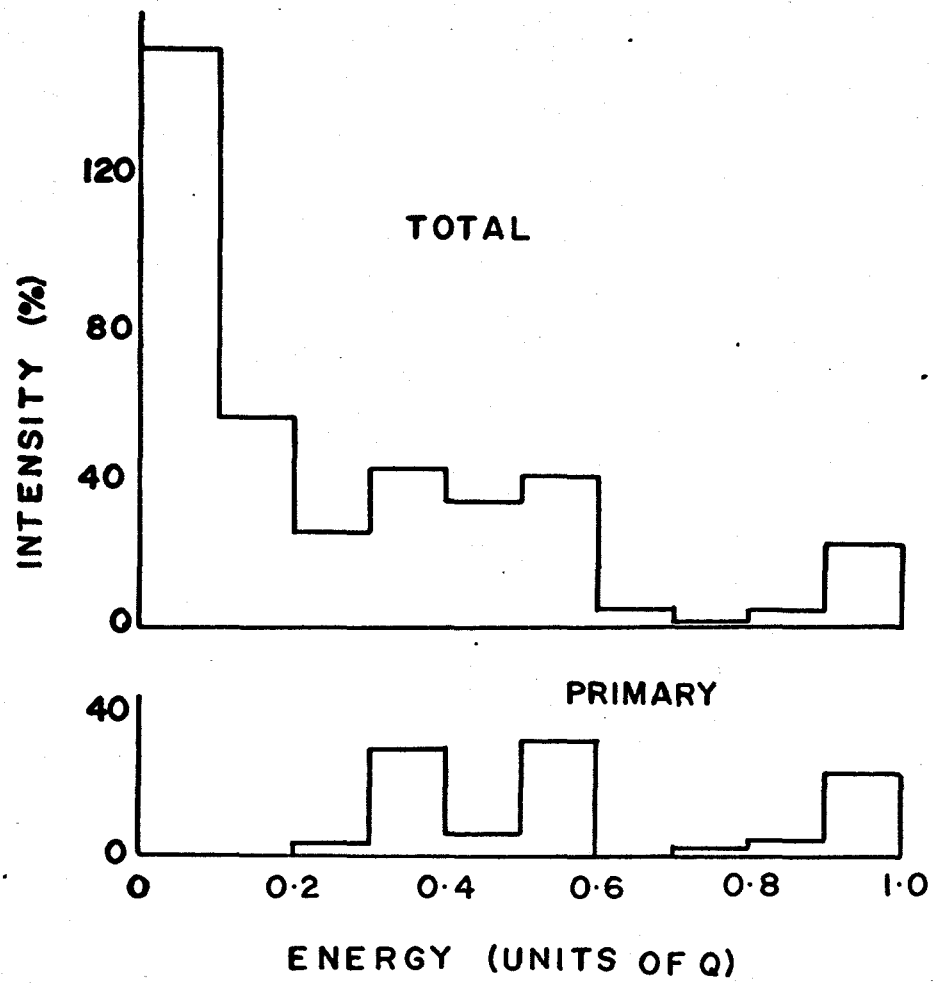

Fig. 5-2 The spectral distribution of the radiation from the $^{23}Na(n,\gamma)^{24}Na$ reaction.

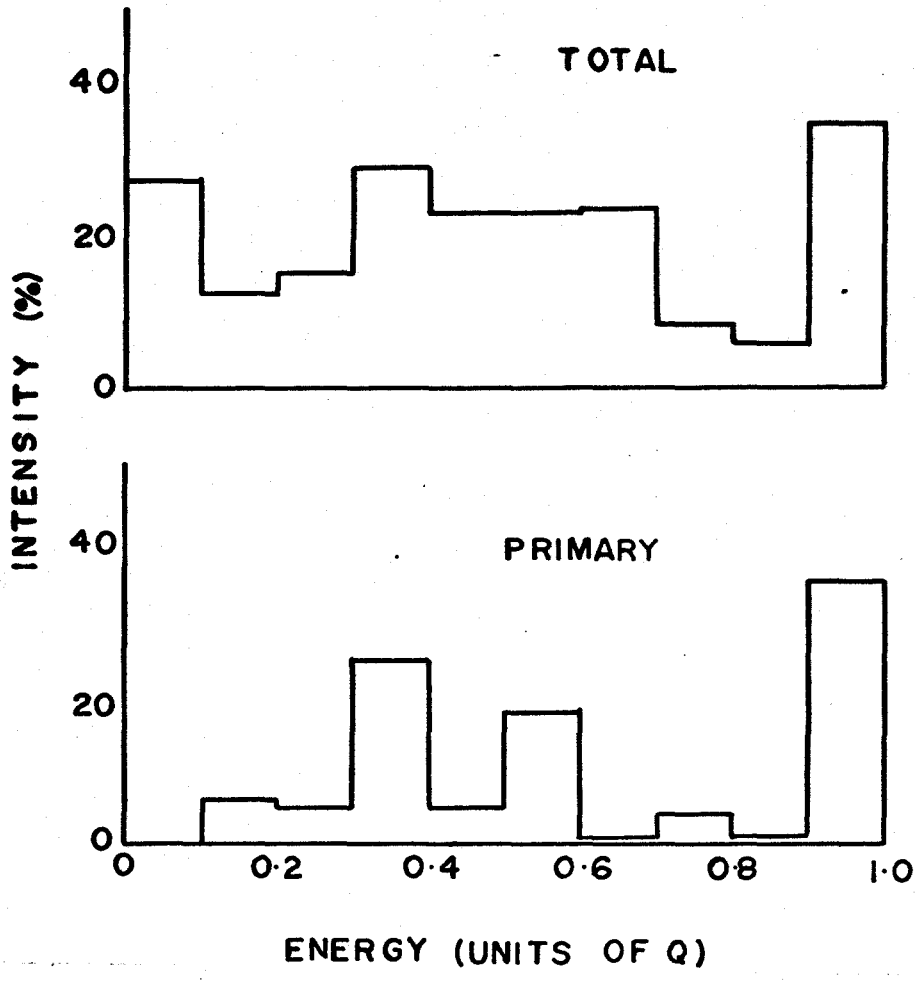

Fig. 5-3 The spectral distribution of the radiation from the $^{27}Al(n,\gamma)^{28}Al$ reaction.

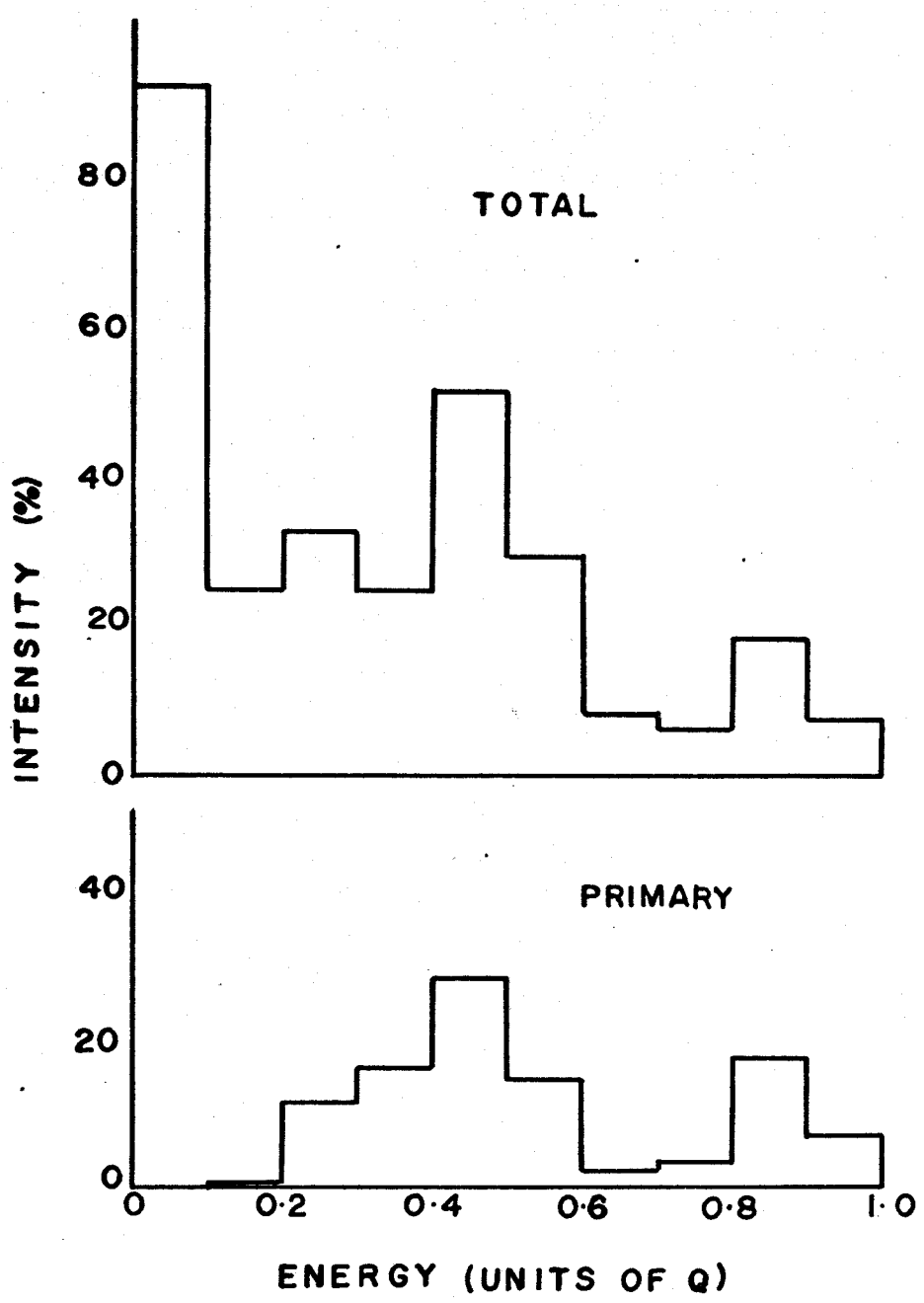

Fig. 5-4 The spectral distribution of the radiation from the $^{31}P(n,\gamma)^{32}P$ reaction.

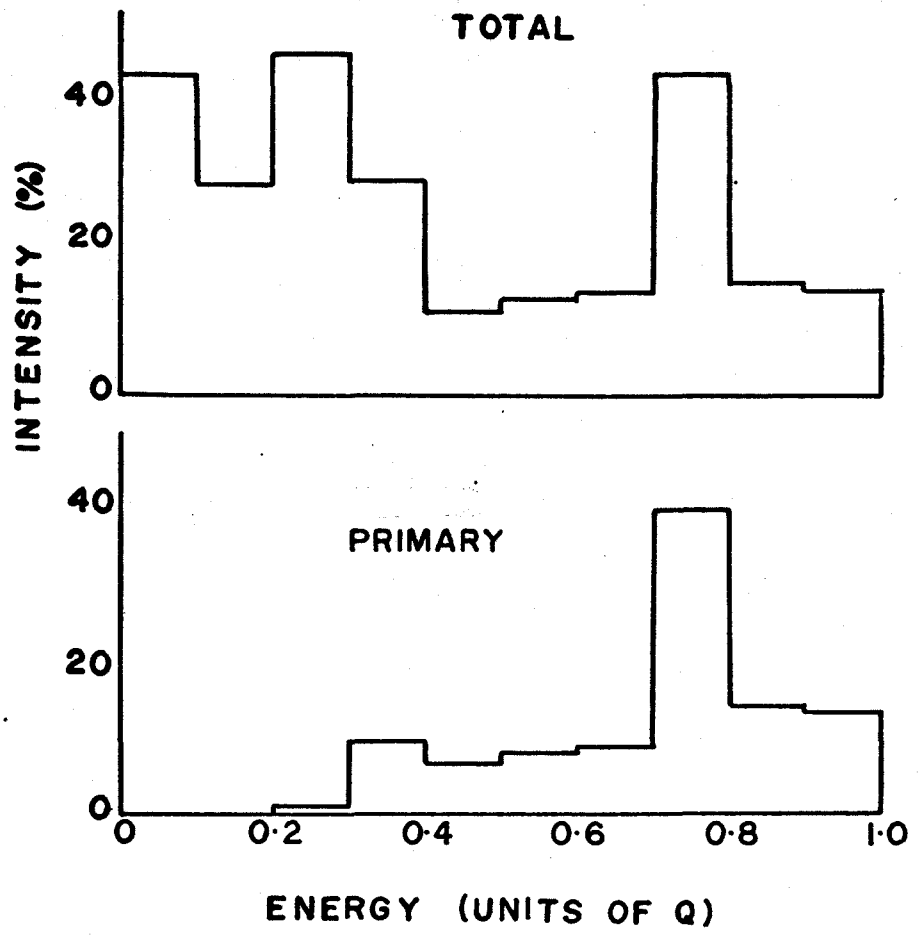

Fig. 5-5 The spectral distribution of the radiation from the $^{35}Cl(n,\gamma)^{36}Cl$ reaction.

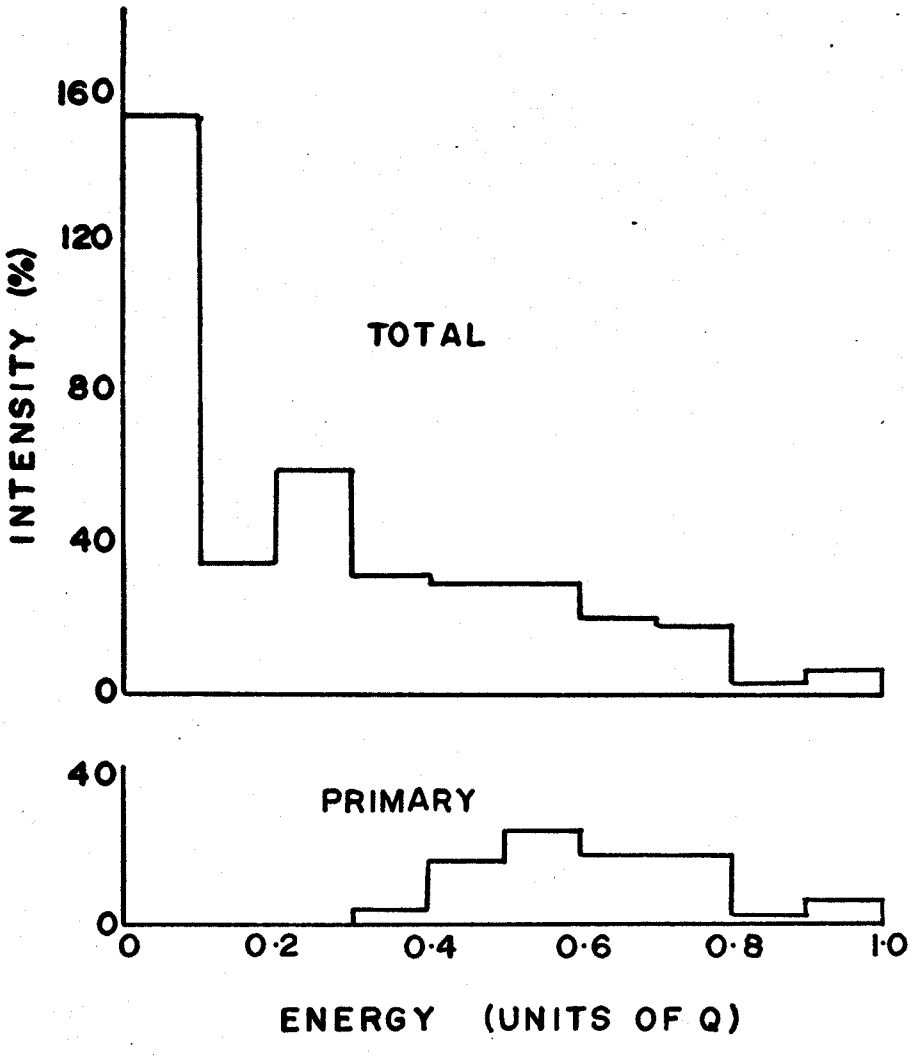

Fig. 5-6 The spectral distribution of the radiation from the $^{39}K(n,\gamma)^{40}K$ reaction.

TABLE 5-3

Average Energies of Primary Transitions

Nucleus	$\bar{E}(P)$ Observed (MeV)	$\bar{E}(P)$ Expected (MeV)
^{24}Na	3.90	4.11
^{28}Al	4.64	4.65
^{32}P	4.39	5.18
^{36}Cl	6.14	4.84
^{40}K	4.31	4.40

ground states. The two strong low energy primary transitions in ^{20}F are responsible for the high intensity at the low energy end of the spectrum as well as for the anomalous shape of the primary spectrum.

In a given mass region, the total intensity contained in the capture gamma ray spectrum (or the multiplicity) will be different for different nuclei being determined by the properties of the low lying levels, but it is possible that the total intensity from a certain energy (above the intense low energy transitions) upto the Q-value will not vary too much from nucleus to nucleus. Assuming that this is true, one could find the lower limit and the total expected intensity which would provide a convenient means of obtaining absolute intensities from the observed relative intensities. The total intensity, I_x, contained in the spectrum from the energy E_x to Q is given by,

$$I_x = \int_{E_x}^{Q} I(E)\ dE \qquad (5.4)$$

where E_x and I_x could be determined from systematics. The results of evaluations of I_x for different E_x are presented in Table 5-4. An examination of the results suggests 0.3 Q as the best value for E_x and averaging over the six nuclei one finds $\bar{I}_x$ = 142%. It is seen that the maximum deviation, for ^{24}Na, represents an error of about 7%.

An attempt was made to see if this agreed with other nuclei in the mass region. An evaluation of I_x with E_x = 0.3 Q for ^{33}S, ^{29}Si and ^{41}Ar, averaging over the data

TABLE 5-4

Variation of I_x with E_x[a]

Nucleus	Total Intensity, I_x (%)			
	E_x = 0.5 Q	E_x = 0.4 Q	E_x = 0.3 Q	E_x = 0.2 Q
^{20}F	89	116	138	163
^{24}Na	78	110	152	177
^{28}Al	96	118	148	163
^{32}P	70	121	145	178
^{36}Cl	96	106	134	180
^{40}K	76	106	138	197

[a] I_x and E_x are defined by equation (5.4).

reported in the compilation of Bartholomew et al[Ba 67] gave the results 133, 149 and 128% respectively. This shows very reasonable consistency.

If valid, this could provide a convenient method for the normalization of gamma ray intensities from neutron capture in resonances where one is generally interested mainly in obtaining the absolute yields of the primary transitions. Since this method does not require a knowledge of the low energy part of the spectrum, it is ideally suited for pair spectrometer measurements.

5.3 Detailed Analysis of the ^{36}Cl Spectrum

In the present work, ^{36}Cl is the only nucleus studied for which capture is dominated by a single resonance. It is worthwhile to consider the gamma ray spectrum of ^{36}Cl in more detail.

The ^{36}Cl spectrum is reasonably complex, yet does permit analysis and the construction of a decay scheme. Usually, for more complex spectra, where the statistical model is applicable, one is unable to make a significant analysis of the observed spectrum.

Using a statistical cascade model, one can calculate the probability that an observed gamma ray of a certain energy would be the mth member of an n step cascade. A model developed in this manner would be very helpful in constructing the decay schemes of more complex nuclei for which level information from other reactions is incomplete or scarce.

Although, it is observed that the simple expression (5.1) does not reproduce the observed primary spectrum satisfactorily, one can hope that a more refined model will be able to predict the primary spectrum more accurately. In order to be able to build such a model, one needs to obtain refined data on different cascade orders for nuclei like ^{36}Cl which be in the transition region from simple to complex spectra.

The analysis of the cascade order in the case of ^{36}Cl indicates the total intensities for 1, 2, 3, 4 and 5 step cascades to be 3.4, 57.3, 31.9, 7.1 and 0.3 percent respectively. This distribution may provide a constraint upon any cascade model. The cumulative spectra for different members of two and three step cascades are shown in Figs. 5-7 and 5-8.

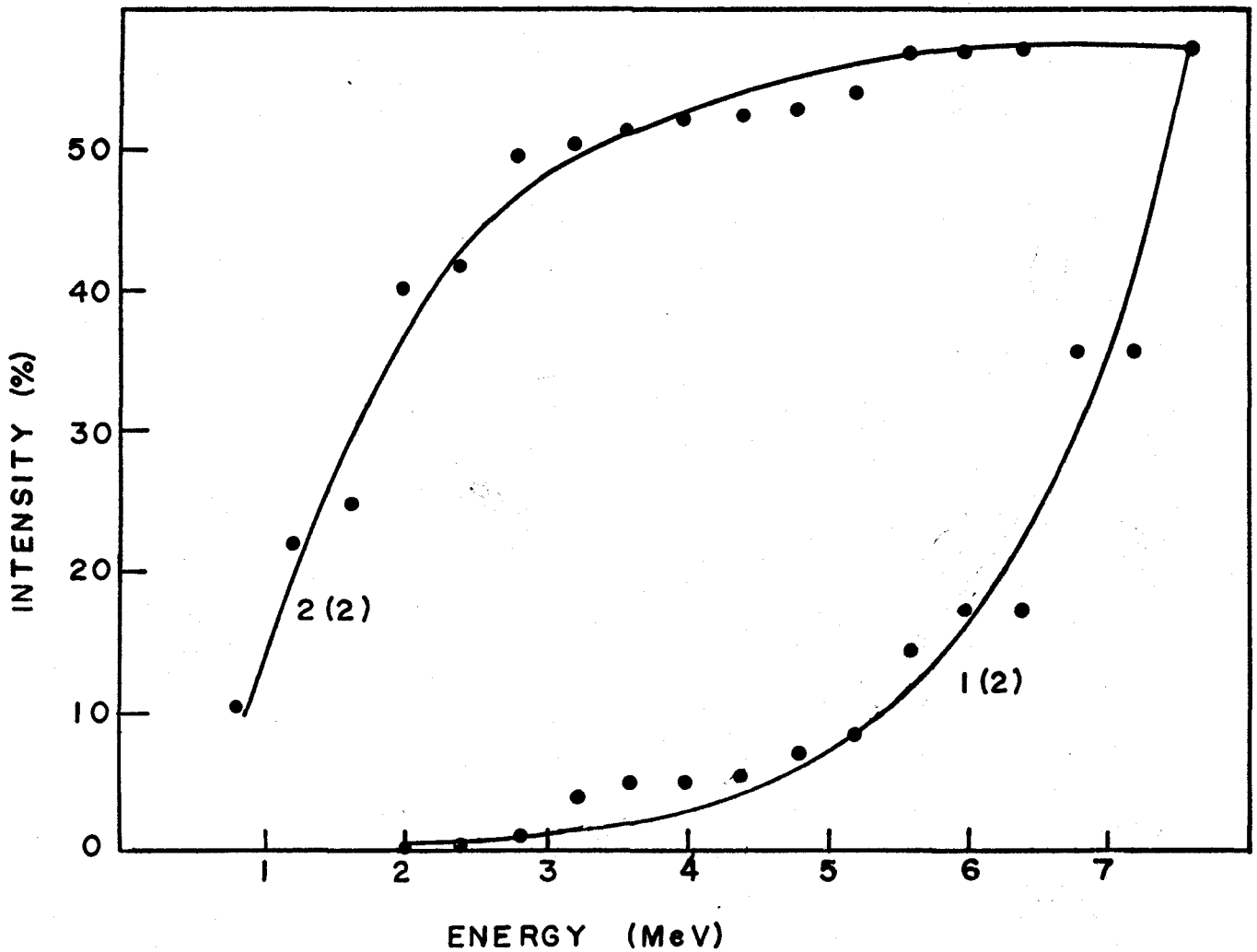

Fig. 5-7 The cumulative spectra of first and second members of two step cascades in ^{36}Cl.

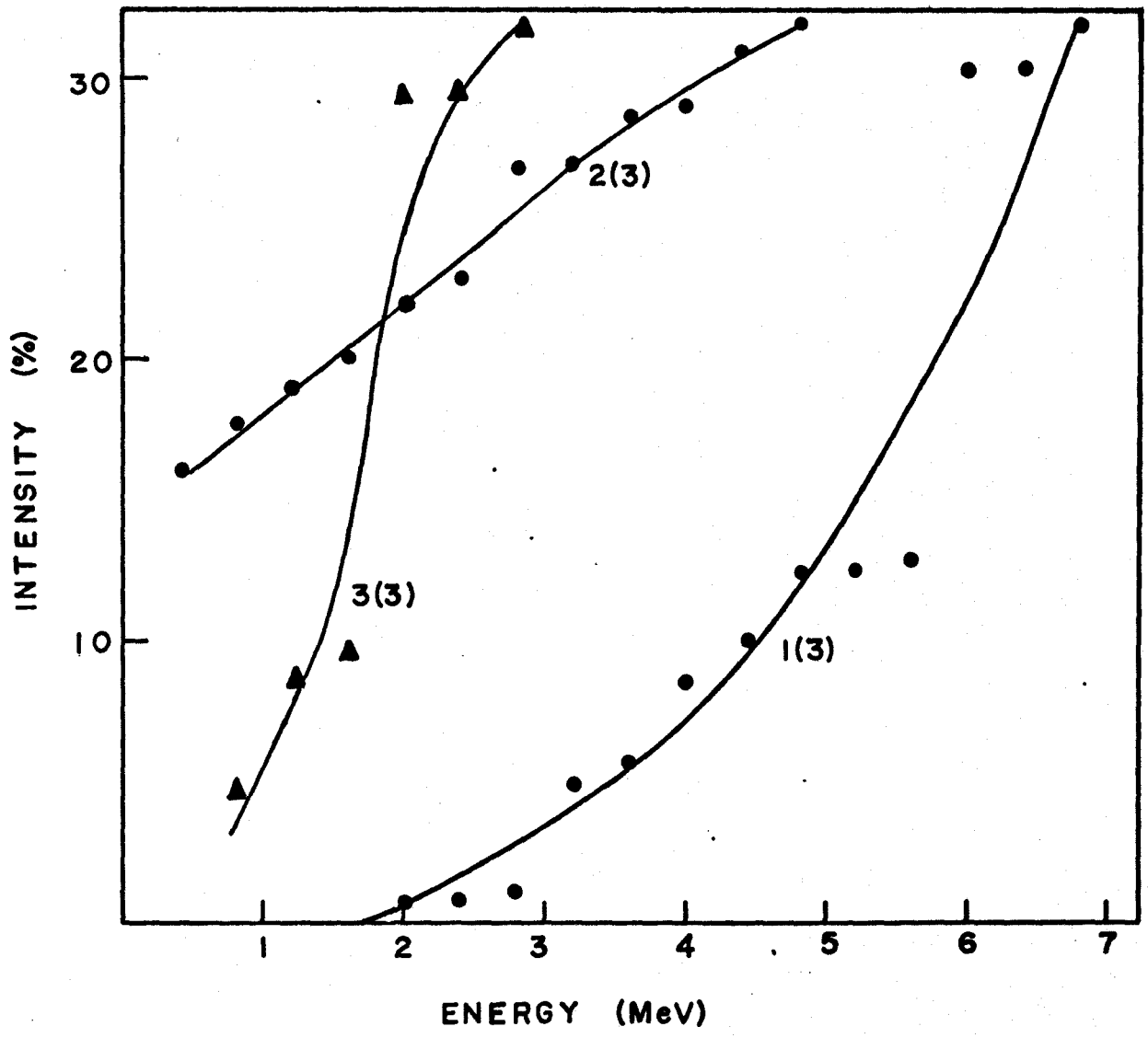

Fig. 5-8 The cumulative spectra of first, second and third members of three step cascades in ^{36}Cl.

REFERENCES

Ad 71 Adelberger, E. G. and Balamuth, D. P., Phys. Rev. Lett. 27, 1597(1971).

Aj 59 Ajzenberg-Selove, F. and Lauritsen, T., Nucl. Phys. 11, 265(1959).

Al 64 Allas, R. G., Hanna, S. S., Meyer-Schutzmeister, L. and Segel, R. E., Nucl. Phys. 58, 122(1964).

Al 69 Alburger, D. E. and Harris, W. R., Phys. Rev. 185 1495(1969).

Ax 62 Axel, P., Phys. Rev. 126, 671(1962).

Ba 58 Bartholomew, G. A. and Higgs, L. A., AECL-669, (1958).

Ba 60 Bartholomew, G. A., Neutron-Capture Gamma Rays, in Nuclear Spectroscopy, Part A, ed. Ajzenberg-Selove, Academic Press, New York, (1960).

Ba 61 Bartholomew, G. A., Ann. Rev. Nucl. Sci. 11, 259(1961).

Ba 67 Bartholomew, G. A., Doveika, A., Eastwood, K. M., Monaro, S., Groshev, L. V., Demidov, A. M., Petekhov, V. I. and Sokolovskii, L. L., Nucl. Data, A3, 367 (1967).

Be 36 Bethe, H. A., Phys. Rev., 50, 332 (1936).

Be 37 Bethe, H. A., Rev. Mod. Phys. 9, 69 (1937).

Be 67 Bergqvist, I., Biggerstaff, J. A., Gibbons, J. H. and Good, W. M., Phys. Rev. 158, 1049 (1967).

Be 71 Betts, R. R., Fortune, H. T., Garrett, J. D., Middleton, R., Pullen, D. J. and Hansen, O., Phys. Rev. Lett. 26, 1121 (1971).

Be 71a Beckstrand, D. F. and Shera, E. B., Phys. Rev. C3, 208 (1971).

Bi 67 Bissinger, G. A., Mueller, R. M., Quin- P. A. and Chagnon, P. R., Nucl. Phys. A90, 1 (1967).

Bl 52 Blatt, J. M. and Weisskopf, V. F., Theoretical Nuclear Physics, John Wiley & Sons, New York (1952).

Bo 59 Bockelman, C. K., Nucl. Phys. 13, 205 (1959).

Bo 62 Bowman, C. D., Bilpuch, E. G. and Newson, H. W., Annals of Physis 17, 319 (1962).

Bo 67 Bollinger, L. M. and Thomas, G. E., Phys. Rev. Lett. 18, 1143 (1967).

Bo 70 Bollinger, L. M., Gamma Rays from Neutron Capture in Resonances, in Experimental Neutron Resonance Spectroscopy, ed. J. A. Harvey, Academic Press., New York (1970).

BO 71 Boerma, D. O., Smith, Ph. B., Phys. Rev. C4, 1200 (1971).

Bo 71a Bollinger, L. M., Phys. Rev. C3, 2071 (1971).

Br 56 Brugger, R. M., Evans, J. E., Joki, E. G. and Shankland, R. S., Phys. Rev. 104, 1054 (1956).

Bu 56 Buechner, W. W., Mazari, M. and Sperduto, A., Phys. Rev. 101, 188 (1956).

Ca 58 Cameron, A. G. W., Can. J. Phys. 36, 1040 (1958).

Ca 62 Carpenter, R. T., ANL-6589 (1962).

Ca 71 Carola, T. P. G. and van der Baan, J. G., Nucl. Phys. A173, 414 (1971).

Da 63 Daum, C., Nucl. Phys. 45, 273 (1963).

De 64 De Lopez, M. E. O., Rickards, J. and Mazari, M., Nucl. Phys. 51, 321 (1964).

De 71 Decowski, P., Nucl. Phys. A169, 513 (1971).

Dr 63 Draper, J. E. and Bostrom, C. O., Nucl. Phys. 47, 108 (1963).

El 64 El-Behay, A. Z., Farouk, M. A., Gontchar, V. J., Loutsik, V. A., Nassef, M. H. and Zaloubovsky, I. I., Nucl. Phys. 56, 224 (1964).

En 59 Enge, A. H., Irwin, E. J. and Weaner, D. H. Phys. Rev. 115, 949 (1959).

En 67 Endt, P. M. and van der Leun, C., Nucl. Phys. A105, 1 (1967).

En 71 Engelbertink, G. A. P. and Olness, J. W., Phys. Rev. C3, 180 (1971).

En 72 Engelbertink, G. A. P. and Olness, J. W., Phys. Rev. C5, 431 (1972).

Er 59 Ericson, T., Nucl. Phys. 11, 481 (1959).

Er 60 Ericson, T., Advan. in Phys. 9, 425 (1960).

Fi 66 Fiedler, H. J., Hughes, L. B., Kennett, T. J., Prestwich, W. V. and Wall, B. J., Nucl. Instr. Methods, 40, 229 (1966).

Fo 70 Fortune, H. T., Bearse R. C., Morrison, G. C., Yntema, J. L. and Wildenthal, H., Bull. Am. Phys. Soc., 15, 483 (1970).

Fo 71 Fortune, H. T., Garrett, J. D., Powers, J. R. and Middleton, R., Phys. Revl, C4, 850 (1971).

Fo 72 Fortune, H. T., Morrison, G. C., Bearse, R. C., Yntema, J. L. and Wildenthal, B. H., Phys. Rev. C6, 21 (1972).

Fr 70 Freeman, R. M. and Gallmann, A., Nucl. Phys. A156, 305 (1970).

Fu 71 Fubini, A., Popa, M., Prosperi, D. and Terrasi, F., Nuovo Cimento, 2A, 109 (1971).

Gi 65 Gilbert, A. and Cameron, A. G. W., Can. J. Phys. 43 1446 (1965).

Gi 65a Gilbert, A., Chen, F. S. and Cameron, A. G. W., Can. J. Phys. 43, 1248 (1965).

Gr 58 Groshev, L. V., Demidov, A. M., Lutsenko, V. N. and Pelikhov, V. I., Atlas of Thermal Neutron Capture Gamma Rays, Atomizdat, Moscow (1958).

Gr 65 Greenwood, R. C. and Reed, H. J., IITRI-1193-53, Vol. 1 (1965).

Gr 66 Greenwood, R. C., Phys. Lett. 23, 482 (1966).

Ha 68 Hardell, R. and Hasselgren, A., Nucl. Phys. A123, 215 (1968).

Ha 69 Hardell, R., Idetjarn, A. O. and Ahlgren, H., Nucl. Phys. A126, 392 (1969).

Ha 70 Hardy, J. C., Brunnader, H. and Cerny, J., Phys. Rev. C1, 561 (1970).

Hi 59 Hibdon, C. T., Phys. Rev. 114, 179 (1959).

Hi 60 Hibdon, C. T., Phys. Rev. 118, 514 (1960).

Ho 62 Hoogenboom, A. M., Kashy, E. and Buechner, W. W., Phys. Rev. 128, 305 (1962).

Ho 62a Holtebeckk, T., Nucl. Phys. 37, 353 (1962).

Ho 69 Holtebekk, T., Tryti, S. and Vamraak, G., Nucl. Phys. A134, 353 (1969).

Ho 71 Honzatko, J., Kajfosz, J. and Kosina, Z., Nucl. Phys. A174, 668 (1971).

Hu 70 Hughes, L. B. and Kennett, T. J., Can. J. Phys. 48, 1130 (1970).

Ja 65 Jackson, H. E., Namenson, A. I. and Thomas, G. E., Phys. Lett. 17, 324 (1965).

Ja 67 Jahr, R., Pflegar, J. A. H. and Zell, H., Phys. Lett. 25B, 113 (1967).

Jo 70 Johnson, L. V. and Kennett, T. J., Can. J. Phys. 48, 1109 (1970).

Ke 71 Keverling Buisman, A. S., Smith, Ph. B., Smulders, P. J. M. and Gruppelaar, H., Nucl. Phys. A176, 161 (1971).

Ko 69 Kopecky, J. and Warming, E., Nucl. Phys. A127, 385 (1969).

La 60 Lane, A. M. and Lynn, J. E., Nucl. Phys. 17, 586 (1960).

Ly 67 Lycklama, H. and Kennett, T. J., Can. J. Phys. 45, 3039 (1967).

Ly 68 Lycklama, H. and Kennett, T. J., Nucl. Instr. Methods 59, 56 (1968).

Ly 69 Lycklama, H., Ph.D. Thesis, McMaster University, (1969).

Ly 69a Lycklama, H., Kennett, T. J. and Hughes, L. B., Can. J. Phys. 47, 665 (1969).

Ma 65 Mattauch, J. H. E., Thiele, W. and Wapstra, A. H., Nucl. Phys. 67, 32 (1965).

Ma 68 Marion, J. B., Nucl. Data, A4, 301 (1968).

Ma 68a Main, I. G., Dawson, N, Kewley, D., Lewley, N, Thomas, M. F. and Twin P. J., Phys. Lett. 26B, 295 (1968).

Mc 69 McDonald, R. E., Becker, J. A., Jones, A. D. W. and Poletti, A. R., Phys. Rev. 181, 1631 (1969).

Mo 55 Moszkowski, S. A., in Beta- and Gamma-Ray Spectroscopy, ed. K. Siegbahn, North Holland, Amsterdam (1955).

Mo 65 Motz, H. and Backstrom, G., in Alpha- Beta- and Gamma-Ray Spectroscopy, ed. K. Siegbahn, North Holland, Amsterdam (1965).

Mo 70 Motz, H. T., Ann. Rev. Nucl. Sci. 20, 1 (1970).

Mu 50 Muchlhause, C. O., Phys. Rev. 79, 277 (1950).

Na 63 Nadjakov, E. G., Nucl. Phys. 48, 492 (1963).

Ni 69 Nichol, L. W., Colenbrander, A. H. and Kennett, T. J., Can. J. Phys. 47, 953 (1969).

Ni 70 Nichol, L., Lopez, A., Robertson, A., Prestwich, W. V. and Kennett, T. J., Nucl. Instr. Methods 81, 263 (1970).

Ni 72 Nichol, L. W. and Kennett, T. J., Can. J. Phys. 50, 553 (1972).

Op 72 Op den Kamp, A. M. F. and Spits, A. M. J. Nucl. Phys. A180, 569 (1972).

Pa 55 Paris, C. H., Buechner, W. W. and Endt, P. M., Phys. Rev. 100, 317 (1955).

Pi 60 Piraino, D., Paris, C. M. and Buechner, W. W., Phys. Rev. 119, 732 (1960).

Po 56 Porter, C. E. and Thomas, R. G., Phys. Rev. 104, 483 (1956).

Pr 65 Prestwich, W. V., Kennett, T. J., Hughes, L. B. and Fiedler, J., Can. J. Phys. 43, 2086 (1965).

Pr 67 Prestwich, W. V., Cote', R. E. and Thomas, G. E., Phys. Rev. 161, 180 (1967).

Qu 67 Quin, P. A., Rollefson, A. A., Gissinger, G. A., Browne, C.P. and Chagnon, P. R., Phys. Rev. 157, 991 (1967).

Qu 70 Quin, P. A., Bissinger, G. A. and Chagnon, P. R., Nucl. Phys. A155, 495 (1970).

Ra 69 Rasmussen, N. C., Hukai, Y., Inouye, T. and Orphan, V. J., MITNE-85 (1969).

Ro 63 Rout, V. M., Jones, W. M. and Waters, D. G., Nucl. Phys. 45, 369 (1963).

Ro 70 Rollefson, A. A., Jano, P. F. and Shea, R. J., Phys. Rev. C1, 1761 (1970).

Sk 66 Skorka, S. J., Hertel, J. and Retz-Schmidt, T. W., Nucl. Data A2, 347 (1966).

Sk 69 Skeppstedt, O., Proc. of the Int. Symp. on Neutron Capture Gamma Ray Spectroscopy, Studsvik, p. 217 (1969).

Sp 52 Sperduto, A. and Buechner, W. W., Phys. Rev. 88, 574 (1952).

Sp 68 Spilling, P., Gruppelaar, H., de Vries, H. F. and Spits, A. M. J., Nucl. Phys. A113, 395 (1968).

St 64 Stehn, J. R., Goldberg, M. D., Magurno, B. A. and Wiener-Chasman, R., BNL-325, 2nd ed., Suppl. 2, Vol. I (1964).

Te 68 Teterin, E. D., Denisov, A. E., Kolalis, R. P., Nemilov, Yu. A., Pomytkin, V. F. and Sadkovskii, V. S., Sov. J. Nuc. Phys. 7, 446 (1968).

Tw 69 Twin, P. J., Olsen, W. C. and Wong, E., Phys. Lett. 29B, 570 (1969).

Tw 70 Twin, P. J., Olsen, W. C. and Sheppard, D. M., Nucl. Phys. A143, 481 (1970).

Va 65 Van Middelkoop, G. and Spilling, P., Nucl. Phys. 72, 1 (1965).

Va 67 Van Middelkoop, G., Nucl. Phys. A97, 209 (1967).

We 51 Weisskopf, V. F., Phys. Rev. 83, 1073 (1951).

Wi 60 Wilkinson, D. H., Analysis of Gamma Decay Data, in Nuclear Spectroscopy, Part B, ed. F. Ajzenberg-Selove, Academic Press, New York (1960).